Mathematical Simulation and Visualization of Sediment Distribution

at Bandon Bay in Surat Thani

Nitinun Pongsiri

A Thesis Submitted in Partial Fulfillment of the Requirements for the Degree of

Master of Science in Applied Mathematics

Prince of Songkla University

2017

Thesis Title   Mathematical Simulation and Visualization of Sediment

Distribution at Bandon Bay in Surat Thani

Author   Miss Nitinun Pongsiri

Major Program   Applied Mathematics

Major Advisor   **Examining Committee:**

……………………………   ……………………….Chairperson
(Dr. Somporn Chuai-Aree)   (Dr. Pakwan Riyapan)

                                         ……………………………
                                         (Dr. Somporn Chuai-Aree)

                                         ……………………………
                                         (Dr. Nifatamah Makaje)

                                         ……………………….
                                         (Dr. Anurak Busaman)

                                         ………………………..………
                                         (Asst. Prof. Dr. Sanae Rujivan)

The Graduate School, Prince of Songkla University, has approved this thesis as partial fulfillment of the requirements for the Master of Science Degree in Applied Mathematics.

……………………………………
(Assoc. Prof. Dr. Teerapol Srichana)

Dean of Graduate School

This is to certify that the work here submitted is the result of the candidate's own investigations. Due acknowledgement has been made of any assistance received.

…………………………….…Signature

(Dr. Somporn Chuai-Aree)

Major Advisor

…………………………….…Signature

(Miss Nitinun Pongsiri)

Candidate

I hereby certify that this work has not been accepted in substance for any other degree, and is not being currently submitted in candidature for any degree.

………………..………….…Signature

(Miss Nitinun Pongsiri)

Candidate

ชื่อวิทยานิพนธ์	แบบจำลองทางคณิตศาสตร์และการสร้างภาพนามธรรมของการกระจายตัวของตะกอนในอ่าวบ้านดอน จังหวัดสุราษฎร์ธานี
ผู้เขียน	นางสาวนิธินันท์ พงษ์ศิริ
สาขาวิชา	คณิตศาสตร์ประยุกต์
ปีการศึกษา	2559

บทคัดย่อ

การเคลื่อนที่ของตะกอนเป็นปัญหาสำคัญที่ก่อให้เกิดการเปลี่ยนแปลงทางด้านสิ่งแวดล้อม ในการศึกษาครั้งนี้ทำการประยุกต์ตัวแบบทางคณิตศาสตร์เพื่อทำการจำลองและแสดงภาพนามธรรม การเคลื่อนที่ของตะกอน ในอ่าวบ้านดอน จังหวัดสุราษฎร์ธานี ตัวแบบทางคณิตศาสตร์ที่ใช้ใน การศึกษาการฟุ้งกระจายของตะกอน ใช้สมการน้ำตื้นรวมกับสมการการเคลื่อนที่ของตะกอนโดยใช้ แนวความคิดเดียวกับการเคลื่อนที่ของน้ำภายใต้กฎการอนุรักษ์มวล และได้ทำการเปรียบเทียบความ ถูกต้องของสมการการเคลื่อนที่ของตะกอนกับแบบจำลองของ Grass โดยการประมาณค่าเชิงตัวเลข ใช้วิธีระเบียบวิธีปริมาตรสืบเนื่อง ภายใต้ปริพันธ์ และใช้วิธีกูดูนูฟ เป็นพื้นฐานในการแก้ปัญหาการ ประมาณค่ารีมันน์โดยฟังก์ชันกูดูนูฟ ประมาณค่าโดยใช้วิธีการ Harten Lax VanLee (HLL) เพื่อ ประมาณหาค่าฟลักซ์ แบบจำลองนี้ได้พัฒนาขึ้นเป็นซอฟต์แวร์ชื่อ VirtualSed3D พบว่าการเคลื่อนที่ ของตะกอนจะช้าหรือเร็วขึ้นอยู่กับค่าความพรุนของตะกอน ความต่อเนื่องของคลื่น และความลึกของ พื้นที่ที่ศึกษา ผลงานจากงานวิจัยนี้สามารถนำไปประยุกต์ใช้กับพื้นที่อื่น ๆ ในลักษณะรูปแบบเดียวกัน ได้

Thesis Title   Mathematical Simulation and Visualization of Sediment

Distribution at Bandon Bay in Surat Thani

Author   Miss Nitinun Pongsiri

Major Program   Applied mathematics

Academic Year   2016

ABSTRACT

Sediment transport is an issue that calls for changes in the environment. In this study, mathematical models are applied to simulate and visualize the movement of sediments at Bandon Bay in Surat Thani province as a case study. A mathematical model is used to study the sediment distribution. This is done by using the Shallow Water Equations (SWEs) combined with a sediment transport Equation which is based on the conservation of mass equation. The model equations for the sediment distribution are validated by comparing it with the Grass Model. The model is solved numerically by using the finite volume methods which are based on the integral form of the conservation laws. Godunov method is used to approximate the functions for solving the model which is a Riemann problem. The functions of Godunov method is computed by using the Harten Lax VanLee approach (HLL) to approximate the numerical flux. Simulation is carried out and visualization by VirtualSed3D program. The result shows that the sediment distribution depends on the porosity of sediment, the continuous movement of wave and also the depth of a particular area under consideration. This research can be applied for other regions based on the same procedure.

Acknowledgements

Foremost, I would like to express my gratitude to my supervisor Dr. Somporn Chuai-Aree for the continuous support of my master study, research, invaluable guidance and assistance throughout the completion of this thesis. Besides my supervisor, I would like to thank Dr. Anurak Boosamun for invaluable guidance in programming part. Special thanks go to all lecturers in Applied Mathematics program, especially Asst. Prof. Dr. Areeyuth Sama-Ae, Asst. Prof. Dr. Arthit Intarasit, Asst. Prof. Dr. Aniruth Phon-On, Dr. Rattikan Saelim, Dr. Nifatamah Makaje, Dr. Pakwan Riyapan, Dr. Saofee Busaman and Dr. Areena Hazanee for their assistance and guidance. Also, I would like to thank Emeritus Prof. Dr. Don McNeil for his enormous contribution and advice.

Furthermore, I am thankful to the Centre of Excellence in Mathematics (CEM), Commission on Higher Education, Thailand and Graduate school, Prince of Songkla University for roviding the scholarship.

I also like to thank the Department of Mathematics and Computer Science and as well as PB Watch in facilitating this study at Prince of Songkla University.

Finally, my sincere thanks also go to my family for their encouragement throughout my study, especially my mother, Mrs. Ratchanee, my father, Mr. Udom, my sister Mrs. Nitinart and my brother Mr. Chayapol. I also thank my friends, especially Benjamin Atta Owusu, Collins Bekoe and Syafika Ulfah for helping and friendship.

Nitinun Pongsiri

Table of Contents

Table of Figures

Chapter 1

Introduction

This research presents a mathematical model to study the distribution of sediment in shallow water. In this chapter, the overview of sediment distribution, problems and motivation of the research as well as the aims and objectives are discussed.

1.1 Background

Sediment distribution can cause problems to people who live near coastal areas. While sediment is needed to build aquatic habitats and reintroduce nutrients for grasses that grow to the surface of shallow water, too much or little sediment can easily cause ecosystem and safety issues. Whether the concerns are caused by scour, erosion, build up, or simply excessive turbidity, sediment transport rate still remains an important environmental factor.

Sediment refers to the mixture of organic or inorganic materials that can be carried away by water, wind, wave current, tides and other anthropogenic impacts (Langland and Cronin, 2003).

The movement of organic and inorganic particles by water is called **Sediment Transport** (Fundamental of Environmental Measurement, 2015). Water flow can be strong enough to suspend particles in the water column as they move downstream, or simply push them along the bottom of a waterway. Sediment that is transported usually includes mineral matter, chemicals, pollutants, and organic materials (Fundamental of Environmental Measurement, 2015).

Stream particles move in three forms that are bed load, suspended load, and wash load. These are shown in Figure 1 and they are described by the numbered notations (1 to 5).
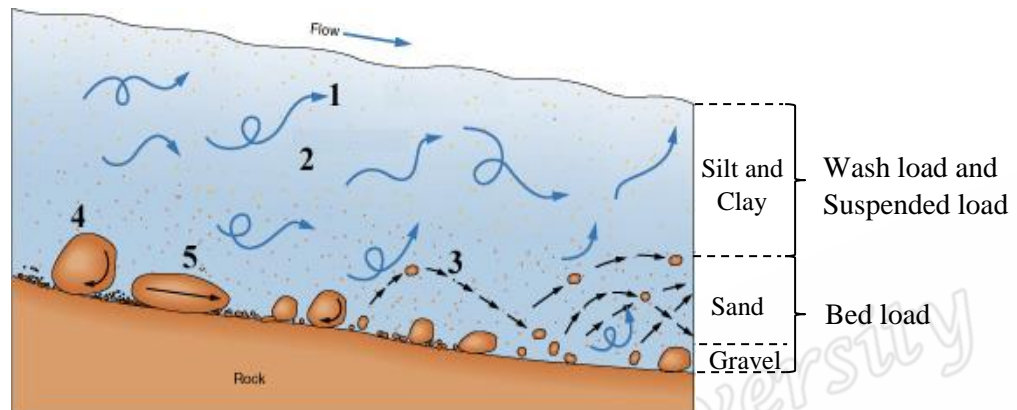
Figure 1 Modes of stream transport

Source/Modify: McGraw-Hill Education (2015)

The bed load contains particles that can slide, roll and jump. The heaviest particles, particle 5 and particle 4, move along the sea bed by sliding and rolling with high energy, respectively. Sand-size particles jump along the sea bed in a way perfectly described as frog leaps (particle 3). Suspended load are small particles like clay and silt. They flow within the water (particles 1 and 2). The wash load is part of the suspended load that is not found in bed such as salts, calcium and magnesium.

This study is to apply mathematical model to analyze, simulate and visualize and to understand the behavior of sediment distribution on the sea bed. Sediment transport can be better explained generally with the normal wave equation. However, this cannot provide full understanding if sediment transport in the shallow water area is considered.

The depths of water (D) have three levels. They are deep water, intermediate and shallow water. This is as shown in Figure 2.
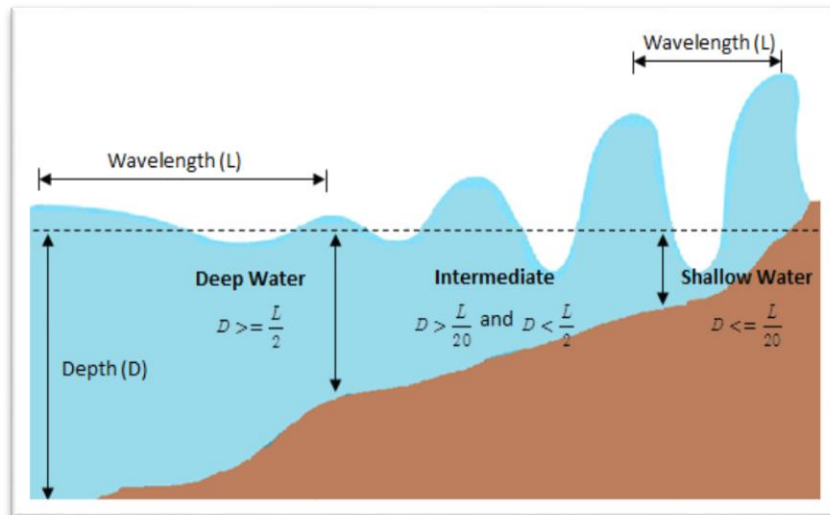
Figure 2 Depth of Water

Source/Modify: Hawai'i Tsunami Education Curriculum : Kai E'e (2016)

It can be distinguished by depth greater than a half of the wavelength $\left(\dfrac{L}{2}\right)$, depth less than $\left(\dfrac{L}{2}\right)$ but greater than $\left(\dfrac{L}{20}\right)$ and depth less than $\left(\dfrac{L}{20}\right)$. They are called deep water, intermediate and shallow water, respectively.
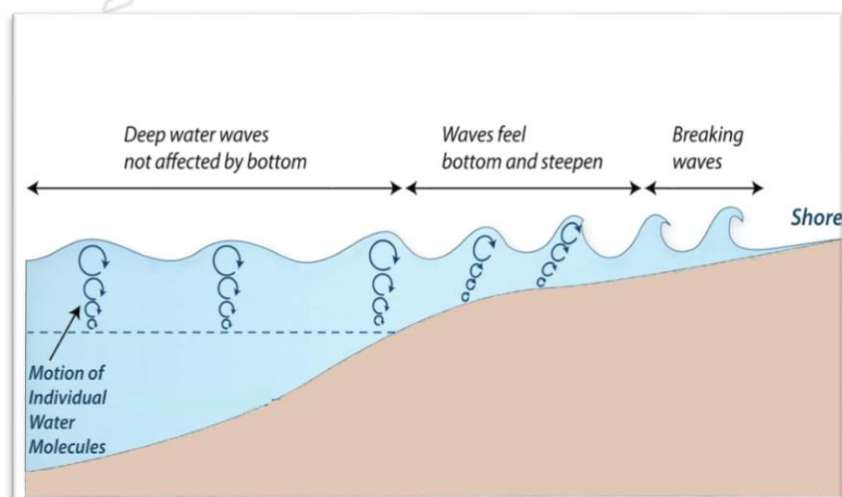
Figure 3 Motion of wave

Source: Satellite Sports Network (2015)

From Figure 3, waves flow from the left to the right hand side. The movement of waves has the motion of individual water column but the deep water waves have no effect on the sea bed. However, in the shallow water area, the motion of waves affects the sea bed and that causes sediment transport in coastal areas. In this research, we focus on the Shallow Water Equations (SWEs).

Mathematical models used in this research are based on the SWEs together with sediment transport equations. The SWEs are based on some basic principles of the laws of conservation of mass and momentum. Also, the idea from the conservation of mass in the SWEs was applied to the sediment transport equation that will be used in this study.

The study area of this research is Bandon Bay in Surat Thani province, Thailand, which is shown in Figure 4.
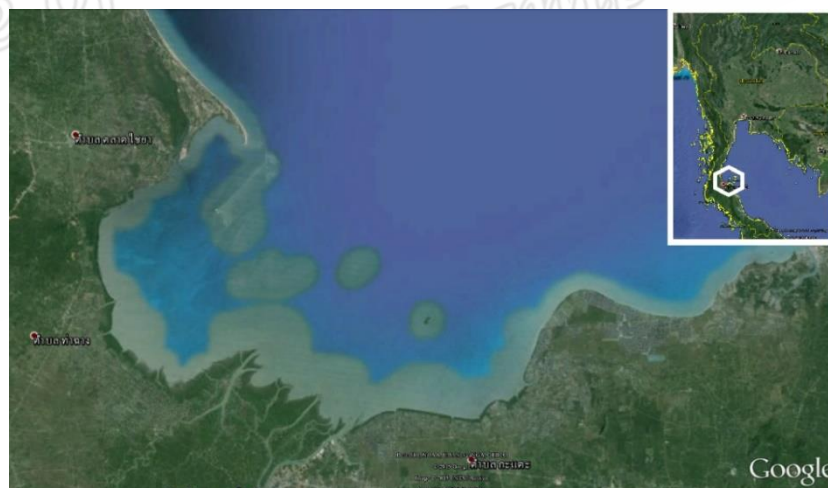
Figure 4 Bandon Bay in Surat Thani, Thailand

Source: Google (2001)

Surat Thani is the largest of the southern provinces of Thailand. The beach just out into the sea which is about 1-2 kilometers from the coast and has a long coastline of about 120 kilometers, covering 6 districts of the province, which are Chaiya, Tha

Chang, Phunphin, Muang Surat Thani, Kanchanadit and Don Sak. Furthermore water from different rivers flow into the bay. This makes the Bandon Bay a deposit point of sediment. The Tapi river is the longest river that flows into the bay and it is has in abundance of marine ecosystems like mangrove, sea grass, and coral reefs. These are important sources of food for fishes and other aquatic species. Surat Thani province also has diverse geographical features such as mountains, plains, rivers, coastlines, and hundreds of islands.

1.2 Motivation for the Study

The transport of organic matter and particles by water in a continuous manner leaves the coastal areas in a vulnerable state water flow can be strong enough to suspend particles as they move downstream.
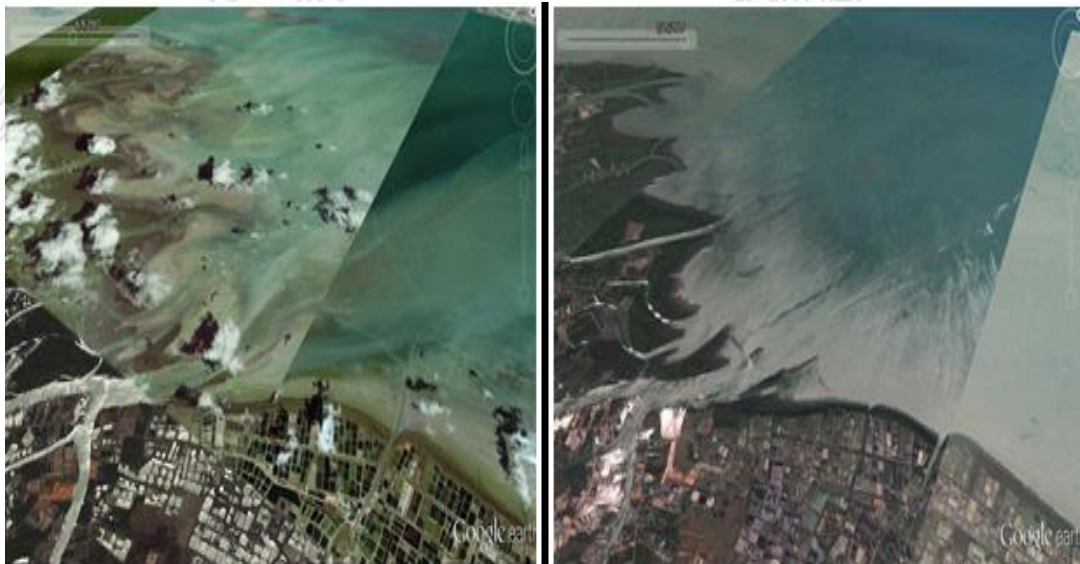
Figure 5 Satellite view of Bandon Bay in Surat Thani, Thailand, 2007 (left panel) and

2015 (right panel)

Source: Google (2001)

Figure 5 shows the satellite view of Bandon Bay in Surat Thani. The left panel shows the sediment distribution in 2007 and the image on the right panel shows the sediment distribution in 2015. Both images show the sediment distribution as worse in 2007 than in 2015. A lot of factors contribute to the transport of sediment and this study, therefore, seeks to use mathematical models to understand the distribution of sediment in Bandon Bay, Surat Thani.

1.3 Objectives

The objectives of this research are

1. To study and apply mathematical model to analyze sediment distribution at Bandon Bay in Surat Thani, Thailand.
2. To use the Shallow Water Equations (SWEs) model to analyze wave movement in the transport of sediment.
3. To develop a program for simulation and visualization of sediment distribution in areas with similar features.

1.4 Expected Advantages of this Study

1. The distribution of sediments in Bandon Bay, Surat Thani in the presence of parameters like manning roughness coefficient and porosity of the sediment, can help to predict future sediment transport at any given time.
2. The sediment transport can be simulated in the shallow water area using the Shallow Water Equations.
3. A computer simulation provides the possibility to predict the sediment transport in other areas with similar features.

This thesis is divided into five chapters according to the following structure. chapter 2 presents the literature review that is relevantly related to this study. The discussion of the mathematical model and how to find the results from the model in chapter 3. The results from simulation of sediment distribution and the conclusion of this thesis are discussed in chapters 4 and 5, respectively.

Research work related to this study would be discussed in the next chapter.

Chapter 2

Literature Review

Mathematical modeling has over the years become an essential tool in understanding how the real world with numerous natural phenomena occurs. Studies into the distribution of sediment have been done extensively in recent times. This chapter therefore presents the mathematical models together with their numerical method for studying sediment transport distribution.

2.1 Mathematical Model

The literatures related to the mathematical models that have been used to study the sediment transport distribution are outlined as follows.

Luchaichana (1987) presented a study on the relationship between the suspended load and the total load of the transport of sediment in river basin. The study was carried out in a recirculant rectangular flume by comparing between the rate of bed material transport measured directly from the tests obtained from computation by using Meyer-Peter and Muller's method (1948) with the following equation

$$g_s = \left(\frac{\gamma_s}{\gamma_s^{''}}\right)\left(\frac{g}{\gamma_w}\right)^{\frac{1}{2}}\left[0.0661\gamma_w\left(\frac{Q_s}{Q}\right)\left(\frac{d_{90}^{3/6}}{n_s}\right)^{\frac{3}{2}}DS - 0.0076\gamma_s^{''}d_m\right]^{\frac{3}{2}}, \qquad (2.1)$$

and Einstein's method (1950) as follows

$$q_s = 11.6 v_* c_a a\left[2.3031\log_{10}\left(\frac{30.2D}{\Delta}\right)I_1 + I_2\right], \qquad (2.2)$$

where g_s is total of sediment flow, γ_s and γ_w are the specific densities of sediment and water, respectively, $\gamma_s^{''} = \gamma_s - \gamma_w$, Q_s is the total bed material sediment load transport, Q is the water discharge released through the reach of the river, d_{90} is the bed material size, n is the manning's roughness coefficient, D is the sediment size in armor layer, S is the channel slope, I_1 and I_2 are integral of Einstein's form of the suspended sediment equation, a is the thickness of the bed layer, $\triangle = k_s / x$, k_s is the hydraulic radius due to skin friction, x is a function of k / δ and δ is the boundary layer thickness. The bed material in this research was sand with a median diameter of 0.70 mm. and a measure of the gradation of sand was 2.134. An analysis of the research showed that the computation from Mayer-Peter and Muller's Equation gave the close results with the experimental data, whiles the Einstein's method showed larger deviations, especially for sand with a bigger mean diameter.

Rattanapitikorn (2008) proposed a mathematical model for computing cross shore sediment transport and beach deformation under the action of irregular waves. The methodology focused on the wave model by comparing between the representative wave approach and the conversion approach for computing representative wave heights which are the essential factors required for the study of beach deformation. The results showed that the representative wave approach was very accurate in computing the energy dissipation whiles the conversion approach was very good in estimating the highest that is one third wave height ($H_{1/3}$) but fair estimation on the maximum wave height ($H_{\max}$).

Castro Diaz, Fernadez-Nieto, Ferreiro and Pares (2009) presented a study on the numerical approximation of sediment transport models in the shallow water. The model is based on the hydro-dynamical component by the shallow water system and the morph dynamical component by a solid transport discharge formula. The bed load transport formula was as follows:

$$\frac{\partial z_b}{\partial t} + \xi \frac{\partial q_{b,1}}{\partial x_1} + \xi \frac{\partial q_{b,2}}{\partial x_2} = 0 , \qquad (2.3)$$

where $\xi = 1 / (1 - \rho_0)$, ρ_0 is the porosity of the sediment layer and $q_b(x,y,t)$ is the solid transport discharge.

The solid transport discharge for this has been proposed by Grass model (1981)

$$\left.\begin{aligned} q_{b,1} &= A_g u_1 (u_1^2 + u_2^2) , \\ q_{b,2} &= A_g u_2 (u_1^2 + u_2^2) , \end{aligned}\right\} \qquad (2.4)$$

where A_g is experiment data (This coefficient takes values between 0 to 1)

and Meyer-Peter and Muller Model

$$\left.\begin{aligned} q_{b,1} &= 8\sqrt{(G-1)gd_i^3} \; \frac{u_1}{\sqrt{u_1^2 + u_2^2}} \max(\tau_* - \tau_{*,c}, 0)^{3/2} , \\ q_{b,2} &= 8\sqrt{(G-1)gd_i^3} \; \frac{u_2}{\sqrt{u_1^2 + u_2^2}} \max(\tau_* - \tau_{*,c}, 0)^{3/2} , \end{aligned}\right\} \qquad (2.5)$$

where $\tau_* = \dfrac{\gamma n^2 (u_1^2 + u_2^2)^{\frac{3}{2}}}{(\wp_s - \wp) d_i h^{\frac{1}{3}}}$, $\wp$ denotes the specific weight of the fluid, $\wp = g\rho$, ρ is the water density, $\wp_s$ is the specific weight of the sediment, $\wp_s = g\rho_s$, ρ_s is the

sediment density, d_i is the sediment grain size, G is the relative density, $G = \dfrac{\rho_s}{\rho}$, $\tau_{*,c}$

is the non-dimensional critical shear stress (for MP&M is equals to 0.047). The numerical method used Roe's scheme based on flux limiter technique to reduce the numerical diffusion whereby the numerical test showed that the Roe schemes are too diffusive as expected.

Meesuk, Boonya-aroonnet, Srimongkol, Chankarn and Chitradon (2009) studied sediment transport in Mahachai Canal and Lung canal, in Samutsakhon Province through simulation of the flow at the different periods of time. This research considered 4 scenarios to operate the water gate in the canal. They were open full-time, keep the lower water level in the inner area, increase flow to Mahachai Canal and increase flow to Lung Canal. The mathematical models used hydraulic-flow with 2-dimensional "CCHE2D" model. The 2-dimensional CCHE2D for water flow was based on Continuity and Momentum Equations which are,

$$
\left.
\begin{aligned}
& \frac{\partial z}{\partial t} + \frac{\partial (hu)}{\partial x} + \frac{\partial (hv)}{\partial y} = 0 \,, \\[2mm]
& \frac{\partial u}{\partial t} + u\frac{\partial u}{\partial x} + v\frac{\partial u}{\partial y} = -g\frac{\partial Z}{\partial x} + \frac{1}{h}\left[\frac{\partial (h\tau_{xx})}{\partial x} + \frac{\partial (h\tau_{xy})}{\partial y} \right] - \frac{\tau_{bx}}{\rho h} + f_{Cor}v \,, \\[2mm]
& \frac{\partial u}{\partial t} + u\frac{\partial v}{\partial x} + v\frac{\partial v}{\partial y} = -g\frac{\partial Z}{\partial x} + \frac{1}{h}\left[\frac{\partial (h\tau_{yx})}{\partial x} + \frac{\partial (h\tau_{yy})}{\partial y} \right] - \frac{\tau_{by}}{\rho h} + f_{Cor}u \,,
\end{aligned}
\right\} \quad (2.6)
$$

where $z(x,y,t)$ is the water surface elevation, $h(x,y,t)$ is local water depth, t is time, $u(x,y,t)$ and $v(x,y,t)$ are the depth-integrated velocity components in the x and y directions, respectively, g is the gravitational acceleration, ρ is water density, f_{Cor} is the Coriolis parameter, $\tau_{xx}, \tau_{xy}, \tau_{yx}$ and τ_{yy} are the depth integrated Reynolds

stresses, τ_{bx} and τ_{by} are shear stresses on the bed surface. And for sediment transport equation,

$$\frac{\partial c_k}{\partial t} + \frac{\partial(uc_k)}{\partial x} + \frac{\partial(vc_k)}{\partial y} + \frac{\partial(wc_k)}{\partial z} - \frac{\partial(w_{sk}c_k)}{\partial y} = \frac{\partial}{\partial x}\left(\varepsilon_s \frac{\partial c_k}{\partial x}\right) + \frac{\partial}{\partial y}\left(\varepsilon_s \frac{\partial c_k}{\partial y}\right) + \frac{\partial}{\partial z}\left(\varepsilon_s \frac{\partial c_k}{\partial z}\right), \quad (2.7)$$

where c_k is the concentration of k-th size class of sediment, $u(x,y,z,t)$, $v(x,y,z,t)$ and $w(x,y,z,t)$ are the velocity components in the x, y and z directions, respectively, the z direction being assigned as the vertical direction along the gravity, w_{sk} is the setting velocity of the k-th size class of sediment, ε_s is the eddy diffusivity of sediment and v_t is the eddy viscosity of flow. The result of this research revealed that the first scenario produced the maximum sediment deposition 0.2 m on the bed load in the center of Mahachai Canal. The third and fourth scenario could remove the partial sediment -0.6 meters and -0.3 meters in the Mahachai canal and Lung Cana respectively.

Cordier, Le and Morales de Luna (2011) studied the sediment transport models in a shallow water. Their models for describing the overland flow were

$$\left.\begin{array}{r} \partial_t h + \partial_x(hu) = 0\,, \\[2mm] \partial_t(hu) + \partial_x(hu^2 + gh^2/2) = -gh\partial_x z_b + gh\partial_x H\,, \\[2mm] \partial_t z_b + \xi\partial_x q_b = 0\,, \end{array}\right\} \qquad (2.8)$$

where $h(x,t)$ is the water depth (m), $u(x,t)$ is the flow velocity (m/s), $z_b(x,t)$ is the thickness of sediment layer, the sediment is fixed the layer at depth H, $\xi = (1-\gamma)^{-1}$, γ is the porosity of sediment and $q_b(x,t)$ is the volumetric bed load sediment transport

rate per unit time. The model is solved numerically based on a splitting method. The result showed that the splitting technique may produce unphysical instabilities and in some cases the resulting instabilities may be avoided by reducing the Courant–Friedrichs–Lewy (CFL) condition and using the upper bound.

2.2 Numerical Method

In modeling, obtaining an exact solution to the mathematical model is sometimes difficult. Numerical Methods are used to find an approximate solution to the various models and this section seeks to describe the numerical method for solving sediment transport model.

Suwannasri (2004) presented SWEs to simulate and visualize the shallow water flow problems for the rectangular and circular dam break by using the finite volume methods to approximate the solution as follows

$$\vec{Q}_{i,j}^{n+1} = \vec{Q}_{i,j}^{n} - \frac{\Delta t}{\Delta x}\left[\vec{F}_{i+\frac{1}{2},j}^{n} - \vec{F}_{i-\frac{1}{2},j}^{n}\right] - \frac{\Delta t}{\Delta y}\left[\vec{G}_{i,j+\frac{1}{2}}^{n} - \vec{G}_{i,j-\frac{1}{2}}^{n}\right], \tag{2.9}$$

where $\vec{Q}_{i,j}^{n}(x,y,t)$ represents a cell average over the (i,j) grid cell at time t_n,

$\vec{F}_{i+\frac{1}{2},j}^{n}(x,y,t)$ and $\vec{G}_{i+\frac{1}{2},j}^{n}(x,y,t)$ are some approximations to the average in the x and

y directions, respectively. The Numerical flux is computed by using a high-resolution Godunov's method based on a second order approximate Riemann solver. The Riemann problem is solved by using Harten, Lax, and Van Leer (HLL) approach and by Roy method to solve the 2D SWEs to compare the performance of computing by using parallel computing technique.

Kanbua and Chuai-Aree (2007) presented the tsunami propagation simulator model which calculated trends to check if the model could predict the tsunami arrival times. The mathematical model was based on the wave equation in Grid which was computed as follows

$$\frac{\partial^2 U}{\partial t^2} = a^2 \left(\frac{\partial^2 U}{\partial x^2} + \frac{\partial^2 U}{\partial y^2} \right), \tag{2.10}$$

where $U(x,y,t)$ is wave height (m), x and y are spatial grid in x and y directions (m), respectively, a is wave propagation speed (m/s), d is water depth (m). The model was solved numerically by using the central difference for finite difference method (FDM) as

$$U_{i,j}^{n+1} = \left(\frac{\triangle t}{\triangle h} \right)^2 \ a_{i-1,j}^2 U_{i-1,j}^n + a_{i+1,j}^2 U_{i+1,j}^n + a_{i,j-1}^2 U_{i,j-1}^n + a_{i,j+1}^2 U_{i,j+1}^n - 4a_{i,j}^2 U_{i,j}^n + 2U_{i,j}^n - U_{i,j}^{n-1}, \tag{2.11}$$

Where $U_{i,j}(x,y,t)$ is the wave height at points i and j, i and j are grid index in the x and y directions, respectively, $\triangle t$ is time step and $\triangle h$ is grid resolution. The results of numerical simulation was compared with the observed time in the case of the 26th December 2004, it showed that the model can predict quite well with the timing.

Boosamun (2010) presented a mathematical model of water flow on area surface by using hydrology and numerical computation to explain the diffusion of water. The model was solved numerically by using finite volume method for SWEs to approximate the solution as follows:

$$\vec{W}_{i,j}^{n+1} = \vec{W}_{i,j}^n - \frac{\triangle t}{\triangle x} \left[\vec{F}_{i+\frac{1}{2},j}^n - \vec{F}_{i-\frac{1}{2},j}^n \right] - \frac{\triangle t}{\triangle y} \left[\vec{G}_{i,j+\frac{1}{2}}^n - \vec{G}_{i,j-\frac{1}{2}}^n \right] + \triangle t \vec{Z}_{i,j}^n + \triangle t \vec{S}_{i,j}^n, \tag{2.12}$$

where $\overrightarrow{W}_{i,j}^{n}(x,y,t)$ represents a cell average over the (i,j) grid cell at time, $\vec{F}_{i+\frac{1}{2},j}^{n}(x,y,t)$ and $\overrightarrow{G}_{i+\frac{1}{2},j}^{n}(x,y,t)$ are some approximations to the average flux in the x and y directions, respectively, $\vec{Z}_{i,j}^{n}(x,y,t)$ is the gravity force vector and $\vec{S}_{i,j}^{n}(x,y,t)$ is the source vector. The Numerical flux is computed by using Harten, Lax, and van Leer (HLL) approach in solving Riemann problem. The result is shown by developing a software to visualize water flow in 2D and 3D and also for predicting the risk area of flooding.

He, Hu, Zhao, Wu and Pahtz (2015) studied a depth-average 2-dimentional wave based on couple flow and sediment transport model to investigate the flow. The governing equations of couple flow and sediment transport used in this study were

$$
\left.\begin{aligned}
\frac{\partial(\rho h)}{\partial t} + \frac{\partial(\rho u h)}{\partial x} + \frac{\partial(\rho v h)}{\partial y} + \rho_b \frac{\partial z_b}{\partial t} = 0 \,, \\[2mm]
\frac{\partial(\rho u h)}{\partial t} + \frac{\partial(\rho u^2 h)}{\partial x} + \frac{\partial(\rho u v h)}{\partial y} + \rho g h \frac{\partial z_s}{\partial x} + \frac{1}{2} g h^2 \frac{\partial \rho}{\partial x} + \rho g \frac{n^2 m_b u U}{h^{\frac{1}{3}}} = 0 \,, \\[2mm]
\frac{\partial(\rho v h)}{\partial t} + \frac{\partial(\rho u v h)}{\partial x} + \frac{\partial(\rho v^2 h)}{\partial y} + \rho g h \frac{\partial z_s}{\partial y} + \frac{1}{2} g h^2 \frac{\partial \rho}{\partial y} + \rho g \frac{n^2 v U}{h^{\frac{1}{3}}} = 0 \,, \\[2mm]
\frac{\partial(h C_t)}{\partial t} + \frac{\partial(h u C_t)}{\partial x} + \frac{\partial(h v C_t)}{\partial y} = -\frac{1}{L_t}(U h C_t - m_b q_{t*}) \,,
\end{aligned}\right\} \quad (2.13)
$$

where t is the time, $h(x,y,t)$ is the flow depth, $u(x,y,t)$ and $v(x,y,t)$ are the flow velocities in the x and y directions, respectively, $U = \sqrt{u^2 + v^2}$, $z_b(x,y,t)$ is the bed surface elevation above datum, $z_s(x,y,t)$ is the water level, $z_s = z_b + h$, C_t is the actual volumetric total-load sediment concentration, $\rho(x,y,t)$ is the density of the

water and sediment mixture in the water column determined by $\rho = \rho_w(1 - C_t) + \rho_s C_t$, ρ_s is density of the water and sediment mixture in the bed surface layer determined by $\rho_b = \rho_w \rho'_m + \rho_s (1 - \rho'_m)$, ρ'_m is the porosity of the surface-layer bed material, ρ_w and ρ_s are the water and sediment density, respectively $m_b = \sqrt{1 + (\partial z_b / \partial x)^2 + (\partial z_b / \partial y)^2}$, q_{t*} is the total load sediment transport capacity and L_t is the saturation length of sediment transport. The models are solved numerically by using the explicit finite volume method with the Godunov-type central upwind scheme and the nonnegative reconstruction of the water depth method. The results of the bed change showed that the erosion occurs at the beach and at the initial stage by the lateral erosion for simulating by without wave and erosion occurring faster by computing the wave.

The various literatures are put together and the appropriate mathematical model for studying sediment transport distribution in Bandon Bay is presented in the next chapter.

Chapter 3

Mathematical Model

This chapter presents the mathematical model and the computational methods that would be used in this study. Some assumptions were made to provide a better explanation of the model used in this study. The Shallow water equations (SWEs) used in the study of Suwannasri (2004) and Boosamun (2010) which was discussed in the previous section was put to use in this research. The idea from conservation of mass of SWEs was applied to the sediment transport equation in this study. Validation of the model will be carried out by comparing with standard Grass model (1981) which was proposed by Castro Diaz, Fernadez-Nieto, Ferreiro and Pares (2009). SWEs, sediment transport, initial & boundary conditions, inflow condition, and numerical method are presented.

Figure 6 shows the work flow of this study whereby the sediment transports is of much interest. The proposed mathematical model is based on SWEs and sediment transport. The SWEs is derived from the conservation of mass and momentum whereby the conservation of momentum consists of 3 forces which are pressure, gravitational and bed friction force. The model is solved numerically by using the finite volume method which is based on the integral form of the conservation laws to get the discretization form. The flux unknowns are solved by using Godunov method. The Godunov method is used to approximate the flux using the HLL approach. The boundary and stability condition are needed to compute the discretization form. The discretization form then is computed by integration in time using Total Variation

Diminishing (TVD) Runge - Kutta and friction force using the semi-implicit method.
By these procedures, the solution will be obtained.
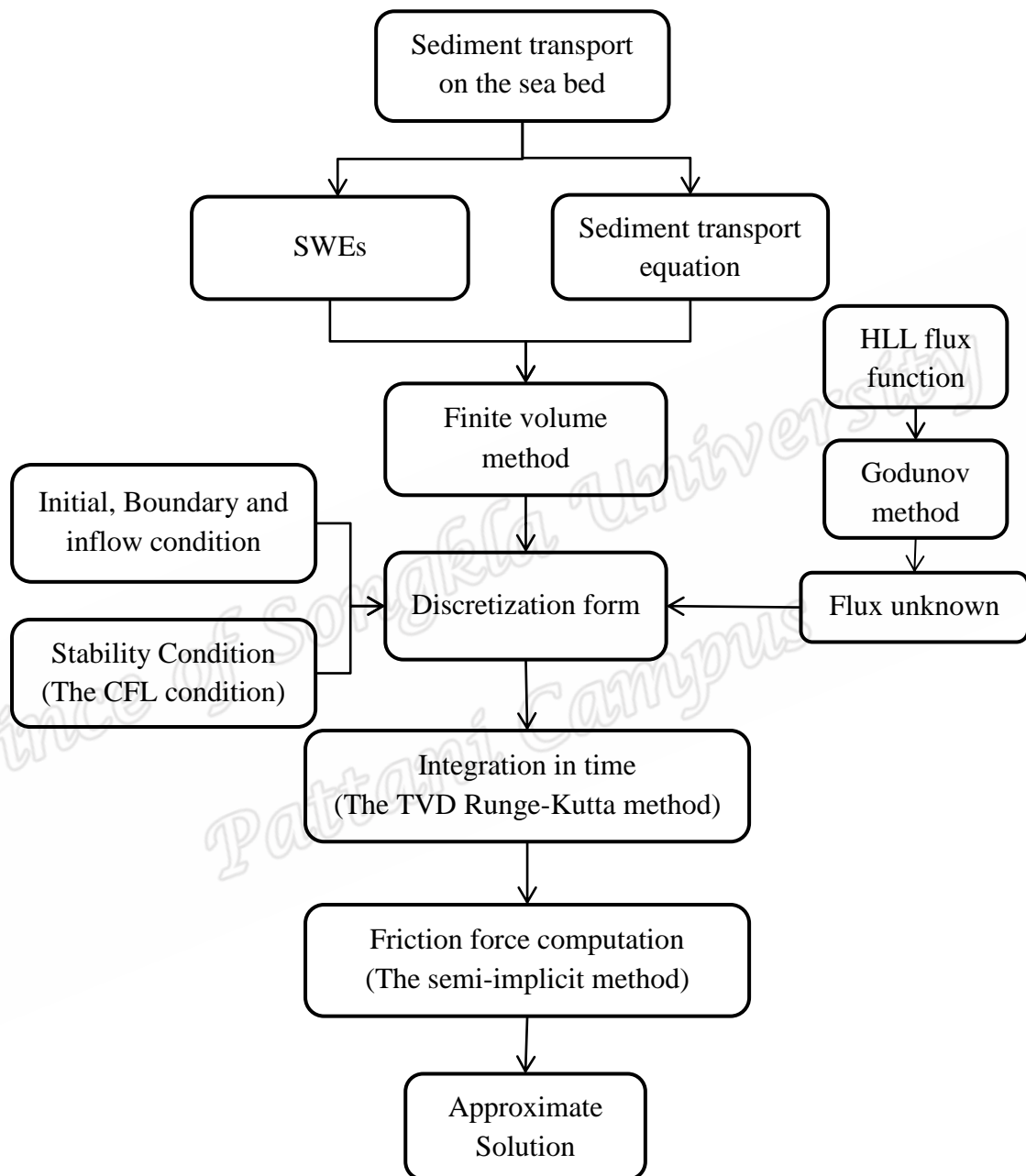
Figure 6 Work flow diagram of sediment transport model

　　　The derivations of the SWEs as well as other mathematical formulations would be discussed in the next section.

3.1 Shallow Water Equations

The Navier – Stoke Equation is useful in simplifying the mathematical formulation of the SWEs. The SWEs are derived based on some basic principles of the laws of conservation of mass and momentum. These are done together with a set of constitutive laws related to fluid properties and motion.

3.1.1 Conservation of Mass

(a)   (b)
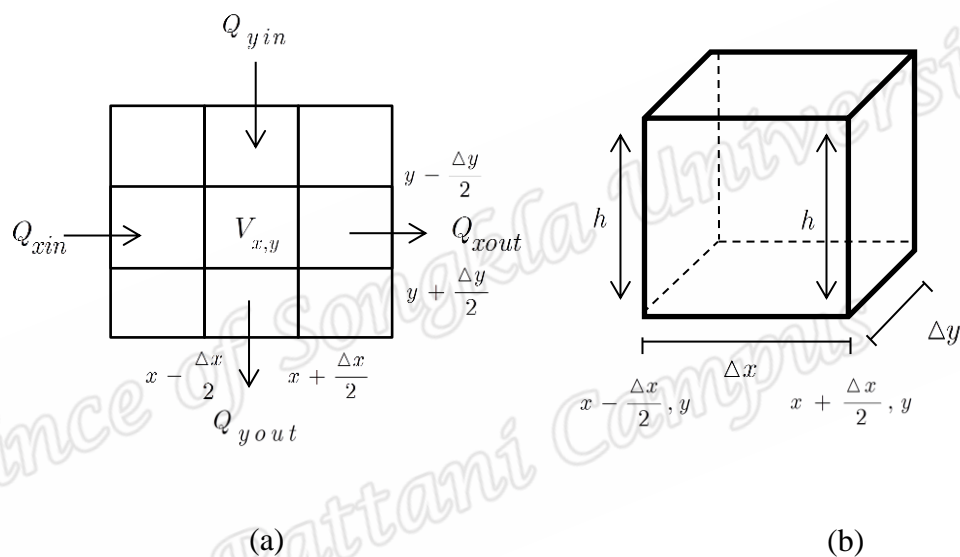
Figure 7 (a) Water direction in grid form and (b) depth of water in the x and y directions

Wave propagation is considered in the x and y directions. In Figure 7(a), the wave moves in the x direction which then moves out in the opposite direction (from left to right). There is another wave moving in the positive y direction which moves out in the negative (opposite) y direction (from top to down). The volume of water at one point can be found by adding the wave coming in the x and y directions and subtracting the wave going out in the opposite directions. In Figure 7(b), the height h (depth of water) is considered and also the distances $\triangle x$ and $\triangle y$ are measured in their respective directions.

From Figure 6 and Figure 7, the rate of change of volume of water at points x and y directions can be written as

$$\frac{\partial V}{\partial t} = Q_{xin} - Q_{xout} + Q_{yin} - Q_{yout}, \tag{3.1}$$

The distance between the grid points in the x and y directions that $\triangle x$ and $\triangle y$ are fixed but the volume of water in the box can change if and only if the depth changes. The corresponding rate of change of water flow ($Q_{in/out}$) can be obtained from multiplying cross-section of the water flow with the velocity of the water and water depth. The volume of the water (V) at points x and y can be obtained from multiplying the water depth with the base area.

This gives

$$\frac{\partial(\triangle x \triangle y h)}{\partial t} = (hu\triangle y)_{xin} - (hu\triangle y)_{xout} + (hv\triangle x)_{yin} - (hv\triangle x)_{yout}, \tag{3.2}$$

where u and v are the velocities of water flow in the x and y directions, respectively, h is the depth of water at points x and y, $\triangle x$ and $\triangle y$ are the length and width of volume control, respectively.

We now divide both sides of the equations by $\triangle x$ and $\triangle y$, since they are constants. This can then be written as

$$\frac{\partial h}{\partial t} = \frac{(uh)_{xin} - (uh)_{xout}}{\triangle x} + \frac{(vh)_{yin} - (vh)_{yout}}{\triangle y},$$

$$\frac{\partial h}{\partial t} = \frac{(uh)_{x-\triangle x/2, y} - (uh)_{x+\triangle x/2, y}}{\triangle x} + \frac{(vh)_{x, y-\triangle y/2} - (vh)_{x, y+\triangle y/2}}{\triangle y}, \tag{3.3}$$

Using the Taylor series expansion and omitting higher order terms in dx and dy, we have

$$(uh)_{x-\Delta x/2,y} = (uh)_{x,y} - \frac{\partial(uh)}{\partial x}\frac{\triangle x}{2} + O(\triangle x^2),$$

$$(uh)_{x+\Delta x/2,y} = (uh)_{x,y} + \frac{\partial(uh)}{\partial x}\frac{\triangle x}{2} + O(\triangle x^2),$$

$$(vh)_{x,y-\Delta y/2} = (vh)_{x,y} - \frac{\partial(vh)}{\partial y}\frac{\triangle y}{2} + O(\triangle y^2),$$

$$(vh)_{x,y+\Delta y/2} = (vh)_{x,y} + \frac{\partial(vh)}{\partial y}\frac{\triangle y}{2} + O(\triangle y^2),$$

$$\tag{3.4}$$

Substituting equation (3.4) in to equation (3.3), we obtain

$$\frac{\partial h}{\partial t} = \frac{\left[(uh)_{x,y} - \frac{\partial(uh)}{\partial x}\frac{\triangle x}{2} + O(\triangle x^2)\right] - \left[(uh)_{x,y} + \frac{\partial(uh)}{\partial x}\frac{\triangle x}{2} + O(\triangle x^2)\right]}{\triangle x}$$

$$+ \frac{\left[(vh)_{x,y} - \frac{\partial(vh)}{\partial y}\frac{\triangle y}{2} + O(\triangle y^2)\right] - \left[(vh)_{x,y} + \frac{\partial(vh)}{\partial y}\frac{\triangle y}{2} + O(\triangle y^2)\right]}{\triangle y}$$

$$= \left[\frac{-\frac{\partial(uh)}{\partial x}\frac{\triangle x}{2} - \frac{\partial(uh)}{\partial x}\frac{\triangle x}{2}}{\triangle x}\right] + \left[\frac{-\frac{\partial(vh)}{\partial y}\frac{\triangle y}{2} - \frac{\partial(vh)}{\partial y}\frac{\triangle y}{2}}{\triangle y}\right]$$

$$= \left[\frac{-2\frac{\partial(uh)}{\partial x}\frac{\triangle x}{2}}{\triangle x}\right] + \left[\frac{-2\frac{\partial(vh)}{\partial y}\frac{\triangle y}{2}}{\triangle y}\right]$$

$$\frac{\partial h}{\partial t} = -\frac{\partial(uh)}{\partial x} - \frac{\partial(vh)}{\partial y}.$$

The conservation of mass equation can then be expressed quantitatively as

$$\frac{\partial h}{\partial t} + \frac{\partial(uh)}{\partial x} + \frac{\partial(vh)}{\partial y} = 0. \tag{3.5}$$

3.1.2 Conservation of Momentum

The Conservation of Momentum is similar to the conservation of mass equation. The depth of water in equation (3.5) h is changed to be the momentum in the control volume (M) and this is equal to the net influx of momentum plus the net force acting on the control volume

$$\frac{\partial M}{\partial t} + \frac{\partial (uM)}{\partial x} + \frac{\partial (vM)}{\partial y} = F. \tag{3.6}$$

where F is the force acting on the control volume.

Since momentum in the control volume is $\rho Q_x \triangle x$ and having ρ as the pressure of water, and Q_x as the rate of flow of water in the x direction.

Then the rate of momentum in the control volume will now be

$$\frac{\partial (\rho Q_x \triangle x)}{\partial t} + \frac{\partial (u\rho Q_x \triangle x)}{\partial x} + \frac{\partial (v\rho Q_x \triangle x)}{\partial y} = F. \tag{3.7}$$

The forces and momentum fluxes on the control volume are in the 3 forms: F_p is the pressure force, F_g is the gravitational force (due to sloping bed) and F_{fx} is the bed friction force.

So then the equation (3.7) can be written as

$$\frac{\partial (\rho Q_x \triangle x)}{\partial t} + \frac{\partial (u\rho Q_x \triangle x)}{\partial x} + \frac{\partial (v\rho Q_x \triangle x)}{\partial y} = F_p + F_g + F_{fx}. \tag{3.8}$$

3.1.2.1 The Pressure Force (F_p)
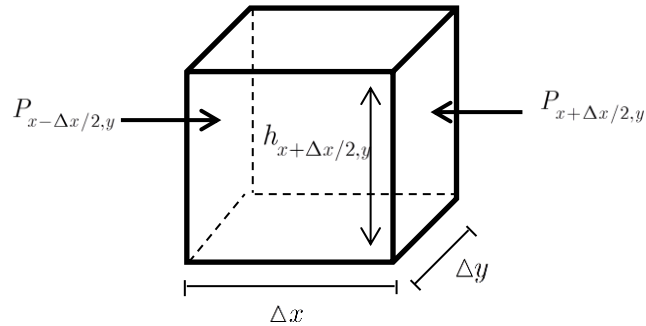
Figure 8 Pressure in fluid in the opposite direction

Consider pressure forces at points x and y in Figure 8. Then

$$F_p = \triangle P = P_{x-\Delta x/2,y} - P_{x+\Delta x/2,y}.$$

From $P = \rho gh$, we get

$$F_p = (\rho gh)_{x-\Delta x/2,y} - (\rho gh)_{x+\Delta x/2,y}. \tag{3.9}$$

Using the Taylor series expansion and omitting higher order terms in $\triangle x$

yields

$$
\left.
\begin{aligned}
(\rho gh)_{x-\Delta x/2,y} &= (\rho gh)_{x,y} - \frac{\partial(\rho gh)}{\partial x}\frac{\triangle x}{2} + O(\triangle x^2), \\
(\rho gh)_{x+\Delta x/2,y} &= (\rho gh)_{x,y} + \frac{\partial(\rho gh)}{\partial x}\frac{\triangle x}{2} + O(\triangle x^2).
\end{aligned}
\right\} \tag{3.10}
$$

Substituting equation (3.10) in to equation (3.9), we obtain

$$
\begin{aligned}
F_p &= \left[(\rho gh)_{x,y} - \frac{\partial(\rho gh)}{\partial x}\frac{\triangle x}{2} + O(\triangle x^2)\right] - \left[(\rho gh)_{x,y} + \frac{\partial(\rho gh)}{\partial x}\frac{\triangle x}{2} + O(\triangle x^2)\right] \\
&= -\frac{\partial(\rho gh)}{\partial x}\frac{\triangle x}{2} - \frac{\partial(\rho gh)}{\partial x}\frac{\triangle x}{2} \\
&= -\triangle x\frac{\partial(\rho gh)}{\partial x}. \tag{3.11}
\end{aligned}
$$

Since, the pressure exerted on the cross sectional area of the water is

$$F_p = -\triangle x \triangle y h \frac{\partial(\rho g h)}{\partial x}. \tag{3.12}$$

3.1.2.2 The Gravitational Force (F_g)
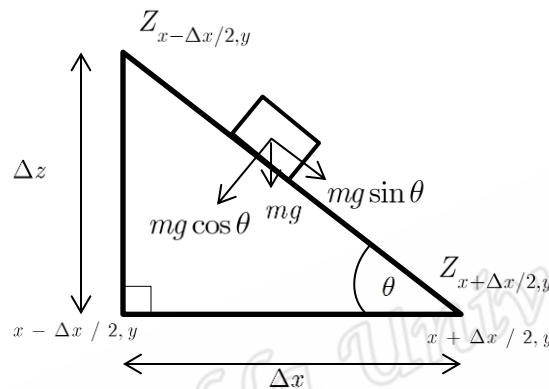
Figure 9 Height of terrain

In Figure 9, we consider a triangle with $\triangle x$ as the length of the slope bed and $\triangle z$ as the height of the slope bed with θ as the angle between the height and length of the slope bed.

The pressure force due to the slope bed is

$$F_g = mg \sin \theta.$$

Since from the Newton law, $m = \rho v$ then

$$F_g = \rho V g \sin \theta = \rho \triangle x \triangle y h g \sin \theta.$$

From Figure 9, the value of $\sin \theta$ is

$$\sin \theta = \frac{\triangle z}{\sqrt{(\triangle x)^2 + (\triangle z)^2}},$$

where z is height of slope bed which can be written as

$$F_g = \rho g \triangle x \triangle y h \frac{\triangle z}{\sqrt{(\triangle x)^2 + (\triangle z)^2}} \,. \tag{3.13}$$

Since $\triangle z = z_{x+\triangle x/2,y} - z_{x-\triangle x/2,y}$ and using the Taylor series expansion and

omitting higher terms in dx of $z_{x+\triangle x/2,y}$ and $z_{x-\triangle x/2,y}$ the equation now becomes

$$\left. \begin{aligned} z_{x+\triangle x/2,y} &= z + \frac{\partial z}{\partial x}\frac{\triangle x}{2} + O(\triangle x^2), \\ z_{x-\triangle x/2,y} &= z - \frac{\partial z}{\partial x}\frac{\triangle x}{2} + O(\triangle x^2). \end{aligned} \right\} \tag{3.14}$$

Substituting equation (3.14) in to equation (3.13), we obtain

$$F_g = \rho g \triangle x \triangle y h \frac{\left[\left(z + \frac{\partial z}{\partial x}\frac{\triangle x}{2} + O(\triangle x^2)\right) - \left(z - \frac{\partial z}{\partial x}\frac{\triangle x}{2} + O(\triangle x^2)\right)\right]}{\sqrt{\triangle x^2 + \left[\left(z + \frac{\partial z}{\partial x}\frac{\triangle x}{2} + O(\triangle x^2)\right) - \left(z - \frac{\partial z}{\partial x}\frac{\triangle x}{2} + O(\triangle x^2)\right)\right]^2}},$$

algebraic cancellation results in,

$$F_g = \rho g \triangle x \triangle y h \frac{\frac{\partial z}{\partial x}\triangle x}{\sqrt{(\triangle x)^2 + \left(\frac{\partial z}{\partial x}\triangle x\right)^2}}$$

$$= \rho g \triangle x \triangle y h \frac{\partial z}{\partial x} \frac{\triangle x}{\sqrt{(\triangle x)^2 + \left(\frac{\partial z}{\partial x}\right)^2 (\triangle x)^2}}$$

$$= \rho g \triangle x \triangle y h \frac{\partial z}{\partial x} \frac{\triangle x}{\sqrt{(\triangle x)^2 \left(1 + \left(\frac{\partial z}{\partial x}\right)^2\right)}}$$

$$F_g = \rho g \triangle x \triangle y h \frac{\partial z}{\partial x} \frac{\triangle x}{\sqrt{(\triangle x)^2} \sqrt{\left(1 + \left(\frac{\partial z}{\partial x}\right)^2\right)}}$$

$$= \rho g \triangle x \triangle y h \frac{\partial z}{\partial x} \frac{\triangle x}{\triangle x \sqrt{\left(1 + \left(\frac{\partial z}{\partial x}\right)^2\right)}}$$

$$= \rho g \triangle x \triangle y h \frac{\partial z}{\partial x} \frac{1}{\sqrt{\left(1 + \left(\frac{\partial z}{\partial x}\right)^2\right)}} \ .$$

Using the polynomial division in $\dfrac{1}{\sqrt{\left(1 + \left(\frac{\partial z}{\partial x}\right)^2\right)}}$, we have

$$\frac{1}{\sqrt{\left(1 + \left(\frac{\partial z}{\partial x}\right)^2\right)}} = \sqrt{1 - \left(\frac{\partial z}{\partial x}\right)^2 + \left(\frac{\partial z}{\partial x}\right)^4 + \dots .}$$

Since the gravitational force due to the slope bed is

$$F_g = \rho g \triangle x \triangle y h \frac{\partial z}{\partial x} \sqrt{1 - \left(\frac{\partial z}{\partial x}\right)^2 + \left(\frac{\partial z}{\partial x}\right)^4 + \dots}$$

$$= \rho g \triangle x \triangle y h \sqrt{\left(\frac{\partial z}{\partial x}\right)^2 - \left(\frac{\partial z}{\partial x}\right)^4 + \dots}$$

$$= \rho g \triangle x \triangle y h \sqrt{\left(\frac{\partial z}{\partial x}\right)^2 + O\left(\left(\frac{\partial z}{\partial x}\right)^4\right)}$$

$$F_g = \rho g \triangle x \triangle y h \frac{\partial z}{\partial x} \ . \tag{3.15}$$

3.1.2.3 The Bed Friction Force (F_{fx} and F_{fy})

The bed function can be estimated by using the Manning resistance law as

$$S_{fx} = \frac{\left(n^2\sqrt{u^2 + v^2}\right)u}{h^{4/3}} \text{ and } S_{fy} = \frac{\left(n^2\sqrt{u^2 + v^2}\right)v}{h^{4/3}}.$$

So, the resisting force at the bottom becomes

$$F_{fx} = -\rho g V S_{fx}$$

$$= -\rho g \triangle x \triangle y h S_{fx}$$

$$F_{fx} = -\rho g \triangle x \triangle y h \frac{n^2\sqrt{u^2 + v^2}u}{h^{4/3}}. \tag{3.16}$$

Equating terms, the conservation of momentum is obtained by substituting equations (3.12), (3.15) and (3.16) in equation (3.8) to get

$$\frac{\partial(\rho Q_x \triangle x)}{\partial t} + \frac{\partial(u\rho Q_x \triangle x)}{\partial x} + \frac{\partial(v\rho Q_x \triangle x)}{\partial y} = -\triangle x \triangle y h \frac{\partial(\rho g h)}{\partial x} + \rho g \triangle x \triangle y h \frac{\partial z}{\partial x}$$

$$-\rho g \triangle x \triangle y h \frac{n^2\sqrt{u^2 + v^2}u}{h^{4/3}}. \tag{3.17}$$

$$\frac{\partial(\rho Q_x \triangle x)}{\partial t} + \frac{\partial(u\rho Q_x \triangle x)}{\partial x} + \frac{\partial(v\rho Q_x \triangle x)}{\partial y} = \rho \triangle x \triangle y \left[-g \frac{\partial(h)}{\partial x} h + g h \frac{\partial z}{\partial x} - g \frac{n^2\sqrt{u^2 + v^2}uh}{h^{4/3}} \right].$$

Since $\rho \triangle x \triangle y$ is constant, we divide by $\rho \triangle x \triangle y$ on both sides of equation (3.17)

$$\frac{1}{\rho \triangle x \triangle y h} \frac{\partial(\rho Q_x \triangle x)}{\partial t} + \frac{1}{\rho \triangle x \triangle y h} \frac{\partial(u\rho Q_x \triangle x)}{\partial x} + \frac{1}{\rho \triangle x \triangle y h} \frac{\partial(v\rho Q_x \triangle x)}{\partial y} = -g \frac{\partial(h)}{\partial x} h + g h \frac{\partial z}{\partial x}$$

$$-g \frac{n^2\sqrt{u^2 + v^2}uh}{h^{4/3}}$$

$$\frac{1}{\triangle y}\frac{\partial Q_x}{\partial t}+\frac{1}{\triangle y}\frac{\partial uQ_x}{\partial x}+\frac{1}{\triangle y}\frac{\partial vQ_x}{\partial y}=-g\frac{\partial h}{\partial x}h+gh\frac{\partial z}{\partial x}-g\frac{n^2\sqrt{u^2+v^2}\,uh}{h^{4/3}}$$

$$\frac{1}{\triangle y}\frac{\partial(hu\triangle y)}{\partial t}+\frac{1}{\triangle y}\frac{\partial u(hu\triangle y)}{\partial x}+\frac{1}{\triangle y}\frac{\partial v(hu\triangle y)}{\partial y}=-g\frac{\partial h^2}{\partial x}+gh\frac{\partial z}{\partial x}-g\frac{n^2\sqrt{u^2+v^2}\,uh}{h^{4/3}}$$

$$\frac{\partial uh}{\partial t}+\frac{\partial u^2h}{\partial x}+\frac{g}{2}\frac{\partial h^2}{\partial x}+\frac{\partial vuh}{\partial y}=gh\frac{\partial z}{\partial x}-g\frac{n^2\sqrt{u^2+v^2}\,uh}{h^{4/3}}$$

$$\frac{\partial uh}{\partial t}+\frac{\partial u^2h}{\partial x}+\frac{g}{2}\frac{\partial h^2}{\partial x}+\frac{\partial vuh}{\partial y}=gh\frac{\partial z}{\partial x}-g\frac{n^2\sqrt{u^2+v^2}\,uh}{h^{4/3}} \qquad (3.18)$$

where $\dfrac{g}{2}\dfrac{\partial h^2}{\partial x}=\dfrac{g}{2}2h\dfrac{\partial h}{\partial x}=g\dfrac{\partial h}{\partial x}h$.

Similarly, the momentum gives

$$\frac{\partial vh}{\partial t}+\frac{\partial vuh}{\partial x}+\frac{\partial v^2h}{\partial y}+\frac{g}{2}\frac{\partial h^2}{\partial y}=gh\frac{\partial z}{\partial y}-g\frac{n^2\sqrt{u^2+v^2}\,vh}{h^{4/3}} . \qquad (3.19)$$

Equations (3.5), (3.18) and (3.19) are called the two-dimensional SWEs which are stated as follows

$$\frac{\partial h}{\partial t}+\frac{\partial(uh)}{\partial x}+\frac{\partial(vh)}{\partial y}=0,$$

$$\frac{\partial uh}{\partial t}+\frac{\partial u^2h}{\partial x}+\frac{g}{2}\frac{\partial h^2}{\partial x}+\frac{\partial vuh}{\partial y}=gh\frac{\partial z}{\partial x}-g\frac{n^2\sqrt{u^2+v^2}\,uh}{h^{4/3}},$$

$$\frac{\partial vh}{\partial t}+\frac{\partial vuh}{\partial x}+\frac{\partial v^2h}{\partial y}+\frac{g}{2}\frac{\partial h^2}{\partial y}=gh\frac{\partial z}{\partial y}-g\frac{n^2\sqrt{u^2+v^2}\,vh}{h^{4/3}},$$

$$(3.20)$$

where g is the acceleration due to gravity, $h(x,y,t)$ is the water depth, $u(x,y,t)$ and $v(x,y,t)$ are the flow velocities in the x and y directions, respectively, $z(x,y,t)$ is the height of slope bed and n is the Manning roughness coefficient.

In our attempt to simulate the wave moment in shallow water these three coupled partial differential equations have been derived to enable the visualization of sediment distribution in the studied area.

3.2 Sediment Transport Equations

In this section, we present the sediment transport model and the Grass Model. The sediment transport is obtained by using the idea from water flow in conservation of mass equation. Since the flow of water and sediment are different, the parameter porosity of sediment denoted with ρ is used to multiply with the flow of sediment as shown in equation (3.21). The porosity of sediment is the empty space in a material as shown in Figure 10

<div align="center">(a)   (b)</div>
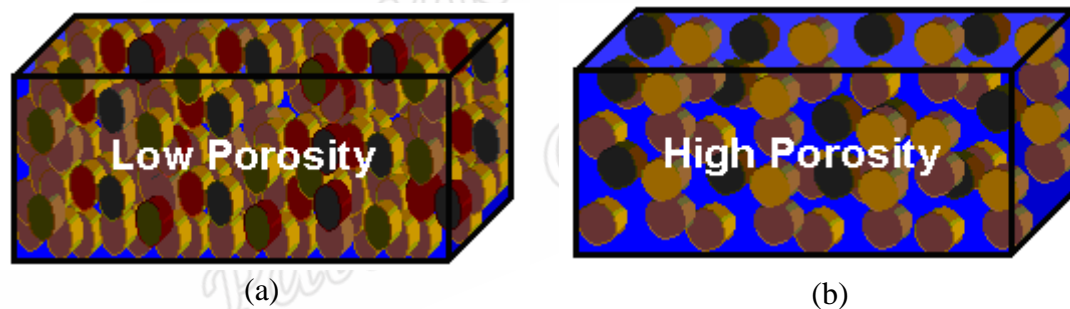
Figure 10 porosity of sediment

Source: Blaskó Lajos (2008)

The porosity of sediment takes a value between 0 to 1. If the value close to 0, then the sediment is said to be fine however, if value close to 1 rough sediment is obtained as described in Figure 10(a) and Figure 10(b), respectively. The Grass model (Grass, 1981) is shown in equation (3.22). The validation of one dimension sediment transport model proposed in this study can be confirmed by comparing with the Grass model. In this study, The Grass model was chosen to compare with the sediment

transport model because the Grass model is efficient in sandy areas and it's similar with our study area.

The sediment transport and the Grass model equation are as follow

$$\frac{\partial z}{\partial t} + \rho_x \frac{\partial uz}{\partial x} = 0 \,, \tag{3.21}$$

$$\frac{\partial z}{\partial t} + \xi \frac{\partial q_{bx}}{\partial x} = 0, \tag{3.22}$$

where $\xi = \dfrac{1}{1 - \rho_x}$ and ρ_x is the porosity of the sediment layer, u represents the velocity in the x direction and $z(x,t)$ is the height of slope bed.

Following the Grass model (Grass, 1981), the formula for the solid transport discharge is given by

$$q_{bx} = A_g u \left| u \right|^{mg-1} ; 1 \le m_g \le 4 \,,$$

where A_g is the constant determined from the experimental data. This constant value is between 0 and 1 according to Grass model, the bed-load sediment transport begins as soon as the fluid starts to move.

This study focuses on a two dimensional sediment transport model by using conservation of mass equation from the SWEs in equation (3.23).

$$\frac{\partial z}{\partial t} + \rho_x \frac{\partial uz}{\partial x} + \rho_y \frac{\partial vz}{\partial y} = 0 \,, \tag{3.23}$$

Where ρ_x and ρ_y represent the porosity of the sediment in the x and y directions, $u(x,y,t)$ and $v(x,y,t)$ represent the velocities in the x and y directions and $z(x,y,t)$ is the height of slope bed.

Finally, the SWEs and the sediment transport equations used in this study are put together as follows

$$
\left.
\begin{array}{c}
\dfrac{\partial h}{\partial t} + \dfrac{\partial (uh)}{\partial x} + \dfrac{\partial (vh)}{\partial y} = 0, \\[2ex]
\dfrac{\partial uh}{\partial t} + \dfrac{\partial u^2 h}{\partial x} + \dfrac{g}{2}\dfrac{\partial h^2}{\partial x} + \dfrac{\partial vuh}{\partial y} = gh\dfrac{\partial z}{\partial x} - g\dfrac{n^2\sqrt{u^2+v^2}\,uh}{h^{4/3}}, \\[3ex]
\dfrac{\partial vh}{\partial t} + \dfrac{\partial vuh}{\partial x} + \dfrac{\partial v^2 h}{\partial y} + \dfrac{g}{2}\dfrac{\partial h^2}{\partial y} = gh\dfrac{\partial z}{\partial y} - g\dfrac{n^2\sqrt{u^2+v^2}\,vh}{h^{4/3}}, \\[3ex]
\dfrac{\partial z}{\partial t} + \rho_x\dfrac{\partial uz}{\partial x} + \rho_y\dfrac{\partial vz}{\partial y} = 0,
\end{array}
\right\}
\qquad (3.24)
$$

with the initial condition given as follows:

$$
h(x,y,0) = h_0, \qquad u(x,y,0) = u_0, \qquad v(x,y,0) = v_0, \qquad z(x,y,0) = z_0,
$$

For the boundary condition, it is considered to be open and closed boundary which are defined from the Figure 11(a) and Figure 11(b), respectively.

Figure 11 (a) Open and (b) closed boundary condition

From Figure 11(a), open boundary can be defined as

$$\frac{\partial h}{\partial \vec{n}} = 0\,, \qquad \frac{\partial u}{\partial \vec{n}} = 0\,, \qquad \frac{\partial v}{\partial \vec{n}} = 0\,, \qquad \frac{\partial z}{\partial \vec{n}} = 0\,, \qquad \forall (x,y) \in \partial\Omega$$

and closed boundary from Figure 11(b) for (i), (ii), (iii) and (iv) as;

$$h(x,0,t) = 0\,, \qquad u(x,0,t) = 0\,, \qquad v(x,0,t) = 0\,, \qquad z(x,0,t) = z_{l\arg e}\,,$$

$$h(m_x - 1, y, t) = 0\,, \quad u(m_x - 1, y, t) = 0\,, \quad v(m_x - 1, y, t) = 0\,, \quad z(m_x - 1, y, t) = z_{l\arg e}\,,$$

$$h(x, m_y - 1, t) = 0\,, \quad u(x, m_y - 1, t) = 0\,, \quad v(x, m_y - 1, t) = 0\,, \quad z(x, m_y - 1, t) = z_{l\arg e}\,,$$

$$h(0,j,t) = 0\,, \qquad u(0,j,t) = 0\,, \qquad v(0,j,t) = 0\,, \qquad z(0,j,t) = z_{l\arg e}\,,$$

where h_0, u_0, v_0 and z_0 are the height of wave, velocities of water flow in the x direction, velocities of water flow in the y direction and height of sediment, respectively at time $t=0$. They are input from the user, $\vec{n}$ is the normal vector on the boundary $\partial\Omega$ and $z_{l\arg e}$ is the large value for height of topography data.

In this study, the SWEs and the sediment transport equations would be considered with some assumptions:

1. In the real world, the ocean is spherical however for this study it is assumed that the ocean is plain.

2. The erosion is not considered.

3. The sediment along the sea bed is considered homogenous.

4. The emission of wave is continuous.

From equation (3.24) the value of z in the $\frac{\partial z}{\partial t}$ term would be calculated at each time step when the time changes. That is, in simulating the wave from the SWEs, the height of the sediment changes and this can be known or calculated at each time

step. The value of the sediment transport in the shallow water can be approximated by using the finite volume methods.

Equation (3.24) can be written in the matrix form as

$$\frac{\partial \vec{w}}{\partial t} + \frac{\partial f(\vec{w})}{\partial x} + \frac{\partial g(\vec{w})}{\partial y} = \vec{z} + \vec{s}\,, \tag{3.25}$$

where $\vec{w} = \begin{bmatrix} h \\ uh \\ vh \\ z \end{bmatrix}$, $f(\vec{w}) = \begin{bmatrix} uh \\ u^2h + g\dfrac{h^2}{2} \\ uvh \\ \rho_x uz \end{bmatrix}$, $g(\vec{w}) = \begin{bmatrix} vh \\ vuh \\ v^2h + g\dfrac{h^2}{2} \\ \rho_y vz \end{bmatrix}$, $\vec{z} = \begin{bmatrix} 0 \\ gh\dfrac{\partial z}{\partial x} \\ gh\dfrac{\partial z}{\partial y} \\ 0 \end{bmatrix}$ and

$$\vec{s} = \begin{bmatrix} 0 \\ -\dfrac{gn^2\sqrt{u^2 + v^2}\,uh}{h^{4/3}} \\ -\dfrac{gn^2\sqrt{u^2 + v^2}\,vh}{h^{4/3}} \\ 0 \end{bmatrix}.$$

These equations can be written in the quasi linear form as

$$\frac{\partial \vec{w}}{\partial t} + \frac{\partial f(\vec{w})}{\partial \vec{w}}\frac{\partial \vec{w}}{\partial x} + \frac{\partial g(\vec{w})}{\partial \vec{w}}\frac{\partial \vec{w}}{\partial y} = \vec{z} + \vec{s}\,. \tag{3.26}$$

It is essential to note that the term $u(x,y,t)\cdot h(x,y,t) = uh(x,y,t)$ and $v(x,y,t)\cdot h(x,y,t) = vh(x,y,t)$. However, to find the Jacobian matrix only, we have to consider $uh(x,y,t)$ and $vh(x,y,t)$ to be one variable as they cannot be separated.

The Jacobian matrix of $\dfrac{\partial f(\vec{w})}{\partial \vec{w}}$ and $\dfrac{\partial g(\vec{w})}{\partial \vec{w}}$ are

$$\frac{\partial f(\vec{w})}{\partial \vec{w}} = \begin{bmatrix} \dfrac{\partial uh}{\partial h} & \dfrac{\partial uh}{\partial uh} & \dfrac{\partial uh}{\partial vh} & \dfrac{\partial uh}{\partial z} \\[2mm] \dfrac{\partial\left(\dfrac{(uh)^2}{h}+\frac{1}{2}gh^2\right)}{\partial h} & \dfrac{\partial\left(\dfrac{(uh)^2}{h}+\frac{1}{2}gh^2\right)}{\partial uh} & \dfrac{\partial\left(\dfrac{(uh)^2}{h}+\frac{1}{2}gh^2\right)}{\partial vh} & \dfrac{\partial\left(\dfrac{(uh)^2}{h}+\frac{1}{2}gh^2\right)}{\partial z} \\[2mm] \dfrac{\partial\dfrac{uhvh}{h}}{\partial h} & \dfrac{\partial\dfrac{uhvh}{h}}{\partial uh} & \dfrac{\partial\dfrac{uhvh}{h}}{\partial vh} & \dfrac{\partial\dfrac{uhvh}{h}}{\partial z} \\[2mm] \dfrac{\partial\dfrac{\rho_x uhz}{h}}{\partial h} & \dfrac{\partial\dfrac{\rho_x uhz}{h}}{\partial uh} & \dfrac{\partial\dfrac{\rho_x uhz}{h}}{\partial vh} & \dfrac{\partial\dfrac{\rho_x uhz}{h}}{\partial z} \end{bmatrix}$$

$$= \begin{bmatrix} 0 & 1 & 0 & 0 \\ -u^2+gh & 2u & 0 & 0 \\ -uv & v & u & 0 \\ \dfrac{-\rho_x uz}{h} & \dfrac{\rho_x z}{h} & 0 & \dfrac{\rho_x uh}{h} \end{bmatrix}$$

and

$$\frac{\partial g(\vec{w})}{\partial \vec{w}} = \begin{bmatrix} \dfrac{\partial vh}{\partial h} & \dfrac{\partial vh}{\partial uh} & \dfrac{\partial vh}{\partial vh} & \dfrac{\partial vh}{\partial z} \\[2mm] \dfrac{\partial\dfrac{vhuh}{h}}{\partial h} & \dfrac{\partial\dfrac{vhuh}{h}}{\partial uh} & \dfrac{\partial\dfrac{vhuh}{h}}{\partial vh} & \dfrac{\partial\dfrac{vhuh}{h}}{\partial z} \\[2mm] \dfrac{\partial\left(\dfrac{(vh)^2}{h}+\frac{1}{2}gh^2\right)}{\partial h} & \dfrac{\partial\left(\dfrac{(vh)^2}{h}+\frac{1}{2}gh^2\right)}{\partial uh} & \dfrac{\partial\left(\dfrac{(vh)^2}{h}+\frac{1}{2}gh^2\right)}{\partial vh} & \dfrac{\partial\left(\dfrac{(vh)^2}{h}+\frac{1}{2}gh^2\right)}{\partial z} \\[2mm] \dfrac{\partial\dfrac{\rho_x vhz}{h}}{\partial h} & \dfrac{\partial\dfrac{\rho_x vhz}{h}}{\partial uh} & \dfrac{\partial\dfrac{\rho_x vhz}{h}}{\partial vh} & \dfrac{\partial\dfrac{\rho_x vhz}{h}}{\partial z} \end{bmatrix}$$

$$= \begin{bmatrix} 0 & 0 & 1 & 0 \\ -uv & v & u & 0 \\ -v^2+gh & 0 & 2v & 0 \\ \dfrac{-\rho_x vz}{h} & 0 & \dfrac{\rho_x z}{h} & \rho_x v \end{bmatrix}.$$

The characteristic polynomial equation of the given matrix $\dfrac{\partial f(\vec{w})}{\partial \vec{w}}$ can be defined by

$$\det\left(\frac{\partial f(\vec{w})}{\partial \vec{w}} - \lambda I\right) = 0\,,$$

$$\det\left(\frac{\partial f(\vec{w})}{\partial \vec{w}} - \lambda I\right) = \begin{vmatrix} -\lambda & 1 & 0 & 0 \\ -u^2 + gh & 2u - \lambda & 0 & 0 \\ -uv & v & u - \lambda & 0 \\ \dfrac{-\rho_x uz}{h} & \dfrac{\rho_x z}{h} & 0 & \rho_x u - \lambda \end{vmatrix} = 0\,.$$

Finally, we have the characteristic polynomial equation

$$\lambda^4 + (-u\rho_x - 3u)\lambda^3 + (3u^2\rho_x + 3u^2 - gh)\lambda^2 + (-3u^3\rho_x + ghu\rho_x - u^3 + ghu)\lambda$$

$$-\rho_x u^2(-u^2 + gh) = 0\,.$$

It can be rewritten as

$$-\lambda(2u - \lambda)(u - \lambda)(\rho_x u - \lambda) - (-u^2 + gh)(u - \lambda)(\rho_x u - \lambda) = 0\,.$$

So, the eigenvalues of $\dfrac{\partial f(\vec{w})}{\partial \vec{w}}$ are the roots of the characteristic polynomial,

$$\lambda_{x_1} = u - \sqrt{gh}\,,\ \lambda_{x_2} = u\,,\ \lambda_{x_3} = u + \sqrt{gh}\,,\ \lambda_{x_4} = \rho_x u\,.$$

Similarly, the eigenvalues of $\dfrac{\partial g(\vec{w})}{\partial \vec{w}}$ are

$$\lambda_{x_1} = v - \sqrt{gh}\,,\ \lambda_{x_2} = v\,,\ \lambda_{x_3} = v + \sqrt{gh}\,,\ \lambda_{x_4} = \rho_y v\,.$$

The eigenvalues of $\dfrac{\partial f(\vec{w})}{\partial \vec{w}}$ and $\dfrac{\partial g(\vec{w})}{\partial \vec{w}}$ will be used to compute the speed of the wave for simulating and visualizing the sediment transport in shallow water.

3.3 Numerical Methods

The numerical solution to the proposed mathematical model is obtained by using the finite volume methods. This is done on the basis of the integral form of the conservation laws by approximating laws of conservation directly once formulated and it is therefore considered a flux conserving method by construction. The calculations are based on the approximation to the integral of certain quantities over each of the volumes. Furthermore it is more effective than the finite element method in which the incorporation of topological laws and time dependent problem is more complex. The finite volume method is also considered to be better than the finite difference method as the finite difference method is limited to structured grids and cell complexity. In deriving the two-dimensional conservation laws, the numerical domain is subdivided into rectangular grid cells ($C_{i,j}$).

Integrating equation (3.25) over each grid cell, gives

$$\frac{\partial}{\partial t}\iint\limits_{C_{i,j}} \vec{w}dxdy + \iint\limits_{C_{i,j}}\frac{\partial f(\vec{w})}{\partial x}dxdy + \iint\limits_{C_{i,j}}\frac{\partial g(\vec{w})}{\partial y}dxdy = \iint\limits_{C_{i,j}}(\vec{z}+\vec{s})dxdy \,,$$

$$\frac{\partial}{\partial t}\iint\limits_{C_{i,j}} \vec{w}dxdy + \int_{j-\frac{1}{2}}^{j+\frac{1}{2}} f(\vec{w})\Big|_{i-\frac{1}{2}}^{i+\frac{1}{2}}dy + \int_{i-\frac{1}{2}}^{i+\frac{1}{2}} g(\vec{w})\Big|_{j-\frac{1}{2}}^{j+\frac{1}{2}}dx = \iint\limits_{C_{i,j}}(\vec{z}+\vec{s})dxdy \,.$$

Integrating from t_n to t_{n+1} yields the following equations

$$\iint\limits_{C_{i,j}} \vec{w}\Big|_n^{n+1} dxdy + \int_n^{n+1}\int_{j-\frac{1}{2}}^{j+\frac{1}{2}} f(\vec{w})\Big|_{i-\frac{1}{2}}^{i+\frac{1}{2}}dydt + \int_n^{n+1}\int_{i-\frac{1}{2}}^{i+\frac{1}{2}} g(\vec{w})\Big|_{j-\frac{1}{2}}^{j+\frac{1}{2}}dxdt =$$

$$\int_n^{n+1}\iint\limits_{C_{i,j}}(\vec{z}+\vec{s})dxdydt \,,$$

$$\left[\iint\limits_{C_{i,j}} \vec{w}^{n+1}dxdy - \iint\limits_{C_{i,j}} \vec{w}^{n}dxdy\right] + \left[\int_n^{n+1}\int_{j-\frac{1}{2}}^{j+\frac{1}{2}} f(\vec{w}_{i+\frac{1}{2}})dydt - \int_n^{n+1}\int_{j-\frac{1}{2}}^{j+\frac{1}{2}} f(\vec{w}_{i-\frac{1}{2}})dydt\right]$$

$$+\left[\int_n^{n+1}\int_{i-\frac{1}{2}}^{i+\frac{1}{2}} g(\vec{w}_{j+\frac{1}{2}})dxdt - \int_n^{n+1}\int_{i-\frac{1}{2}}^{i+\frac{1}{2}} g(\vec{w}_{j-\frac{1}{2}})dxdt\right] = \int_n^{n+1}\iint\limits_{C_{i,j}} \vec{z}\,dxdydt + \int_n^{n+1}\iint\limits_{C_{i,j}} \vec{s}\,dxdydt,$$

$$\iint\limits_{C_{i,j}} \vec{w}^{n+1}dxdy - \iint\limits_{C_{i,j}} \vec{w}^{n}dxdy = -\left[\int_n^{n+1}\int_{j-\frac{1}{2}}^{j+\frac{1}{2}} f(\vec{w}_{i+\frac{1}{2}})dydt - \int_n^{n+1}\int_{j-\frac{1}{2}}^{j+\frac{1}{2}} f(\vec{w}_{i-\frac{1}{2}})dydt\right]$$

$$-\left[\int_n^{n+1}\int_{i-\frac{1}{2}}^{i+\frac{1}{2}} g(\vec{w}_{j+\frac{1}{2}})dxdt - \int_n^{n+1}\int_{i-\frac{1}{2}}^{i+\frac{1}{2}} g(\vec{w}_{j-\frac{1}{2}})dxdt\right]$$

$$+\int_n^{n+1}\iint\limits_{C_{i,j}} \vec{z}\,dxdydt + \int_n^{n+1}\iint\limits_{C_{i,j}} \vec{s}\,dxdydt,$$

$$\iint\limits_{C_{i,j}} \vec{w}^{n+1}dxdy = \iint\limits_{C_{i,j}} \vec{w}^{n}dxdy - \left[\int_n^{n+1}\int_{j-\frac{1}{2}}^{j+\frac{1}{2}} f(\vec{w}_{i+\frac{1}{2}})dydt - \int_n^{n+1}\int_{j-\frac{1}{2}}^{j+\frac{1}{2}} f(\vec{w}_{i-\frac{1}{2}})dydt\right]$$

$$-\left[\int_n^{n+1}\int_{i-\frac{1}{2}}^{i+\frac{1}{2}} g(\vec{w}_{j+\frac{1}{2}})dxdt - \int_n^{n+1}\int_{i-\frac{1}{2}}^{i+\frac{1}{2}} g(\vec{w}_{j-\frac{1}{2}})dxdt\right]$$

$$+\int_n^{n+1}\iint\limits_{C_{i,j}} \vec{z}\,dxdydt + \int_n^{n+1}\iint\limits_{C_{i,j}} \vec{s}\,dxdydt\,.$$

Dividing by $\triangle x\triangle y$, we obtain

$$\frac{1}{\triangle x\triangle y}\iint\limits_{C_{i,j}} \vec{w}^{n+1}dxdy = \frac{1}{\triangle x\triangle y}\iint\limits_{C_{i,j}} \vec{w}^{n}dxdy$$

$$-\frac{1}{\triangle x\triangle y}\left[\int_n^{n+1}\int_{j-\frac{1}{2}}^{j+\frac{1}{2}} f(\vec{w}_{i+\frac{1}{2}})dydt - \int_n^{n+1}\int_{j-\frac{1}{2}}^{j+\frac{1}{2}} f(\vec{w}_{i-\frac{1}{2}})dydt\right]$$

$$-\frac{1}{\triangle x\triangle y}\left[\int_n^{n+1}\int_{i-\frac{1}{2}}^{i+\frac{1}{2}} g(\vec{w}_{j+\frac{1}{2}})dxdt - \int_n^{n+1}\int_{i-\frac{1}{2}}^{i+\frac{1}{2}} g(\vec{w}_{j-\frac{1}{2}})dxdt\right]$$

$$+\frac{1}{\triangle x\triangle y}\int_n^{n+1}\iint\limits_{C_{i,j}} \vec{z}\,dxdydt + \frac{1}{\triangle x\triangle y}\int_n^{n+1}\iint\limits_{C_{i,j}} \vec{s}\,dxdydt\,.$$

Introducing $\triangle t$ into the equation above, we obtain the following equation

$$\frac{1}{\triangle x \triangle y}\iint\limits_{C_{i,j}} \vec{w}^{n+1}dxdy = \frac{1}{\triangle x \triangle y}\iint\limits_{C_{i,j}} \vec{w}^{n}dxdy$$

$$-\frac{\triangle t}{\triangle x}\left[\frac{1}{\triangle y \triangle t}\int_{n}^{n+1}\int_{j-\frac{1}{2}}^{j+\frac{1}{2}} f(\vec{w}_{i+\frac{1}{2}})dydt - \frac{1}{\triangle y \triangle t}\int_{n}^{n+1}\int_{j-\frac{1}{2}}^{j+\frac{1}{2}} f(\vec{w}_{i-\frac{1}{2}})dydt\right]$$

$$-\frac{\triangle t}{\triangle y}\left[\frac{1}{\triangle x \triangle t}\int_{n}^{n+1}\int_{i-\frac{1}{2}}^{i+\frac{1}{2}} g(\vec{w}_{j+\frac{1}{2}})dxdt - \frac{1}{\triangle x \triangle t}\int_{n}^{n+1}\int_{i-\frac{1}{2}}^{i+\frac{1}{2}} g(\vec{w}_{j-\frac{1}{2}})dxdt\right]$$

$$+\triangle t\left[\frac{1}{\triangle t\triangle x \triangle y}\int_{n}^{n+1}\iint\limits_{C_{i,j}} \vec{z}dxdydt + \frac{1}{\triangle t\triangle x \triangle y}\int_{n}^{n+1}\iint\limits_{C_{i,j}} \vec{s}dxdydt\right].$$

The above equation can be rewritten in the vector form as follows

$$\vec{W}_{i,j}^{n+1} = \vec{W}_{i,j}^{n} - \frac{\triangle t}{\triangle x}\left[\vec{F}_{i+\frac{1}{2},j}^{n} - \vec{F}_{i-\frac{1}{2},j}^{n}\right] - \frac{\triangle t}{\triangle y}\left[\vec{G}_{i,j+\frac{1}{2}}^{n} - \vec{G}_{i,j-\frac{1}{2}}^{n}\right] + \triangle t\vec{Z}_{i,j}^{n} + \triangle t\vec{S}_{i,j}^{n}, \quad (3.27)$$

where $\vec{W}_{i,j}^{n}$ represents a cell average over the (i,j) grid cell at time t_{n},

$$\vec{W}_{i,j}^{n} \approx \iint\limits_{C_{i,j}} \vec{W}(x,y,t)dxdy,$$

$\vec{F}_{i-\frac{1}{2},j}^{n}$ is the approximation of the average flux along $x = x_{i-\frac{1}{2},j}$,

$$\vec{F}_{i-\frac{1}{2},j}^{n} \approx \frac{1}{\triangle t\triangle y}\int_{n}^{n+1}\int_{j-\frac{1}{2}}^{j+\frac{1}{2}} f(\vec{w}(x_{i-\frac{1}{2}},y,t))dydt,$$

$\vec{G}_{i,j-\frac{1}{2}}^{n}$ is the approximation of the average flux along $y = y_{i,j-\frac{1}{2}}$,

$$\vec{G}_{i-\frac{1}{2},j}^{n} \approx \frac{1}{\triangle t\triangle x}\int_{n}^{n+1}\int_{i-\frac{1}{2}}^{i+\frac{1}{2}} g(\vec{w}(x,y_{i-\frac{1}{2}},t))dxdt,$$

$\vec{Z}_{i,j}^{n}$ is the gravitational force vector,

$$\vec{Z}_{i,j}^{n} \approx \frac{1}{\triangle t \triangle x \triangle y} \int_{n}^{n+1} \iint_{C_{i,j}} \vec{z} dx dy dt \, ,$$

$\vec{S}_{i,j}^{n}$ is the source term vector,

$$\vec{S}_{i,j}^{n} \approx \frac{1}{\triangle t \triangle x \triangle y} \int_{n}^{n+1} \iint_{C_{i,j}} \vec{s} dx dy dt \, .$$

Equation (3.27) will be used to compute the numerical solutions, but they are four unknown value at points $(i-1/2, j)$, $(i+1/2, j)$, $(i, j-1/2)$ and $(i, j+1/2)$. So, we have to approximate the flux at each point.

3.3.1 Flux Calculation

The equation (3.27) cannot be solved numerically by substituting the values directly. The flux functions $F_{i-1/2, j}$, $F_{i+1/2, j}$, $G_{i, j-1/2}$ and $G_{i, j+1/2}$ can be approximated at each cell point. The Figure 11 describes the flux functions and shows how the Godunov Scheme can be applied to approximate the functions
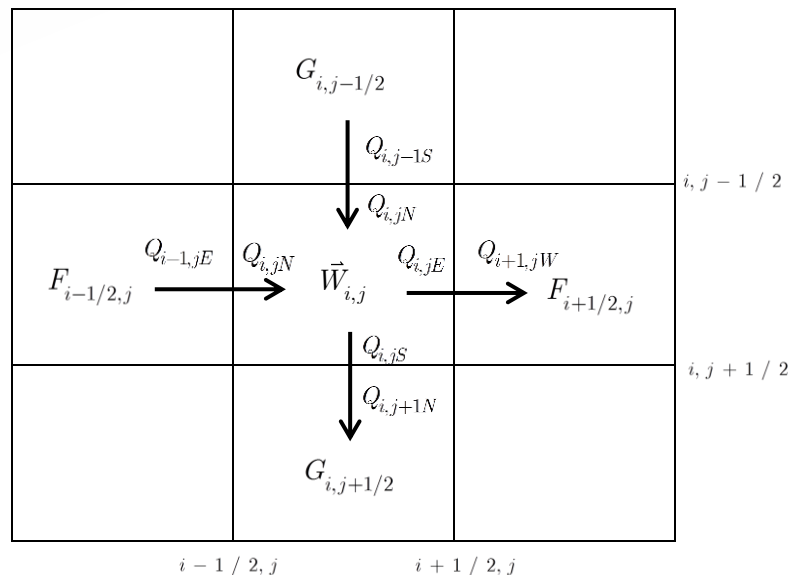
Figure 12 Flux calculation in the x and y directions

The Figure 12 at points $F_{i-1/2,j}$, $F_{i+1/2,j}$, $G_{i,j-1/2}$ and $G_{i,j-1/2}$ can be defined by the Godunov scheme. As suggested by (Godunov, 1959), the Godunov scheme is a conservation numerical scheme for solving partial differential equation. In other words, it is a conservative finite volume method which solves the exact or Riemann problems at each cell boundary.

In the basic and simplest form, Godunov scheme is first order accuracy in time and space. It can also be used as a basic form for developing the high-order schemes. The full Godunov scheme is given by the basic form as follow,

$$F^n_{i-1/2,j} = F(Q^n_{i-1/2}, Q^n_i). \tag{3.28}$$

Therefore from The Godunov scheme in equation (3.28) is to approximate to solve the Riemann problem in basic form it gives

$$
\left.
\begin{aligned}
\vec{F}^n_{i-1/2,j} &= F(\vec{Q}^n_{i-1,jE}, \vec{Q}^n_{i,jW}), \\
\vec{F}^n_{i+1/2,j} &= F(\vec{Q}^n_{i,jE}, \vec{Q}^n_{i+1,jW}), \\
\vec{G}^n_{i,j-1/2} &= G(\vec{Q}^n_{i,j-1S}, \vec{Q}^n_{i,jN}), \\
\vec{G}^n_{i,j+1/2} &= G(\vec{Q}^n_{i,jS}, \vec{Q}^n_{i,j+1N}),
\end{aligned}
\right\} \tag{3.29}
$$

where $\vec{F} = \begin{bmatrix} h \\ uh \\ vh \\ z \end{bmatrix}$, $\vec{G} = \begin{bmatrix} h \\ uh \\ vh \\ z \end{bmatrix}$, and $\vec{Q} = \begin{bmatrix} h \\ u \\ v \\ z \end{bmatrix}$.

The functions $F(\vec{Q}^n_W, \vec{Q}^n_E)$ and $G(\vec{Q}^n_N, \vec{Q}^n_S)$ in equation (3.29) can be computed by using the Harten-Lax-Van Leer approach (HLL), which was developed by (Harten et al., 1983) to approximate the numerical flux as

$$F(\vec{Q}_W^n, \vec{Q}_E^n) = \frac{S_E f(\vec{Q}_W) - S_W f(\vec{Q}_E) + S_E S_W (W(\vec{Q}_E) - W(\vec{Q}_W))}{S_E - S_W},$$

$$G(\vec{Q}_N^n, \vec{Q}_S^n) = \frac{S_S f(\vec{Q}_N) - S_N f(\vec{Q}_S) + S_S S_N (W(\vec{Q}_S) - W(\vec{Q}_N))}{S_S - S_N},$$

$$(3.30)$$

where $f(\vec{Q}) = \begin{bmatrix} uh \\ u^2 h + g\dfrac{h^2}{2} \\ uvh \\ \rho_x uz \end{bmatrix}$, $g(\vec{Q}) = \begin{bmatrix} vh \\ vuh \\ v^2 h + g\dfrac{h^2}{2} \\ \rho_y vz \end{bmatrix}$, $w(\vec{Q}) = \begin{bmatrix} h \\ uh \\ vh \\ z \end{bmatrix}$,

S_W and S_E are the smallest and largest wave speed, respectively in the x direction,

S_N and S_S are the smallest and largest wave speed, respectively in the y direction.

For SWEs the speed of wave S_W, S_E, S_S and S_N can be estimated by

$$S_W = \min\left(u_W - \sqrt{gh_W}, u_E - \sqrt{gh_E}, \rho_x u_W, \rho_x u_E, 0\right),$$

$$S_E = \max\left(u_W + \sqrt{gh_W}, u_E + \sqrt{gh_E}, \rho_x v_W, \rho_x v_E, 0\right),$$

$$(3.31)$$

$$S_N = \min\left(v_N - \sqrt{gh_N}, v_S - \sqrt{gh_S}, \rho_y v_N, \rho_y v_S, 0\right),$$

$$S_S = \max\left(v_N + \sqrt{gh_N}, v_S + \sqrt{gh_S}, \rho_y v_N, \rho_y v_S, 0\right),$$

where $u_W \pm \sqrt{gh_W}$, $u_E \pm \sqrt{gh_E}$, $v_N \pm \sqrt{gh_N}$, $v_S \pm \sqrt{gh_S}$, $\rho_x u_W$, $\rho_x u_E$, $\rho_y u_N$ and

$\rho_y u_S$ are the eigenvalues of Jacobian matrix $\dfrac{\partial f(\vec{w})}{\partial \vec{w}}$ and $\dfrac{\partial g(\vec{w})}{\partial \vec{w}}$.

From the formula to compute the flux each one of them needs data at the edges of the 4 sides of the cell but the data is only at the center of each cell. The data

at each side of the cell needs to be reconstructed so that it can be used to calculate the results.

3.5.2 Flux-limited Reconstruction

The basic limiter formulated for discontinuous scheme depends on the Monotonic Upstream-centered schemes for Conservation Law (MUSCL) slope limiting technique developed by (Van Leer, 1977). MUSCL uses the piecewise linear reconstruction for subgrid-cell distributions which gives a second order accurate scheme. The minmod limiter is applied to the reconstruction process to avoid inaccurate oscillations.

The piecewise linear reconstruction for one grid cell is considered below by using the minmod limiter.
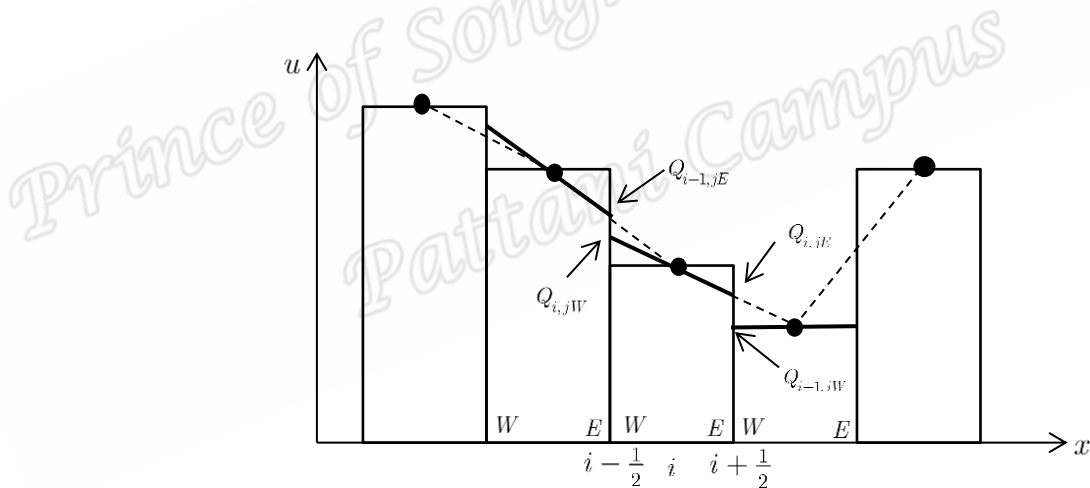
Figure 13 Picewise linear and constant approximation at each cell

Figure 13 shows the piecewise linear reconstruction. The edge of each cell can be calculated by using the following formula.

$$Q_{i,jW} = Q_{i,j} - \frac{1}{2}\sigma_{i,j}\Delta x\,,$$

$$Q_{i,jE} = Q_{i,j} + \frac{1}{2}\sigma_{i,j}\Delta x\,,$$

$$Q_{i,jN} = Q_{i,j} - \frac{1}{2}\delta_{i,j}\Delta y\,,$$

$$Q_{i,jS} = Q_{i,j} + \frac{1}{2}\delta_{i,j}\Delta y\,,$$

$$(3.32)$$

where $\sigma_{i,j}$ and $\delta_{i,j}$ are the slope limiter in x and y direction, respectively and $Q_{i,j}$ are the values needed to create new data such as $h_{i,j}$, $u_{i,j}$, $v_{i,j}$ or $z_{i,j}$.

The slope limiter function are defined by

$$\sigma_{i,j} = \text{minmod}\left(\frac{Q_{i+1,j}-Q_{i,j}}{\Delta x}, \frac{Q_{i,j}-Q_{i-1,j}}{\Delta x}\right),$$

$$\delta_{i,j} = \text{minmod}\left(\frac{Q_{i,j+1}-Q_{i,j}}{\Delta y}, \frac{Q_{i,j}-Q_{i,j-1}}{\Delta y}\right),$$

$$(3.33)$$

where the minmod function is defined by

$$\text{minmod}(a,b) = \begin{cases} a, & if \quad |a| < |b| \quad and \quad ab > 0 \\ b, & if \quad |b| < |a| \quad and \quad ab > 0 \\ 0, & if \quad ab \le 0 \end{cases}$$

$$= \frac{1}{2}\ \text{sgn}(a) + \text{sgn}(b)\ \min\ |a|, |b|\ . \qquad (3.34)$$

It must be noted that, Δt plays an important role in the numerical results and for that matter it calculation needs to be in detail as the divergence of the solution depends on it. The CFL condition is used to compute Δt and this would be discussed in the next section.

3.3.2 Courant–Friedrichs–Lewy (CFL) Condition

A numerical solution converges if and only if its numerical domain contains the exact domain of the partial differential equation. The CFL condition used by Delis (Delis et al. 2005) is necessary to guarantee the stability. The CFL condition is used to calculate the Δt in order to calculate the convert solution. The size of Δt plays a big role to the numerical solution, if the Δt too small the calculation need more time to compute whole system, but if the Δt too large the solution may diverged.

Therefore Δt can be calculated using the CFL condition as follows,

$$\frac{\max(c_x, c_y)\Delta t}{\min(\Delta x, \Delta y)} \leq \frac{1}{2},$$

$$\Delta t \leq \frac{1}{2}\frac{\min(\Delta x, \Delta y)}{\max(c_x, c_y)}, \tag{3.35}$$

where c_x and c_y are based on rough estimates of the eigenvalue of Jacobian matrix $\dfrac{\partial f(\vec{w})}{\partial \vec{w}}$ and $\dfrac{\partial g(\vec{w})}{\partial \vec{w}}$, respectively to satisfy the sub-characteristic condition by

$$\left.\begin{aligned}
c_x &= \max(s_{i-1/2,jW}, s_{i+1/2,jE}, -s_{i-1/2,jW}, -s_{i+1/2,jE}), \\
c_y &= \max(s_{i,j-1/2N}, s_{i,j+1/2S}, -s_{i,j-1/2N}, -s_{i,j+1/2S}).
\end{aligned}\right\} \tag{3.36}$$

Also in equation (3.35), if $\max(c_x, c_y)$ becomes zero, the value of Δt will be infinity and to avoid it, the following formula would be used

$$\Delta t \leq \frac{1}{2}\frac{\min(\Delta x, \Delta y)}{\sqrt{g}}, \tag{3.37}$$

where g is the gravitational constant ($g = 9.814$).

So, the Δt becomes

$$\Delta t = \begin{cases} \dfrac{1}{2} \dfrac{\min(\Delta x, \Delta y)}{\max(c_x, c_y)}, if \max(c_x, c_y) \neq 0 \\ \dfrac{1}{2} \dfrac{\min(\Delta x, \Delta y)}{\sqrt{g}}, Otherwise \end{cases} \tag{3.38}$$

The flux and Δt for the numerical results have been computed and this would be used in the simulation of sediment transport distribution. The next section describes the steps involved in the calculation of the model.

3.3.3 Calculation of the Model

The previous section proposed the equation that would be used in computing numerically flux and Δt associated with equation (3.27). The results in equation (3.27) would be calculated at each time step with the next time (t_{n+1}) calculated using the current time (t_n) and this would be done iteratively.

Equation (3.27) was shown as

$$\vec{W}_{i,j}^{n+1} = \vec{W}_{i,j}^{n} - \frac{\Delta t}{\Delta x}\left[\vec{F}_{i+\frac{1}{2},j}^{n} - \vec{F}_{i-\frac{1}{2},j}^{n}\right] - \frac{\Delta t}{\Delta y}\left[\vec{G}_{i,j+\frac{1}{2}}^{n} - \vec{G}_{i,j-\frac{1}{2}}^{n}\right] + \Delta t \vec{Z}_{i,j}^{n} + \Delta t \vec{S}_{i,j}^{n},$$

where $\vec{W}_{i,j}^{n+1}$ is the new vector values of h, uh, vh and z at the next time t_{n+1}, $\vec{W}_{i,j}^{n+1}$ is still the unknown vector we need to calculate it by using $\vec{W}_{i,j}^{n}$, $\vec{W}_{i,j}^{n}$ is known at time

t_n with defined by $\overrightarrow{W}_{i,j}^{n} = \begin{bmatrix} h_{i,j}^{n} \\ (uh)_{i,j}^{n} \\ (vh)_{i,j}^{n} \\ z_{i,j}^{n} \end{bmatrix}$, $\overrightarrow{Z}_{i,j}^{n} = \begin{bmatrix} 0 \\ gh_{i,j}^{n} \dfrac{z_{i,jW}^{n} - z_{i,jE}^{n}}{\Delta x} \\ gh_{i,j}^{n} \dfrac{z_{i,jN}^{n} - z_{i,jS}^{n}}{\Delta y} \\ 0 \end{bmatrix}$ and

$$\vec{S}_{i,j}^{n} = \begin{bmatrix} 0 \\ -\dfrac{gn^2\sqrt{(u_{i,j}^{n})^2 + (v_{i,j}^{n})^2}\,(uh)_{i,j}^{n}}{(h_{i,j}^{n})^{4/3}} \\ -\dfrac{gn^2\sqrt{(u_{i,j}^{n})^2 + (v_{i,j}^{n})^2}\,(vh)_{i,j}^{n}}{(h_{i,j}^{n})^{4/3}} \\ 0 \end{bmatrix}.$$

To complete equation (3.27) we still need to calculate the flux $\vec{F}_{i-\frac{1}{2},j}^{n}$, $\vec{F}_{i+\frac{1}{2},j}^{n}$,

$\vec{G}_{i-\frac{1}{2},j}^{n}$ and $\vec{G}_{i+\frac{1}{2},j}^{n}$ are the flux can be calculated from equation (3.29), The gravitational

force $\vec{Z}_{i,j}^{n}$ calculated from the height of the terrain reconstruction in equation (3.34)

and the time step $\triangle t$ can be computed by using CFL condition in equation (3.38).

However, the solution of equation (3.27) can be oscillated from each time

step. To solve this problem, we need to average the next solution between the current

time t_n and the next time t_{n+1} as shown in Figure 14. The average of $h_{i,j}^{n+1}$ and $h_{i,j}^{n}$ is

calculated by using Second-Order Total Variation Diminishing (TVD) Runge-Kutta

scheme to guarantee the total variation of the solution. Figure 14 is illustrated the

solution of h, u, v and z at time t_n and t_{n+1} for easy understanding

Figure 14 Depicting the result average between current times

Source: Boosamun (2010)

The Second-Order TVD Runge-Kutta scheme can be calculated the vector $\vec{W}$ as the following steps:

1. Calculate the equation (3.27) for the time t_n by ignoring the source term $\triangle t \vec{S}_{i,j}$

$$\vec{W}_{i,j}^{(1)} = \vec{W}_{i,j}^n - \frac{\triangle t_1}{\triangle x}\left[\vec{F}_{i+\frac{1}{2},j}^n - \vec{F}_{i-\frac{1}{2},j}^n\right] - \frac{\triangle t_1}{\triangle y}\left[\vec{G}_{i,j+\frac{1}{2}}^n - \vec{G}_{i,j-\frac{1}{2}}^n\right] + \triangle t_1 \vec{Z}_{i,j}^n, \qquad (3.39)$$

2. Repeat the calculation of equation (42)

$$\vec{W}_{i,j}^{(2)} = \vec{W}_{i,j}^{(1)} - \frac{\triangle t_2}{\triangle x}\left[\vec{F}_{i+\frac{1}{2},j}^n - \vec{F}_{i-\frac{1}{2},j}^n\right] - \frac{\triangle t_2}{\triangle y}\left[\vec{G}_{i,j+\frac{1}{2}}^n - \vec{G}_{i,j-\frac{1}{2}}^n\right] + \triangle t_2 \vec{Z}_{i,j}^n, \qquad (3.40)$$

3. Find average value between 2 results from equation (3.39) and equation (3.40)

$$\vec{W}_{i,j}^{n+1} = \frac{\vec{W}_{i,j}^{(1)} + \vec{W}_{i,j}^{(2)}}{2}, \qquad (3.41)$$

4. The result of the model from equation (3.41) now is still not included the source function $\triangle t \vec{S}_{i,j}$, so we have to add the source function (friction force) for the flow rate per one unit of time by using semi-implicit method proposed by (Bristeau et al., 2001). The source function can be calculated as follows

and

$$\left.\begin{array}{l} (uh)_{i,j}^{n+1} = \dfrac{(uh)_{i,j}^{(3)}}{\left(1 + \Delta t \dfrac{gn^2\sqrt{u_{i,j}^n{}^2 + v_{i,j}^n{}^2}}{h_{i,j}^{n+1}{}^{4/3}}\right)} \\[40pt] (vh)_{i,j}^{n+1} = \dfrac{(vh)_{i,j}^{(3)}}{\left(1 + \Delta t \dfrac{gn^2\sqrt{u_{i,j}^n{}^2 + v_{i,j}^n{}^2}}{h_{i,j}^{n+1}{}^{4/3}}\right)}, \end{array}\right\} \qquad (3.42)$$

where $\triangle t = \dfrac{\triangle t_1 + \triangle t_2}{2}$, $(uh)_{i,j}^{(3)}$ and $(vh)_{i,j}^{(3)}$ are the results from equation (3.42).

3.3.4 Boundary Condition

$$0 \quad \cdots\cdots\cdots\cdots\cdots\cdots\cdots\cdots\cdots\cdots\cdots\cdots m_x - 1$$
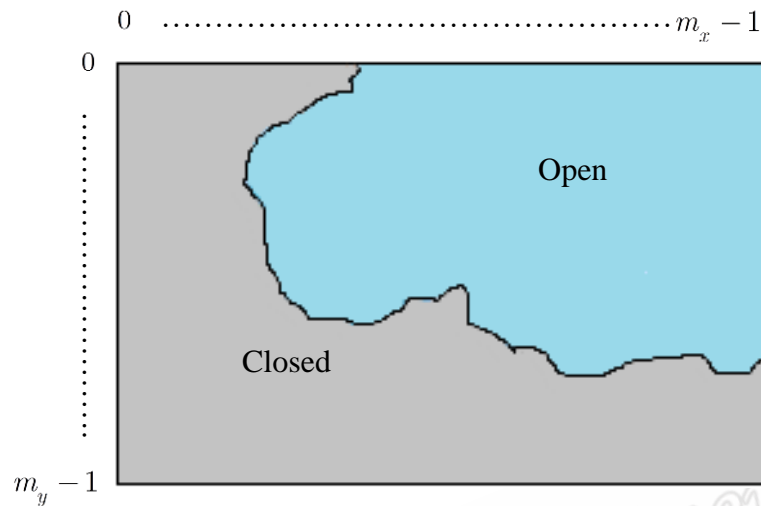
Figure 15 Boundary of grid data

As we mentioned in the previous section, this study considers an open and closed boundary when calculating the entire area. From Figure 15, there are four edges and all values on the boundary cannot be computed by using the equation as internal grid cell to solve this problem, we need to determine the open and closed boundary condition to allow the water flow out from the boundary for open boundary and the water cannot flow out once the boundary is closed. The value at the open boundary is equal to the adjacent edges of the area. The open boundary for four edges is given as follows,

$$
\left.
\begin{array}{llll}
h_{0,j}^{t} = h_{1,j}^{t}, & u_{0,j}^{t} = u_{1,j}^{t}, & v_{0,j}^{t} = v_{1,j}^{t}, & z_{0,j}^{t} = z_{1,j}^{t}; \quad \text{for } h_{i,j}^{0} < 0, \\[2mm]
h_{i,0}^{t} = h_{i,1}^{t}, & u_{i,0}^{t} = u_{i,1}^{t}, & v_{i,0}^{t} = v_{i,1}^{t}, & z_{i,0}^{t} = z_{i,1}^{t}; \quad \text{for } h_{i,j}^{0} < 0, \\[2mm]
h_{i,m_y-1}^{t} = h_{i,m_y-2}^{t}, & u_{m_x-1,j}^{t} = u_{m_x-2,j}^{t}, & v_{m_x-1,j}^{t} = v_{m_x-2,j}^{t}, & z_{m_x-1,j}^{t} = z_{m_x-2,j}^{t}; \text{for } h_{i,j}^{0} < 0, \\[2mm]
h_{m_x-1,j}^{t} = h_{m_x-2,j}^{t}, & u_{i,m_y-1}^{t} = u_{i,m_y-2}^{t}, & v_{i,m_y-1}^{t} = v_{i,m_y-2}^{t}, & z_{i,m_y-1}^{t} = z_{i,m_y-2}^{t}; \text{for } h_{i,j}^{0} < 0,
\end{array}
\right\} \quad (3.43)
$$

For the closed boundary, the depth of water (h) is set to zero indicate the land area (gray color in Figure 15). This is a condition imposed on the system to break the water flow to the land. The closed boundary is

$$h_{i,j}^{t} = 0 \,,\ u_{i,j}^{t} = 0 \,,\ v_{i,j}^{t} = 0 \,,\ z_{i,j}^{t} = z_{l\arg e}^{t} \,; \text{for } h_{i,j}^{0} \geq 0 \,, \tag{3.44}$$

where i and j are the indicated grid size by $i = 0,1,2,...,m_x - 1$ and $j = 0,1,2,...,m_y - 1$, respectively, $z_{l\arg e}^{t}$ is the large value for height of topography data, h is the depth of water by if $h_{i,j} < 0$ is the sea and $h_{i,j} \geq 0$ is the land areas as shown in Figure at 15 blue and gray colors, respectively.

3.3.5 Inflow Condition

In this study, the inflow conditions considered are wave and sediment for the simulation process.

The wave condition is obtained by using the following formula;

$$h_{i,j}^{t} = h_{i,j}^{0} + amp * \sin(\Delta t * \pi / 45) \,; \text{if } h_{i,j}^{0} < 0 \,, \text{ for all } t > 0 \,, \tag{3.45}$$

likewise, the sediment condition is obtained as well by using the formula below;

$$z_{i,j}^{t} = z_{i,j}^{0} + \varepsilon \,; \text{if } h_{i,j}^{0} < 0 \,, \text{ for all } t > 0 \,, \tag{3.46}$$

where $h_{i,j}^{0}$ is the sea water level and at time $t = 0$, this is referred to as the initial condition at the mean sea water level while amp is the amplitude. However $z_{i,j}^{0}$ is the sediment level at time $t = 0$, and ε is the value of sediment to be added. Furthermore position (i, j) for $h_{i,j}$ and $z_{i,j}$ can be obtained from the user.

3.3.6 Topography Interpolation

The land data used in this study is based on the topography of a 1 kilometer grid size. It was derived by using the USGS SRTM30 gridded digital elevation model (DEM) data product. The DEM data was created by NASA shuttle radar topography mission (Becker et al., 2009). The SRTM30 data used for this study was the last updated data which took place on November 29th, 2014. Since the DEM data are coarse grid, it is possible to increase the resolution to be smaller size of grid cell. The bilinear interpolation technique was used to obtain the high resolution topography (Busaman et al., 2011). The high resolution topography at point (i, j) is calculated by the following
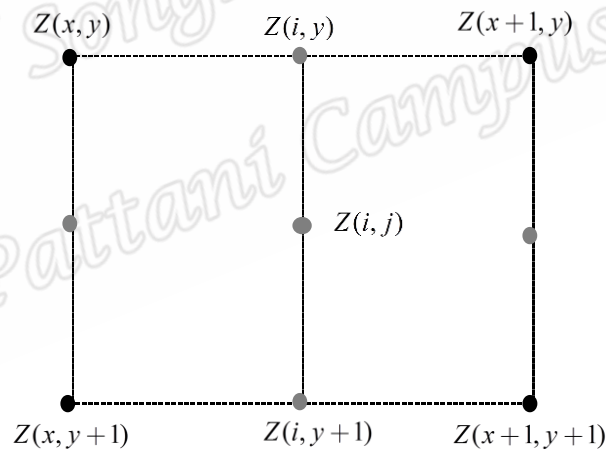
Figure 16 Bilinear interpolation

From Figure 16, the process of the bilinear interpolation is derived based on linear interpolation of second order in the x direction can be defined by

$$F(x) = F(x_1)\left(\frac{x - x_2}{x_1 - x_2}\right) + F(x_2)\left(\frac{x - x_1}{x_2 - x_1}\right). \tag{3.47}$$

To obtain the $Z(i, y)$, we use the points $Z(x, y)$ and $Z(x+1, y)$ as shown

$$Z(i, y) = Z(x, y)\left(\frac{i-(x+1)}{x-(x+1)}\right) + Z(x+1, y)\left(\frac{i-x}{(x+1)-x}\right)$$

$$= Z(x, y)(-i + x + 1) + Z(x+1, y)(i - x). \tag{3.48}$$

Similarly for the points $Z(x, y+1)$ and $Z(x+1, y+1)$, the point $Z(i, y+1)$ can be obtained

$$Z(i, y+1) = Z(i, y+1)\left(\frac{i-(x+1)}{x-(x+1)}\right) + Z(x+1, y+1)\left(\frac{i-x}{(x+1)-x}\right)$$

$$= Z(i, y+1)(-i + x + 1) + Z(x+1, y+1)(i - x). \tag{3.49}$$

From Figure 15, the point $Z(i, j)$ in the y direction, we take points $Z(i, y)$ and $Z(i, y+1)$ to compute using the second order linear interpolation formula in y direction as shown

$$Z(i, j) = F(y_1)\left(\frac{y - y_2}{y_1 - y_2}\right) + F(y_2)\left(\frac{y - y_1}{y_2 - y_1}\right)$$

$$= Z(i, y)\left(\frac{j-(y+1)}{y-(y+1)}\right) + Z(i, y+1)\left(\frac{j - y}{(y+1) - y}\right)$$

$$= Z(i, y) \ -j + y + 1 \ + Z(i, y+1) \ j - y \ . \tag{3.50}$$

Substituting equations (47) and (48) in to equation (49), we obtain

$$Z(i, j) = \ Z(x, y)(-i + x + 1) + Z(x+1, y)(i - x) \ (-j + y + 1)$$

$$+ \ Z(i, y+1)(-i + x + 1) + Z(x+1, y+1)(i - x) \ (j - y).$$

Thus the bilinear interpolation becomes

$$Z(i, j) = Z(x, y)(x - i + 1)(y - j + 1) + Z(x+1, y)(i - x)(y - j + 1) +$$

$$Z(i, y+1)(x - i + 1)(j - y) + Z(x+1, y+1)(i - x)(j - y), \tag{3.51}$$

where (x, y) is the spatial index of the topography data grid cell, (i, j) is the cell approximation.

The bilinear solution obtained in equation (3.51) makes it possible to obtain a more accurate result from the investigated software namely VirtualSed3D Software. The Flowchart diagram of the VirtualSed3D software is explained in the next section.

3.3.7 Flowchart Diagram of VirtualSed3D Software

The VirtualSed3D software is designed to support the simulation and visualization of the sediment transport. It provides to read the topography data and allows the user to simulate the wave movement and sediment transport by given wave direction. The software can visualize the wave propagation and the sediment movement. It allows the user to rotate, zoom in and out from different perspective.
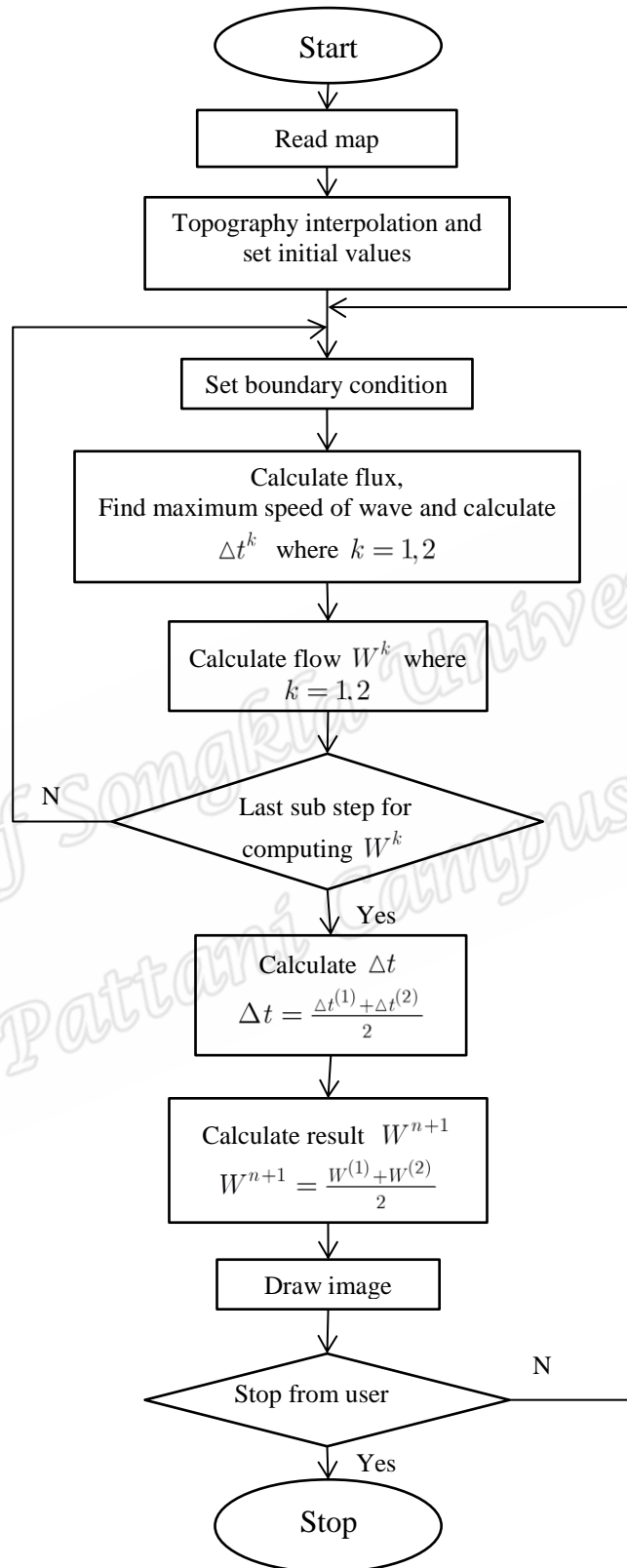
Figure 17 Flow of computation

Simulation for the numerical solution of the sediment transport would be carried out in the next chapter. Discussion on the various figures would be shown as well.

Chapter 4

Results and Discussion

In this chapter the various simulations for the distribution of sediment would be discussed. First of all, the 1-dimensional SWEs would be used to describe the movement of the sediment. Different values for the porosity of the sediment are used to simulate the sediment distribution. The corresponding graphs and figures from the 1-dimensional simulation would be shown as well as any further analysis. The 2-dimensional SWEs representing the physical problem of this study would be used to explain the distribution of sediment in Bandon Bay using the VirtualSed3D software.

The user interface of the program would be presented together with the various buttons, sliders and check boxes. The map of the area under study would be loaded into the program for the simulation and the visualization of sediment distribution.

4.1 The 1-Dimensional Graphic for Sediment Distribution

In order to fully understand the distribution of sediment, the 1-dimensional is presented with the following assumptions as follows

1. The sediment along the sea bed is homogenous case only.

2. The initial wave is considered to commence from the left, right and both.

3. The initial wave is continuous.

 Figure 18 below presents the user interface of the program.
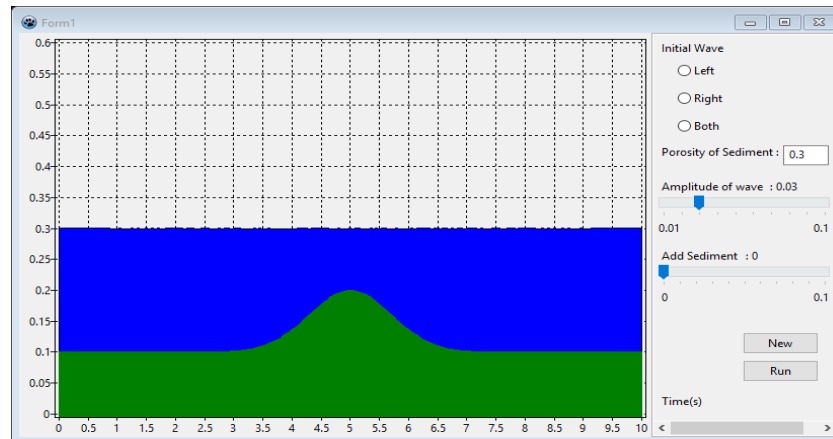
Figure 18 Initial condition for sediment transport in 1-dimensional at time $t = 0$ s.

From Figure 18, the initial wave can be started from the left, right or both. The porosity of the sediment can be inputted and the amplitude of the wave can be adjusted to any desirable value. The time step for the computation can be known when the program starts. The level of water in Figure 18 is at 0.3 meters as shown with blue color while the sediment is at 0.1 meter and rises to 0.2 meters (green) by using the formula $0.1 + 0.1\left(e^{-i(\triangle x - 5)^2}\right)$.

4.1.1 Validation of Models

The simulation carried out in this study was as a result of the conservation of the mass equation. However, this was validated by comparing sediment transport model in this study with standard Grass model.

(a) (b)
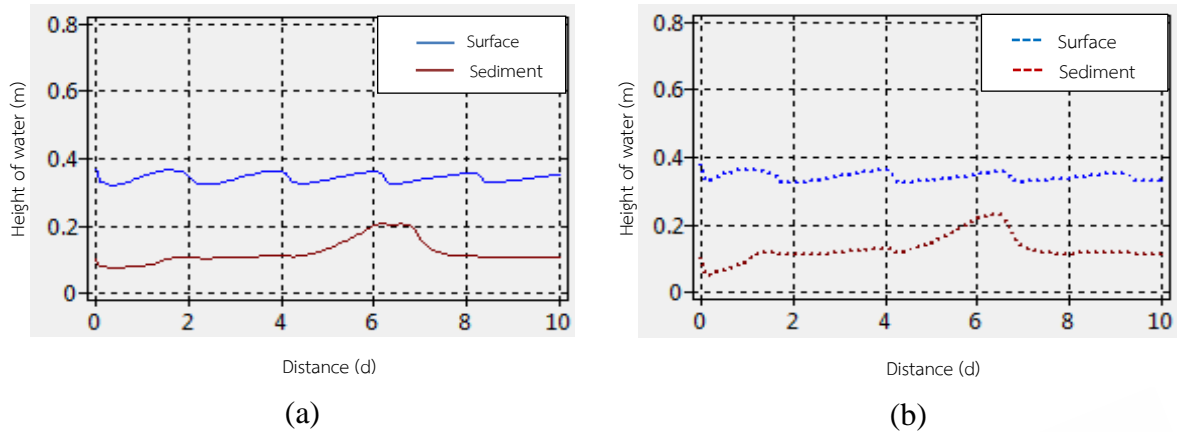
Figure 19 (a) Graph of sediment transport from the conservation of mass equation at time *t = 10* s. and (b) Graph of sediment transport by using the Grass model at time *t = 10* s

Figure 19(a) and Figure 19(b) show the sediment distribution with the conservation of mass equation and the Grass model at time t=10 s. The porosity of sediment used in the simulation is set to 0.43 and A_g constant is set to 0.3 (constant used in the Grass model).
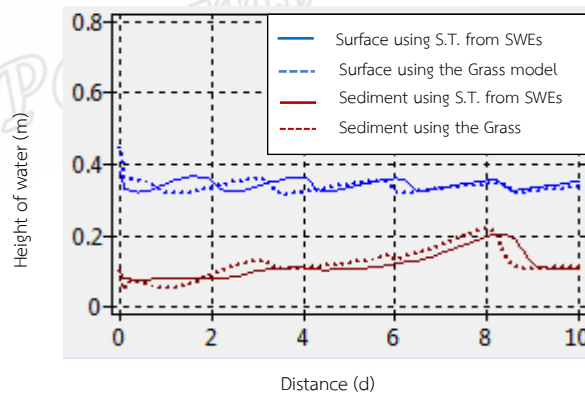
Figure 20 Graph of sediment transport from the conservation of mass equation and the Grass model at time *t = 20* s.
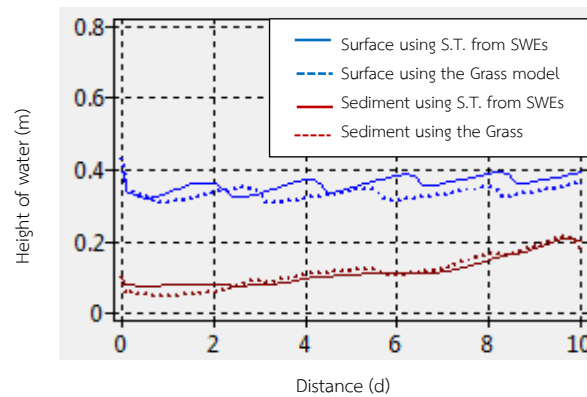
Figure 21 Graph of sediment transport from the conservation of mass equation and
the Grass model at time $t = 30$ s.

Figure 20 and Figure 21 show the sediment distribution by comparing the sediment transport from the conservation of mass equation and the Grass model. Figure 20 presents two models that is the Grass and the sediment transport models at time $t=20$ s. Figure 21 illustrates the difference of two models at time $t=30$ s. If the constant A_g and porosity are increased, the sediment will move faster than the small value of constant. From the results, both models can be used to simulate the distribution of sediment. The next will explain about the result of the sediment distribution by changing the involved parameters such as porosity of the sediment, height of water depth and increment in the sediment level.

4.1.2 Simulation of Sediment Distribution

The result of sediment transport in the 1-dimensional case would be used to explain the distribution of sediment in different category, when the values for the porosity of the sediment are changed, height of water depth is increased and increment of sediment level. The simulated results are shown in Figure 22, Figure 23, Figure 24, Figure 25 and Figure 26.
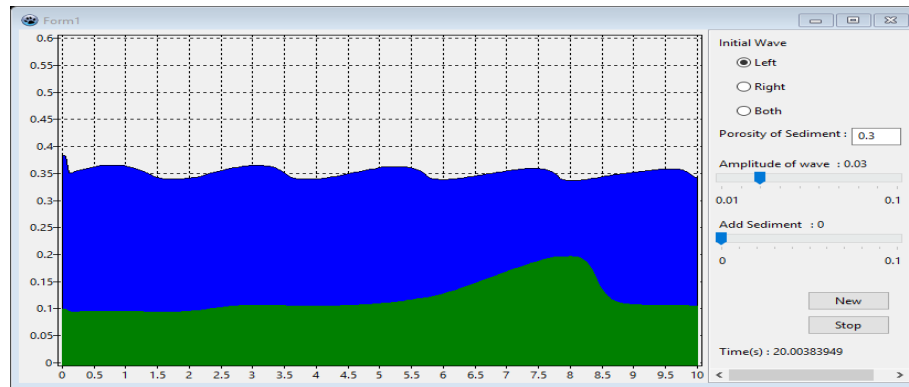
Figure 22 Sediment transport in 1-dimension with porosity of sediment 0.3

at time *t =20* s.
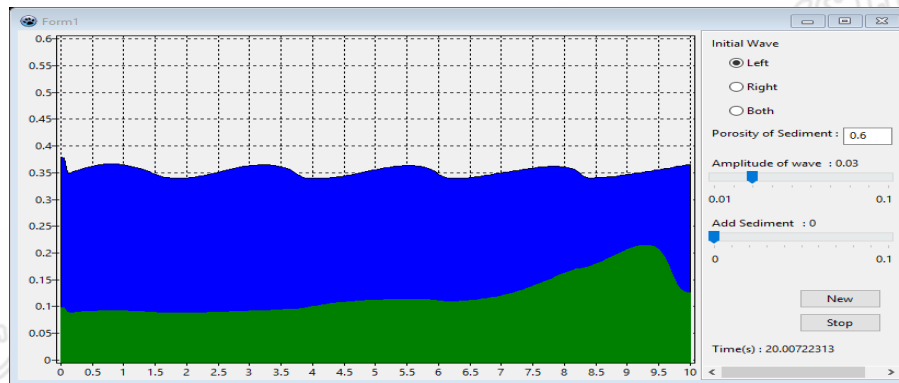
Figure 23 Sediment transport in 1-dimension with porosity of sediment 0.6

at time *t = 20* s.
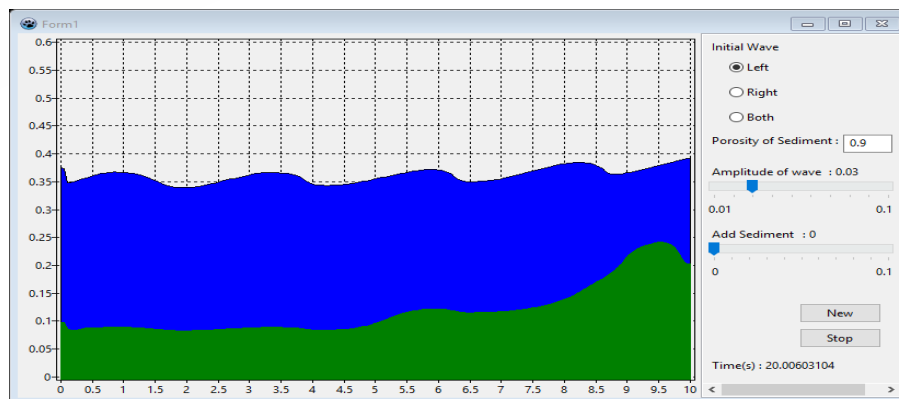
Figure 24 Sediment transport in 1-dimension with porosity of sediment 0.9

at time *t = 20* s.

Figure 22, Figure 23 and Figure 24 present the simulation of sediment distribution in the 1-dimensional case. The porosity of sediment in Figure 22 is set to 0.3 with wave amplitude of 0.03, the sediment displacement can be seen at time $t=20$ s. The porosity is changed from 0.3 (in Figure 22) to 0.6 (in Figure 23), the sediment transport moves faster when the porosity increases. The porosity is further increased to 0.9 and at this point it has become lighter and as a result it moves faster than in Figure 22 and Figure 23, therefore, it can be seen that lighter the sediment becomes, the faster it displaces.
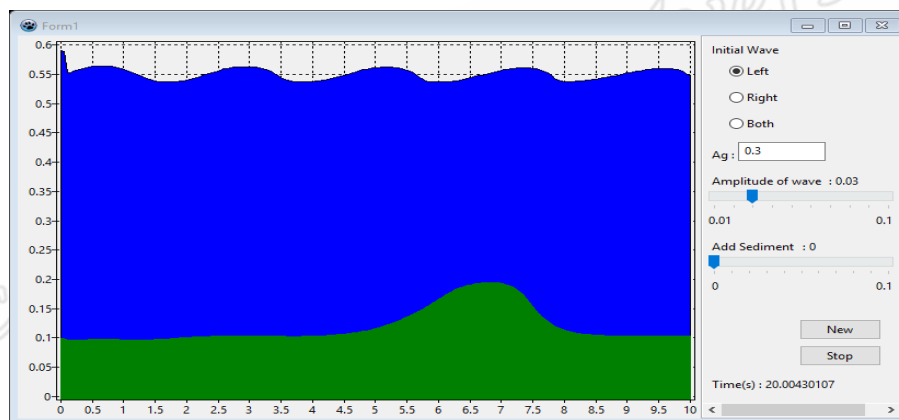
Figure 25 Sediment transport in 1-dimension with porosity of sediment 0.3 and depth of water 0.5 meters at time $t = 20$ s.

Figure 25 shows the sediment distribution when the water level is increased from 0.3 meters in Figure 22 to 0.5 meters with the same amplitude of wave and porosity, the sediment is not displaced much as seen in Figure 25. This is because the depth of water in Figure 25 is higher than the depth of water in Figure 22. As a result the movement of the wave does not affect the sediment distribution when the water is much deeper.
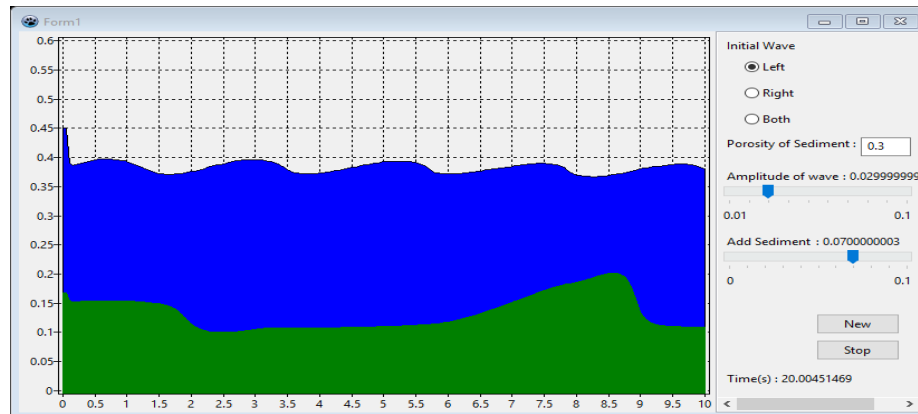
Figure 26 Sediment transport in 1-dimension with the level of sediment increased by

0.07 meters

When the program runs, the level of sediment can be increased and this can be seen in Figure 26. At time $t=0$ s. until 10 s. the program runs without any addition of sediment. From $t=10$ s. to $t=20$ s., the level of sediment is increased by 0.07 meters in the left boundary. This shows the fact that, as river streams flow into the ocean, they can deposit sediment which needs to be accounted for in the simulation.

4.2 The 2-Dimensional Graphic for Sediment Distribution

A two-dimensional SWEs model together with the sediment transport model by using conservation of mass equations was used to read the topography data in VirtualSed3D software as shown in Figure 27.
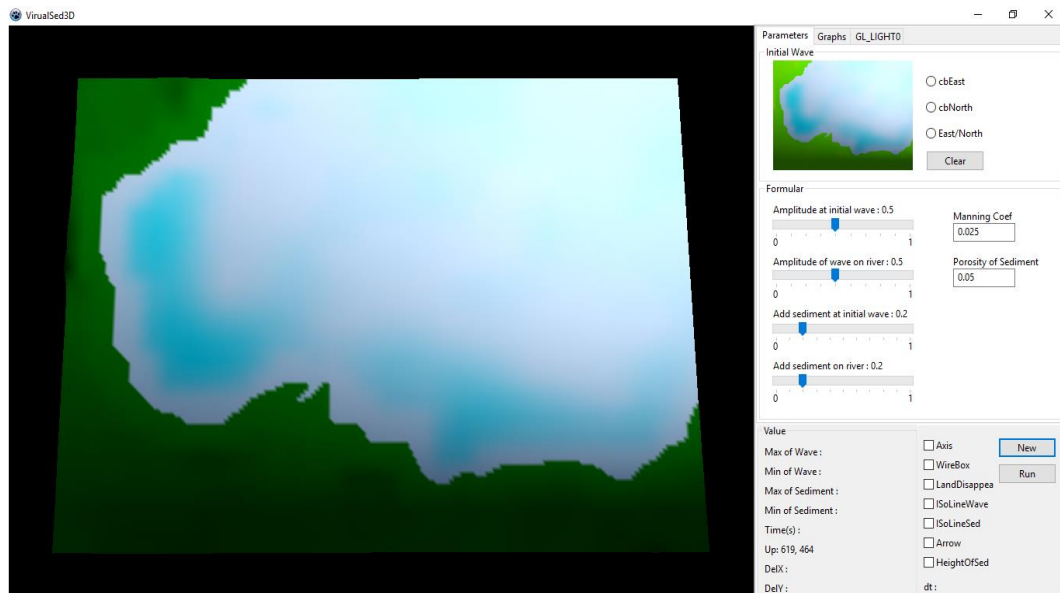
Figure 27 Topography data visualized by the VirtualSed3D

The topography data in this study considered longitude at 99.20416667E to 99.49583333E from the west to the east and latitude at 9.387500N to 9.170833N from the north to south. The file structure of the data is explained in appendix II. Therefore, from one latitude-longitude point, the measurement from the SRTM 30 is approximated to 1 kilometer which gives 36 kilometers from west to east and 27 kilometers from north to south. The topography data are then interpolated using equation (3.51) to 200 meters for higher resolution.

Figure 27 shows the user interface of the VirtualSed3D software. The various buttons, check boxes and radio buttons are used to enter all values to specify the command in the program. The user interface consists of three tabs, the first tab is for setting parameters, the second is to show graph and the third is for setting light parameters.

The parameter tab is for setting all the various parameters used in the model. All parameters can be adjusted and varied in order to simulate the distribution of

sediment. Also, the direction of the initial wave and a button to load the map to the study area as well as the button to run the program are presented.

The graph tab is where the simulation of the sediment distribution is visualized graphically. The "light tab" is used to control the light parameters to aid the visualization process in various light properties at different angles of the study area.

Figure 28, Figure 29 and Figure 30 give a detailed description of the user interface of the program under the parameter tab.

Figure 28 Panel for initializing the initial wave

Figure 28 shows the panel for initializing the wave. The wave can be initialized from the east, the north and both east and north. The initial wave can be drawn by the user in desired direction on the topography map.
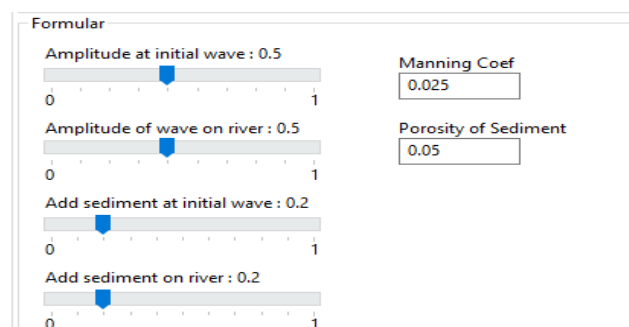
Figure 29 Panel for entering and changing the model parameters

Figure 29 shows the panel for entering and changing the parameters of the model while running the simulation. The porosity value of sediment can be changed on this tab, also the manning coefficient in the bed friction force can be changed as well. The amplitude of the initial wave, the amplitude of wave on the river can all be adjusted using the slider. Sediment can be added at the initial time and during the simulation.
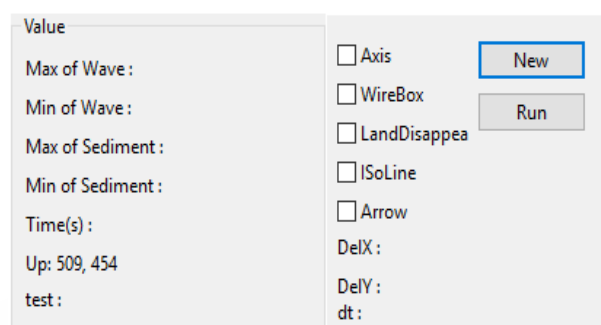
Figure 30 Additional settings for simulation

Figure 30 shows additional setting for more information in the simulation. The New and Run buttons can be used to load the map in the study area and also run the program, respectively.

Figure 31 and Figure 32 show the various features under the graph tab.
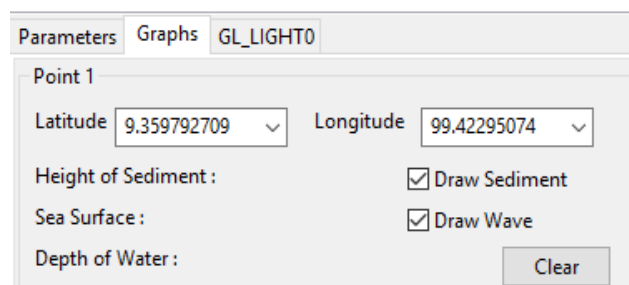
Figure 31 Latitude and longitude for setting the point for plotting graph

Figure 31 shows the panel for plotting the graphs of the various points on the map as well as the latitude and longitude for drawing the positions of the points. The

height of sediment, sea surface and depth of water can be known when the program is running. The graph of the various points can be known by switching between the points on the right pane.
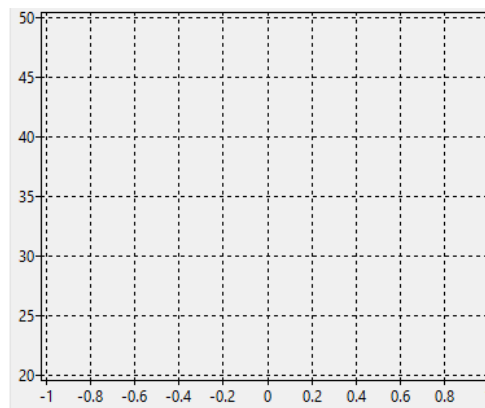

Figure 32 Plotting graph panel

From Figure 32, the sediment level and the wave height can be together plotted on the graph. The end user can change to the another position to measure the sediment level and wave height by selecting in the drop down list.

Figure 33 shows the various sliders for controlling the light in the program.
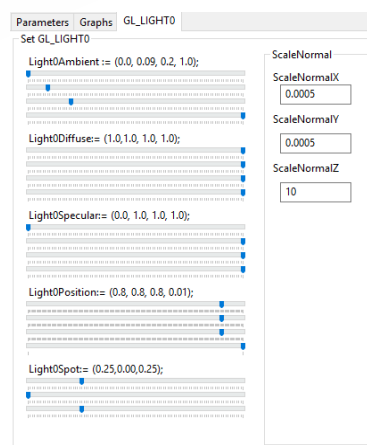
Figure 33 Sliders for controlling the light parameters

The ambient lighting, the diffuse lighting and specular lighting of the area under study can be controlled by using the various sliders.

The ambient lighting is the constant light that prevents the area from being completely dark. The diffuse lighting is responsible for brightening the area when it is directed towards it. The specular lighting simulates a bright spot of a light bright parts of the area. The light parameters can be controlled to see the visualization of the distribution of sediment clearly.
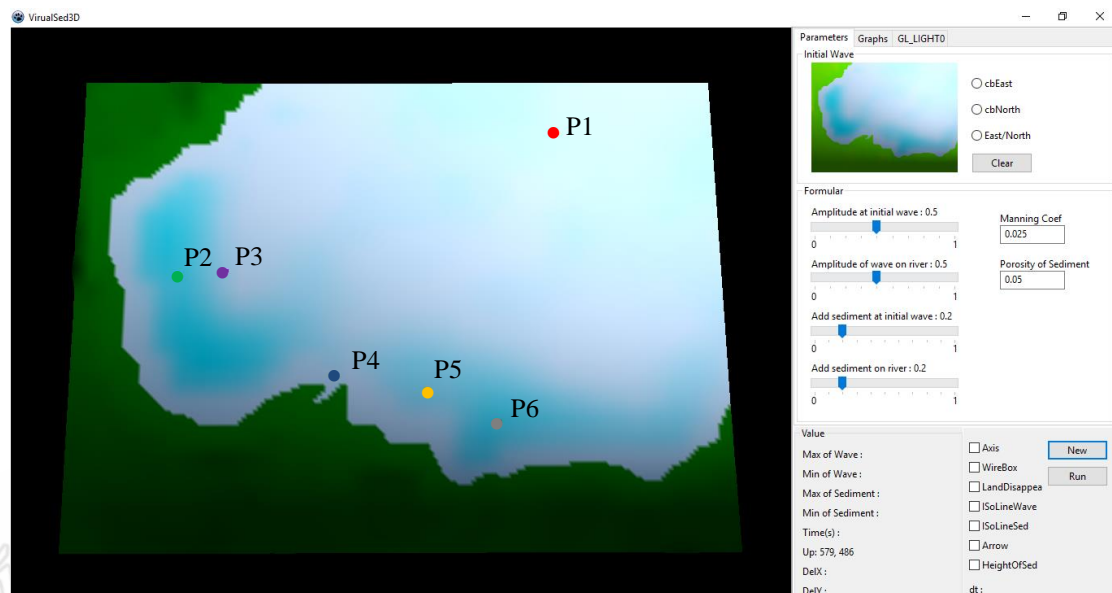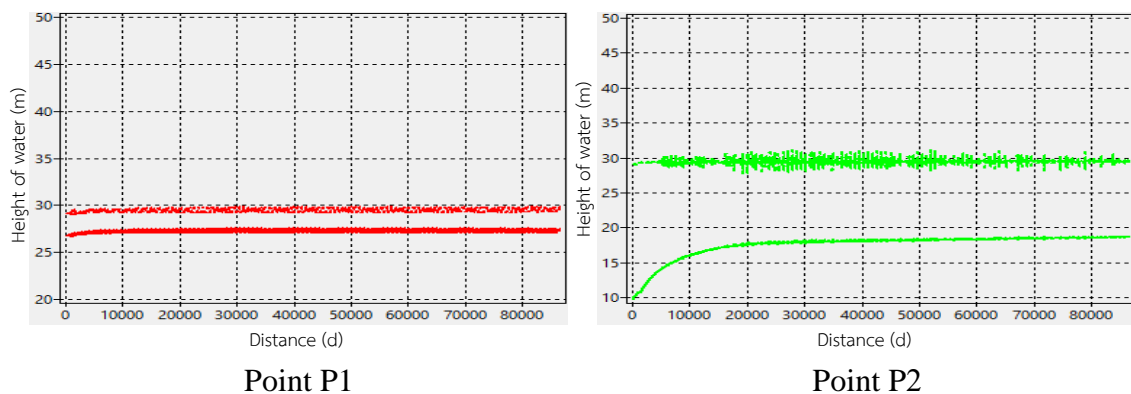

Figure 34 Arbitrary points for simulation

Figure 34 shows the position of the various points that were used to carry out the simulations. The points P1, P2, P3, P4, P5 and P6 are chosen such that the distribution of sediment can be measured.
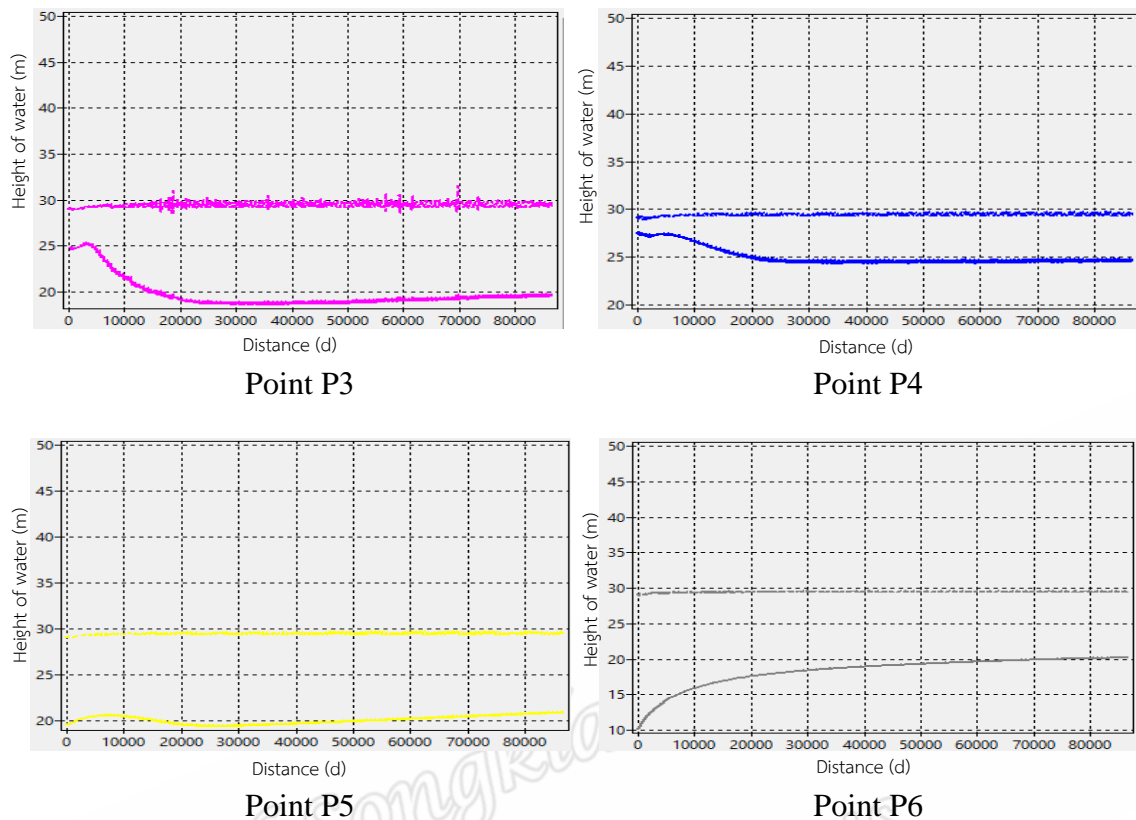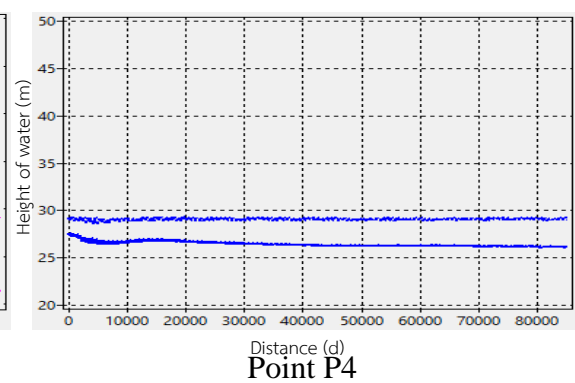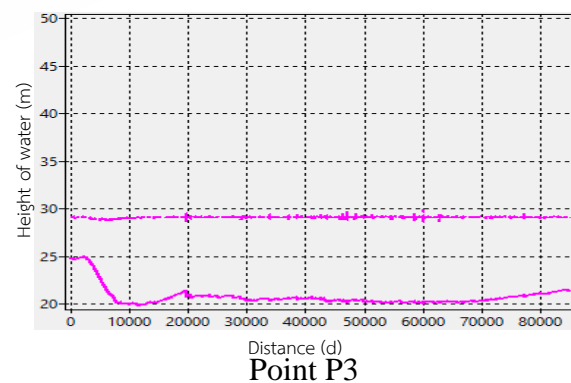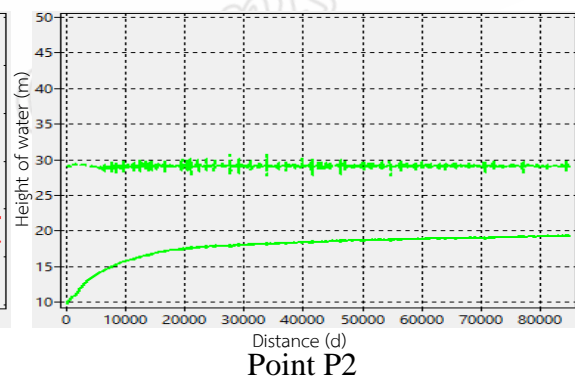

Point P1

Point P2

Point P3   Point P4

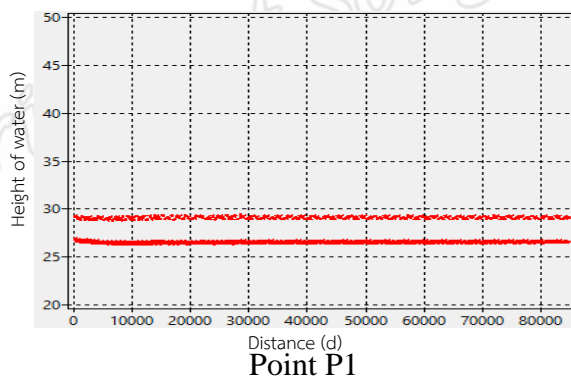Point P5   Point P6

Figure 35 Distribution of sediment with porosity of sediment 0.5 and initial wave

from the east at points P1 to P5

Figure 35 shows the graph of the distribution of sediment for the various points described in Figure 34. The simulations were carried out for more than 24 hours in order to mimic the real world situation. The depth of water at the beginning of the simulation is 2.38, 19.36, 4.27, 1.63, 9.48 and 18.94 meters for points P1, P2, P3, P4, P5 and P6, respectively. The porosity of the sediment is 0.5 for the entire simulation. The manning coefficient in the bed friction force is responsible for the smooth or rough movement of the sediment and this value is fixed at 0.025 according to Kontar et al., 2014.

The amplitude of the initial wave is 0.5 and this can be varied using the slider. The initial wave is started from the east and the graph of the distribution of the

sediment can be seen in Figure 35. The distribution of the sediment can be seen to be constant at point P1 throughout the whole simulation. This is not the case for points P2 and P3. As the initial wave is from the east, the movement of the sediment is much higher at point P3. The sediment is then deposited at point P2 as it is close to point P3. From Figure 35 at point P2, the second graph (the sediment distribution) shows an increasing of the amount of sediment from the beginning of the simulation.

The sediment distribution at point P4 also starts decreasing at the beginning of the simulation. At this point the wave speed is not too strong and as a result, it becomes constant at a point in time. Points P5 and P6 also show the respective distribution of sediment at different positions to fully understanding the sediment movement.
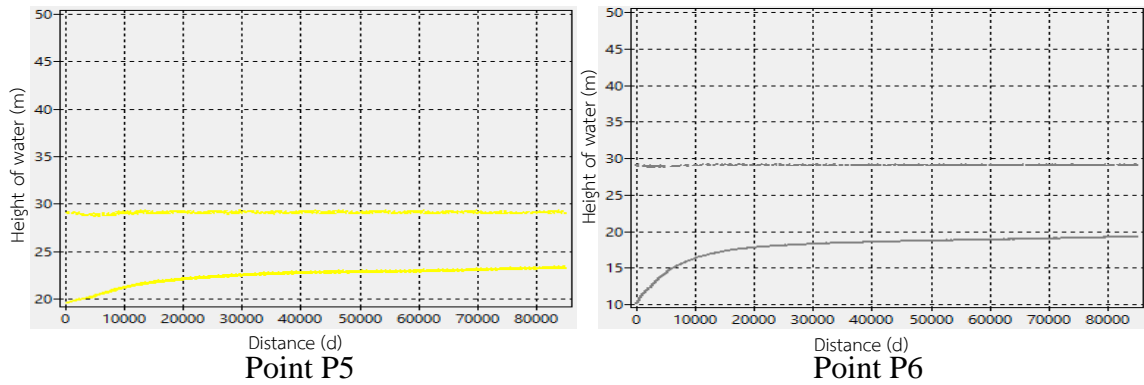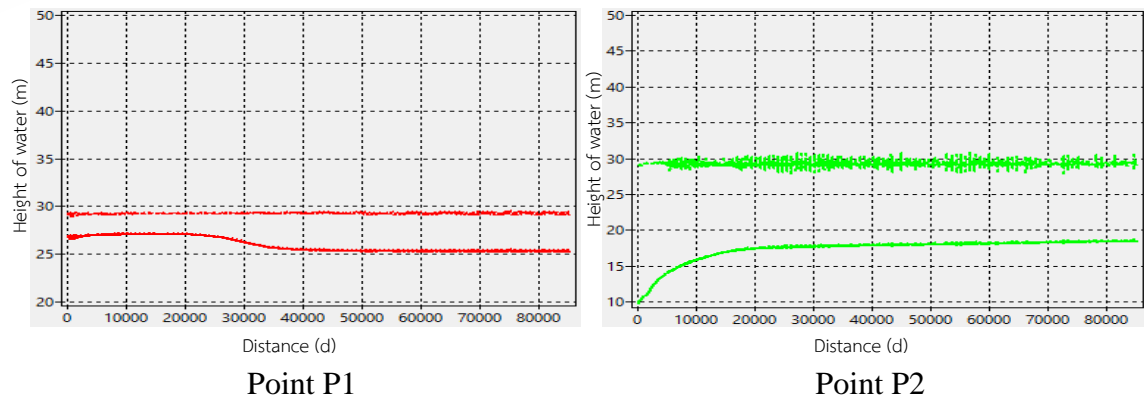

Point P1

Point P2

Point P3

Point P4

Point P5 Point P6

Figure 36 Distribution of sediment with porosity of sediment 0.5 and initial wave

from the north at points P1 to P6

The simulation in Figure 34 is repeated with the initial wave from the initial wave from the north. The porosity of the sediment is 0.5 just as the previous simulation. The distribution of the sediment for the various points can be seen in Figure 36. Point P1 still shows the same behavior as in Figure 35. There is not much of a decrease or increase in the movement of sediment. Points P2 and P3 are also showing similar behavior in Figure 35. In Figure 36, at points P2 and P3, the movement of the sediment is deposited at point P2 from point P3. Points P4, P5 and P6 although they are far from the initial wave, which is a significant change in the distribution of sediment as shown in Figure 36.
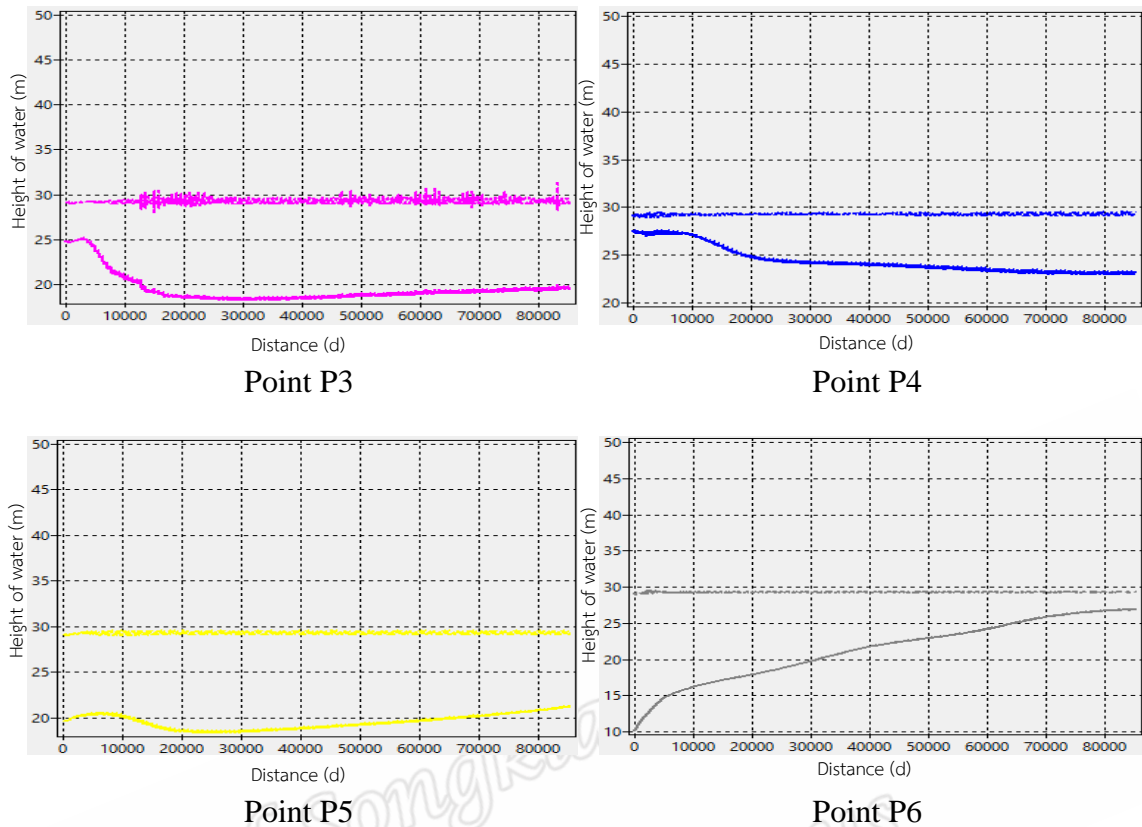

Point P1 Point P2

Figure 37 Distribution of sediment with porosity of sediment 0.5 and initial wave

from the north/east at points P1 to P6

Figure 37 shows the distribution of sediment with the initial wave from both the north and the east. The movement of sediment is greatly affected with the initial wave from both directions. The porosity of sediment is 0.5 and the amplitude of the initial wave is 0.5 meters. At point P1 in Figure 37, the sediment increases at the initial time and this attains a constant movement in the middle of the simulation. With the positions of the various points in Figure 34, the behavior and the distribution of sediment can be seen in Figure 37.

The amount of sediment can be increased or decreased depending on the distance from initial wave, but not only this parameter. There are more parameters needed to be studied such as wave speed, water depth and porosity of sediment.
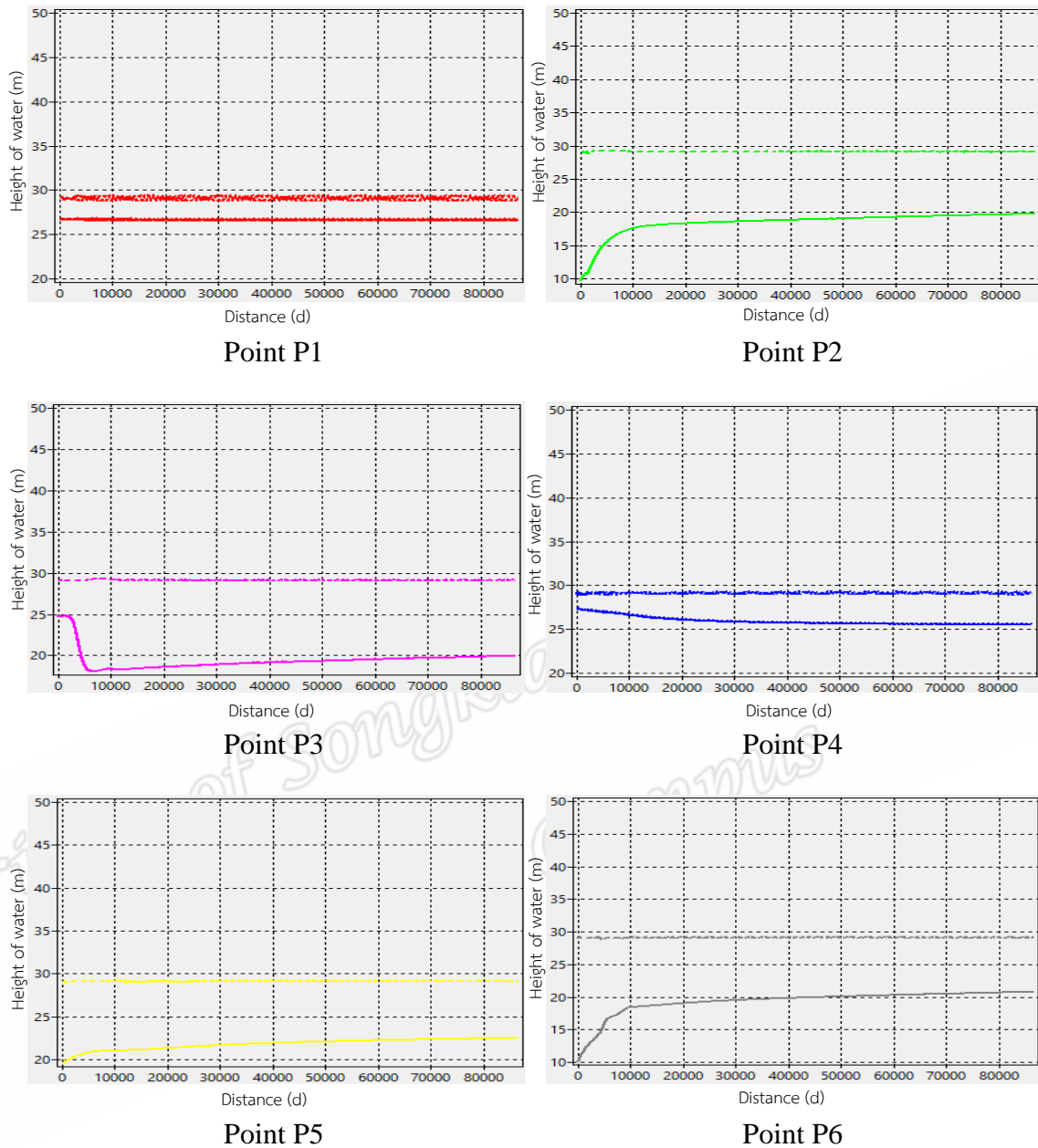
Figure 38 Distribution of sediment with porosity of sediment 0.05 and initial wave

from the north/east at points P1 to P6

Figure 38 shows the sediment distribution with the initial wave from both the

north and east. The porosity of the sediment is reduced from 0.5 to 0.05. The

reduction in the value means that the sediment is rougher in the case of 0.5 and fine in

the case of the 0.05 value. As the result the movement of the sediment is restrained a

bit. This has been shown in Figures 22, 23 and 24 in 1-dimensional case. With the same amplitude of initial wave points P1, P2, P3, P4, P5 and P6 under the 2-dimensional case show the distribution of the sediment at their respective positions in Figure 38.

The sediment at point P1 maintains a constant movement whereas the sediment at point P2 increases at the initial time as a result of sediment from point P3. Point P4 in Figure 38 starts decreasing at the initial time but maintain some level of constancy throughout the simulation. Point P5 in Figure 38 see some increase after the initial time in simulation and point P6 in Figure 38 also increases at the initial time in the simulation and maintains some level of constancy as well.

Simulations for different sediment porosity at different positions have been carried out to understand the distribution of sediment. This has been done in the 1-dimensional case and the 2-dimensional case as well.

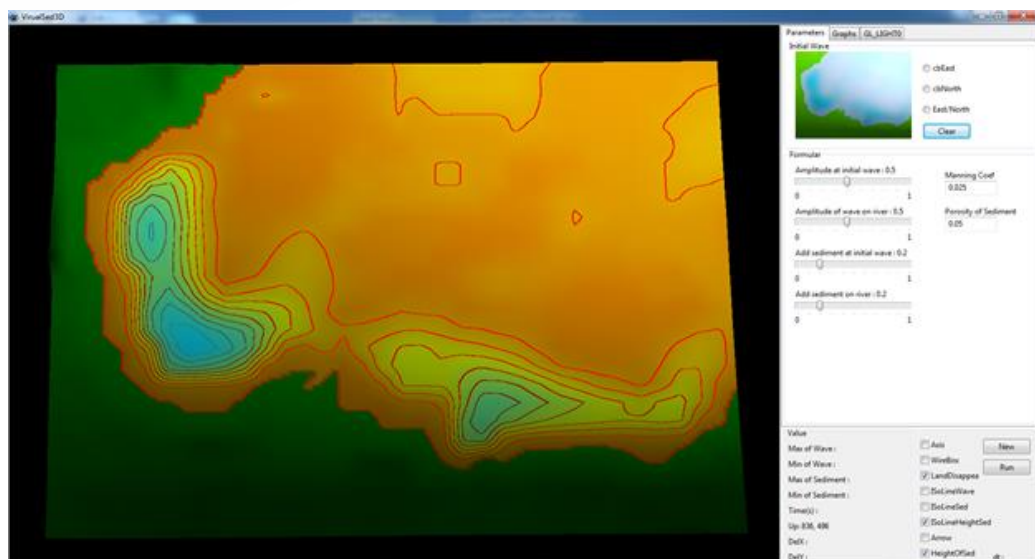However, the distribution of sediment can be described in 3-dimensional and this is shown in Figure 39.

Figure 39 3-dimensional view of the sediments before distribution

Figure 39 shows the 3-dimensional view of the program. After the map is loaded in the program, the area with high sediment can be seen on the map with the description of the color bar (Figure 40) and the contour lines display the same height of sediment with the description of the color bar (Figure 41).

$Z_{\max}$ $Z_{\min}$

Figure 40 Color bar of high and low sediment

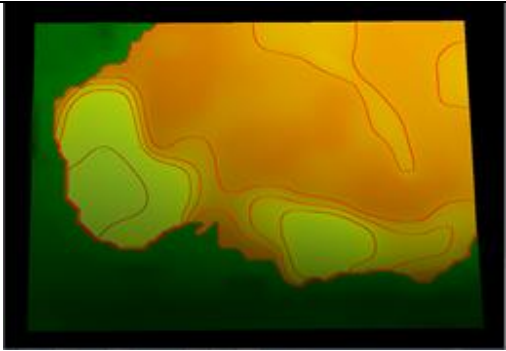$Z_{\max}$ $Z_{\min}$

Figure 41 Color bar of contour lines
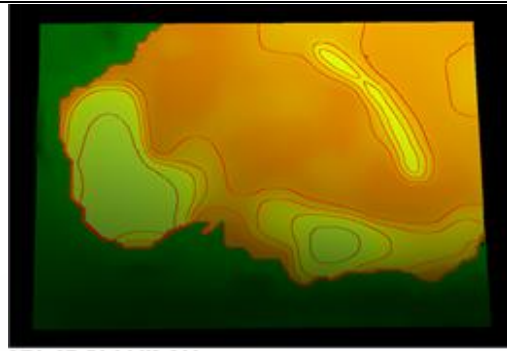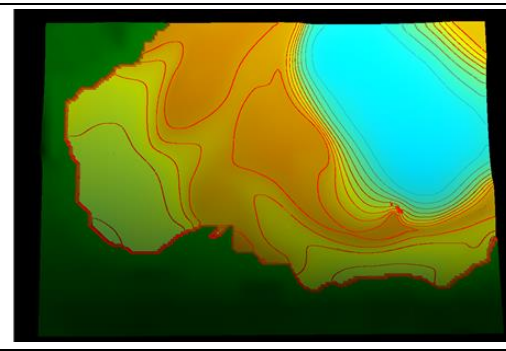
Figure 40 and Figure 41 show the description of the upper bar with the area with high sediment is represented as $Z_{\max}$ and the area with low sediment is represented as $Z_{\min}$. It should be noted that high and low sediment corresponds to the colors and this is used in the result that follow in Figures 43-48.
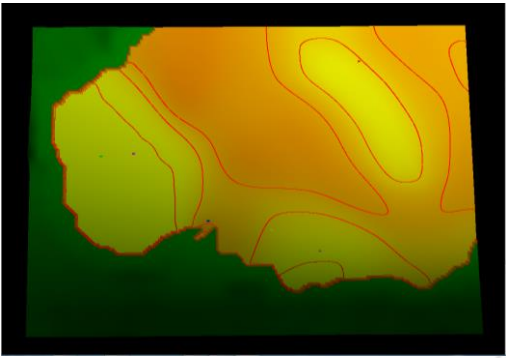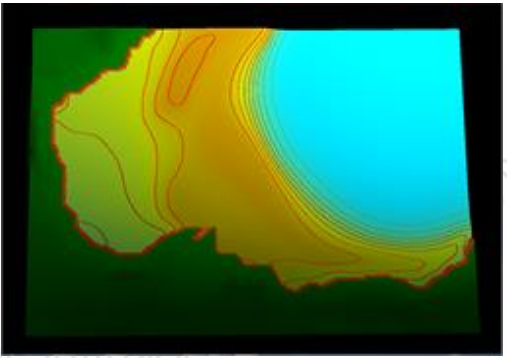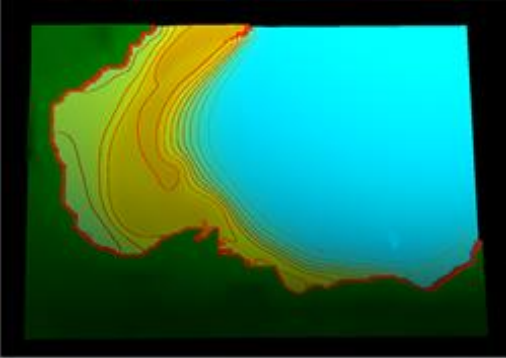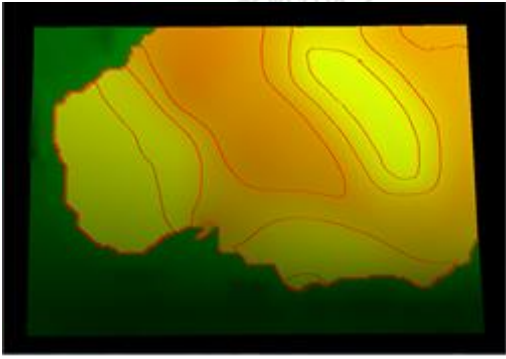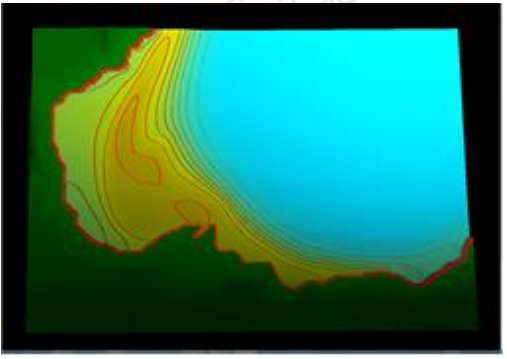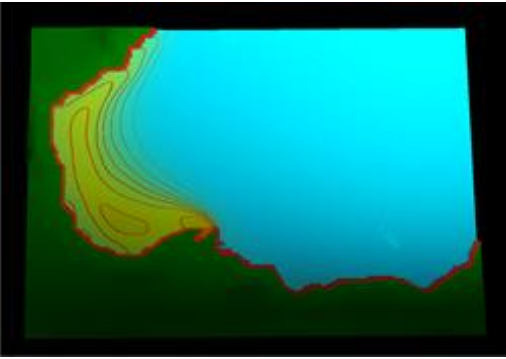
Figure 42 Initial wave for the simulation
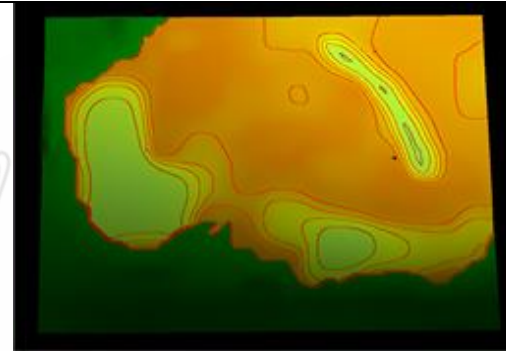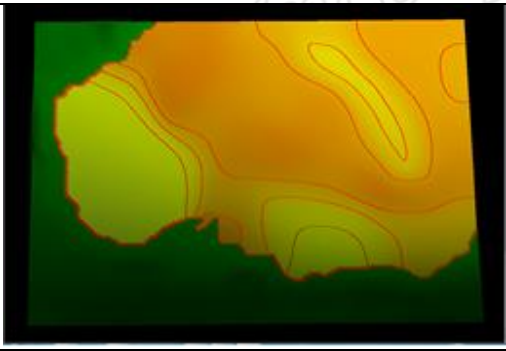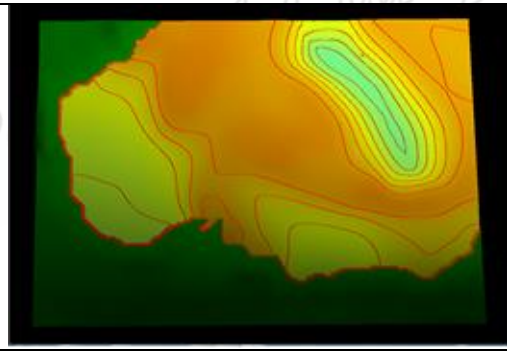
In the 3-dimensional view, the initial wave for the simulation is done by drawing a black line on the ocean. Figure 42 shows an example of a line drawn to initialize the wave for the simulation. The line can therefore be done on any desirable part of the ocean to understand how sediment distributes based on the direction as well as how close they are to the initial wave.

Simulations carried in 3- dimensions are shown in the figures that follow. This is done with three different values of sediment types at different times

Time (s.)	Porosity of sediment (ρ)		
	0.1	0.3	0.5
10,000			
	a	b	c
	Figure 43 Distribution of sediment with porosity of sediment 0.1, 0.3 and 0.5 at time *t=10,000* s.		
50,000			
	a	b	c
	Figure 44 Distribution of sediment with porosity of sediment 0.1, 0.3 and 0.5 at time *t=50,000* s.		

Time (s.)	Porosity of Sediment (ρ)		
	0.1	0.3	0.5
100,000			
	a	b	c
	Figure 45 Distribution of sediment with porosity of sediment 0.1, 0.3 and 0.5 at time *t=100,000* s.		
150,000			
	a	b	c
	Figure 46 Distribution of sediment with porosity of sediment 0.1, 0.3 and 0.5 at time *t=150,000* s.		
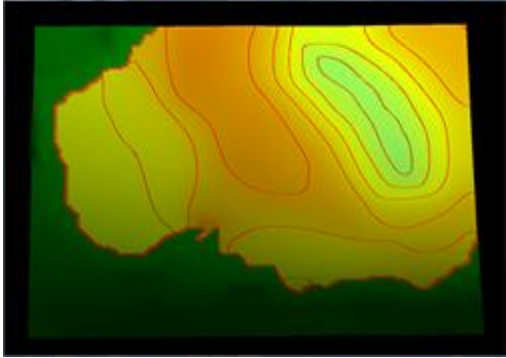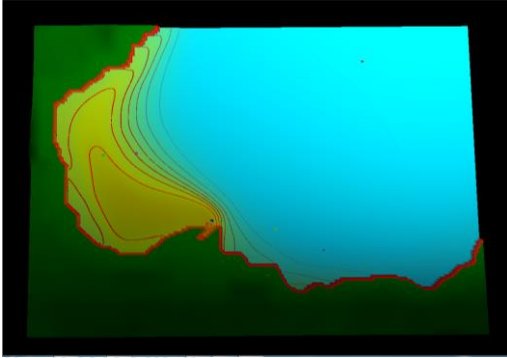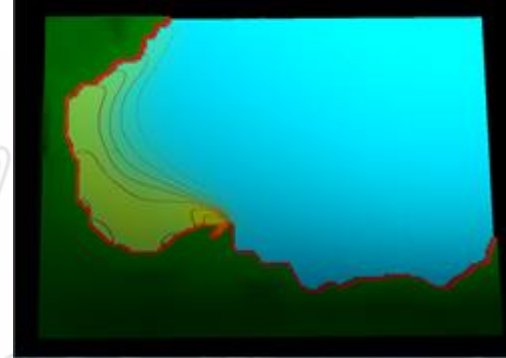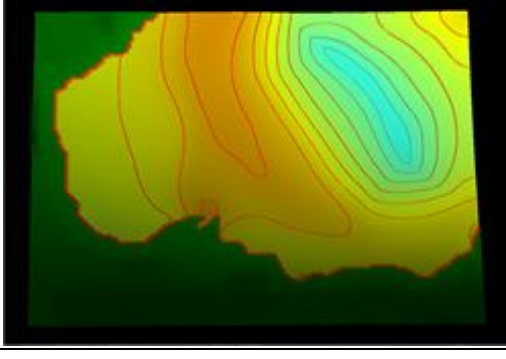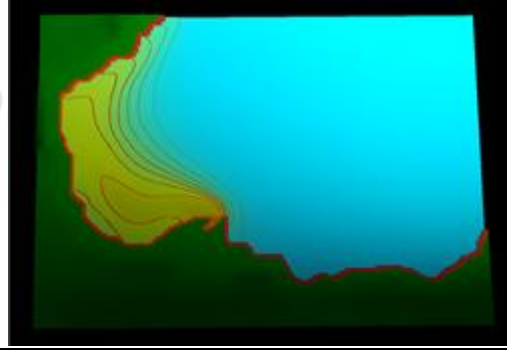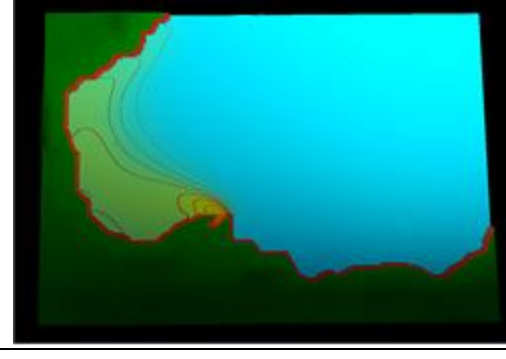
Time (s.)	Porosity of Sediment (ρ)		
	0.1	0.3	0.5
200000			
	a	b	c
	Figure 47 Distribution of sediment with porosity of sediment 0.1, 0.3 and 0.5 at time *t=200,000* s.		
250000			
	a	b	c
	Figure 48 Distribution of sediment with porosity of sediment 0.1, 0.3 and 0.5 at time *t= 250,000* s.		

Figure 43 shows the sediment distribution for sediment type with values 0.1, 0.3 and 0.5 at time $t=10,000$ s. With a porosity of 0.1 and an initial wave drawn as shown in the Figure 42, the sediment does not move that much for $t=10,000$ s. This is because the porosity of sediment is heavy. When the porosity is reduced to 0.3 in Figure 43(b), with the same initial wave, the sediment moves but not too much. The porosity is reduced to 0.5 in Figure 43(c) and the movement is much faster than when the values are 0.1 and 0.3 as now the porosity of the sediment has become lighter than before.

The simulation of the sediment continuous with an increased in the time from 10,000 to 50,000 s. With the same porosity, the wave is initialized by drawing a line on the ocean as described as earlier. Even with an increase in the time, the distribution of the sediment when the porosity is 0.1 does not move fast as shown in Figure 44(a). Figure 44(b) shows a significant movement in the sediment with a porosity of 0.3. As the porosity is increased to 0.5, the sediment moves faster and the colors bar described earlier in Figure 40 shows the area with much sediment in figure 44c.

The change of porosity in Figure 45, Figure 46, Figure 47 and Figure 48 are similar to the Figure 43 and Figure 44 with the same behavior when increasing the porosity with different time $t=100,000$ s. (Figure 45), $t=150,000$ s. (Figure 46), $t=200,000$ s. (Figure 47), $t=250,000$ s. (Figure 48).

Finally, the amount of sediment in this study can be increased or decreased depending on the distance from initial wave, wave speed, water depth and porosity of sediment.

The next chapter describes the inferences and conclusion that can be drawn from the entire study from the modeling though to the simulation.

Chapter 5

Conclusions and Further Research

5.1 Conclusions

Sediment is needed to build aquatic habitats and also reintroduce nutrients for grasses that grow on shallow areas of oceans, sea, and other water bodies and as result, its distribution needs to be monitored as it can create problems for people living along the coast.

In this study, sediment distribution has been studied through mathematical modeling and simulation. This was done by using the Shallow Water Equations (SWEs) combined with sediment transport equation. A sediment transport model has been presented by using the idea following the flow of water from the conservation of mass. However, the flow of water and sediment are different so we add a porosity parameter of sediment to multiply with the rate of sediment flow per one unit. The model was solved numerically by using the finite volume methods which are based on the basis of the integral form of the conservation laws. The calculation of the flux from the numerical solution has been shown. The Godunov method was used to approximate the functions for solving the Riemann problem. The functions of Godunov method were computed by using the Harten Lax Van Lee approach (HLL) to approximate the numerical flux. Also, the data for the area of study was interpolated in order to simulate the entire area for the sediment distribution. Various simulations have been carried out to understand the distribution of sediment. The 1-dimensional SWEs and sediment transport equation were first used under the distribution. The validity of the sediment transport model was compared with the

grass model. The results showed that the sediment transport model is able to describe the distribution of sediment. This has been achieved by using different values of the porosity of sediment. The simulations were carried out for some time to know the sediment distribution between the two models.

The 2-dimensional SWEs together with the sediment model were also used to understand the distribution. With the initial wave from the East, North, East/North and also initialized by drawing the desire direction in the picture pane, the movement of sediment has been described in 2-dimensions for the study. A VirtualSed3D program developed using the Lazarus programming software is used for the simulation. With the latitude and longitude, different positions have been chosen on the map to know the distribution in shallow water or at the deepest parts of the ocean. All the various simulations and graph have been shown and described.

A 3D view of the sediment distribution has also been shown with different colors depicting how much sediment there is at any given area in the ocean. This has been shown with the color bar. As the porosity is reduced, the distribution of the sediment can be seen and understood.

Finally, it can be concluded that the sediment transport model has been able to describe the distribution of sediment and the distribution depends on the porosity of sediment, the continuous movement of wave and also the depth of a particular area under consideration.

5.2 Further Research

This research studied the simulation of sediment transport in order to understand the behavior and also provide some insight on how to prevent the damage

in the future. This study considered the sediment along the sea bed in homogeneous case only, while in fact, the topography of the seabed in the form of stones and rocks cannot move. Also, sediments at each position are of different types. Therefore, it will be very interesting to consider the topography and sediment along sea bed separately in the model.

Since no experimental data exists for the sediment transport model used in this study, the validation of sediment transport equation is deduced by comparing the results obtained in this model with the Grass model. Also, the visualization in the study is not able to account for high slopes which cause sea surface movements. However, these issues could be developed in future researches.

References

Becker, J.J., Sandwell, D.T., Smith, W.H.F., Braud, J,. Binder, B., Depner, J., Fabre, D., Factor, J., Ingalls, S., Kim, S-H., Ladner, R., Marks, K., Nelson, S., Pharaoh, A., Trimmer, R., Von Rosenberg, J., Wallace, G. and Weatherall, P. 2009. Global Bathymetry and Elevation Data at 30 Arc Seconds Resolution: SRTM30_PLUS Marine Geodesy. 32(4), 355-371.

Boosamun, A. 2010. Mathematical Model for Simulation and Visualization of Flood. Master Degree Thesis, Chulalongkorn University.

Bristeau, M.O.and Coussin, B. 2001. Boundary Conditions for the Shallow Water Equations Solved by Kinetic Schemes. Inria report, inria-00072305.

Busaman, A., Mekchay, K., Siripant, S. and Chuai-Aree, S. 2011. Dynamically Adaptive Tree Grid Modeling for Simulation and Visualization of Rainwater Overland Flow, 980–989.

Castro Diaz, M.J., Fernandez, E.D., Ferreiro, A.M. and Pares, C. 2009. Two-Dimensional sediment models in Shallow Water Equations. A Second Order Finite Volume Approach on Structured Meshes. Comput. Methods Appl. Mech. Engrg. 198, 2520-2538.

Cordier, S., Le, M.H. and Morales de Luna, T. 2011. Bedload Transport in Shallow Water Models: Why Splitting (may) Fail, How Hyperbolicity (can) Help. Advances in water Resources. 34, 980-989.

Delis, A.I., Katsaounis, Th. 2005. Numerical Solution of the Two-Dimensional Shallow Water Equations by the Application of Relaxation Methods. Applied Mathematical Modelling. 29, 754-783.

Fundamental of Environmental Measurement. 2015. Sediment Transport and

Deposition. Available online: http://www.fondriest.com/environmental-measurements/parameters/hydrology/sediment-transport-deposition/. [Aug 5, 2015].

Godunov, S. K. 1959. A Difference Scheme for Numerical Solution of Discontinuous Solution of Hydrodynamic Equations. Math. Sbornik. 47, 271–306. translated US Joint Publ. Res. Service, JPRS 7226, 1969.

Google. 2001. Bandon Bay in Surat Thani, Thailand. Available online: http://www.google.co.th/intl/th/earth/download/ge/agree.html. [Oct 8, 2015].

Grass, A.J. 1981. Sediment transport by waves and currents. SERC London Cent. Mar. Technol, Report No. FL29.

Harten A, Lax PD, Leer BV. 1983. On Upstream Di_Erencing and Godunov-Type Schemes for Hyperbolic Conservation Laws. SIAM Review. 25(1), 35-61.

Hawai'i Tsunami Education Curriculum: Kai E'e. 2016. Tsunami Propagation. Available online: http://www.discovertsunamis.org/tsunami_science_u5.html [December 20, 2016].

He, Z., Hu, P., Zhao, L., Wu, G and Pahtz, T. 2015. Modeling of Breaching Due to Overtopping Flow and Waves Based on Coupled Flow and Sediment Transport. Water 2015. Doi : 10.3390/w7084283.

Kanbua, W. and Chuai-Aree, S. 2007. Understanding the Simple Model of Tsunami Propagation by SiTProS Model. Proceedings of the 11th Annual National Symposium on Computational Science and Engineering (ANSCSE11), Phuket, Thailand, March 28-30, 2007.

Kontar, Y. A., Santiago-Fandino, V. and Takahashi, T. 2014. Tsunami Events and

Lessons Learned : Environment and Societal Significance (Springer Dordrecht Heidelberg, New York, London, 2014), pp. 218.

Lajos, B. 2008. Soil Science. Available online: http://www.tankonyvtar.hu/en/ tartalom/tamop425/0032_talajtan/ch06s06.html. [December 20, 2016].

Langland, M. and Cronin, T. 2003. A Summary Report of Sediment Processes in Chesapeake Bay and Watershed. Available online: http://pa.water.usgs.gov/reports/wrir03-4123.pdf. [Aug 5, 2015]

Luchaichana, S. 1987. Flume study of sediment transportation using sand of a given size and gradation as bed material. Ph.D. Thesis, Chulalongkorn University.

McGraw-Hill Education. 2015. Modes of Stream Transport. Available online: http://highered.mheducation.com/novella/MixQuizProcessing Servlet. [Oct 8, 2015].

Meesuk, V., Boonya-aroonnet, S., Srimongkol, S. and Chankarn, A. 2009. Sediment Transport in Mahachai Canal and Lung Canal, Samutsakhon Province. Proceedings of the 14th National Convention on Civil Engineering, Engineering Institute of Thailand, Nakhon Ratchasima, May 13-15, 2009.

Rattanapitikon, W. 2008. Mathematical Modeling for Cross Shore Sediment Transport and Beach Deformation under Irregular Waves. Thailand Reasearch Fund. RMU4880020.

Satellite Sports Network. 2015. Motion of Wave. Available online: http://www.satellitesportsnetwork.com/content.php?contentID=2934. [Oct 7, 2015].

Suwannasri, P. 2004. Parallel Computation of Shallow Water Flow Problem. Ph.D. Thesis, Chulalongkorn University.

Van Leer, B. 1977. Towards the Ultimate Conservative Difference Scheme III. Upstream-Centered Finite-Difference Schemes for Ideal Compressible Flow. Comp. Phys. 23(3), 263–275.

APPENDIXES

APPENDIX I

How to use the program

This section describes how to use the investigated software. The following steps are involved in using the VirtualSed3D program.

1. Set and input the initial values as describe in the figure below:
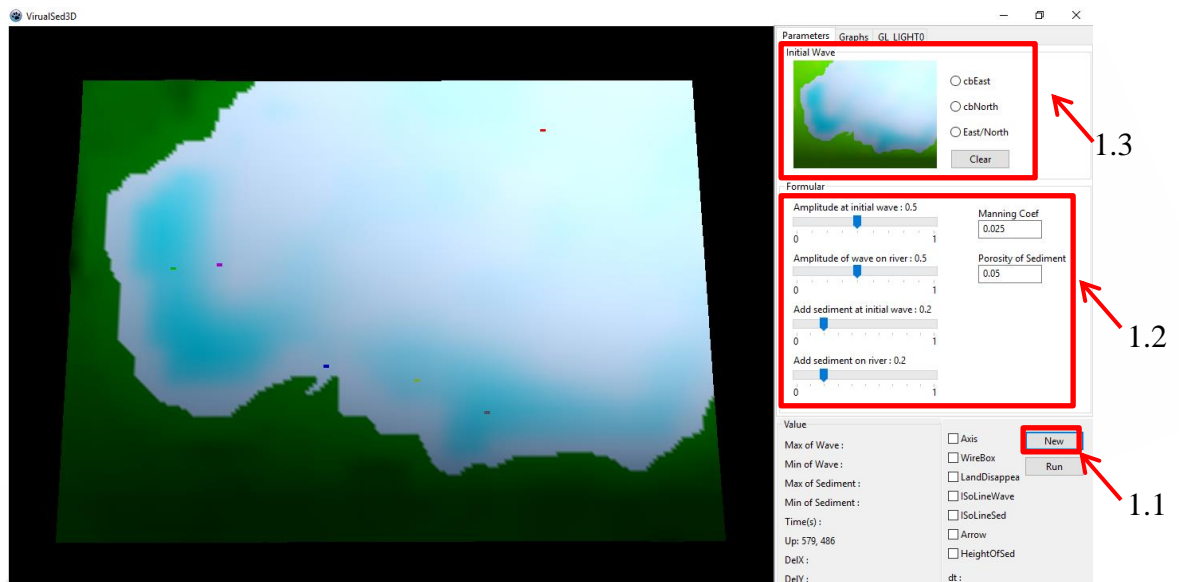
Figure 49 Input and set initial values for the program

1.1. Clicking the New bottom to download the topography data.

1.2. Choosing the direction of the initial wave.

1.3. Inputting the initial value of Manning coefficient, sediment

porosity, amplitude of initial wave, etc.

2. Select the latitude and longitude from the dropdown list as shown in the figure below:
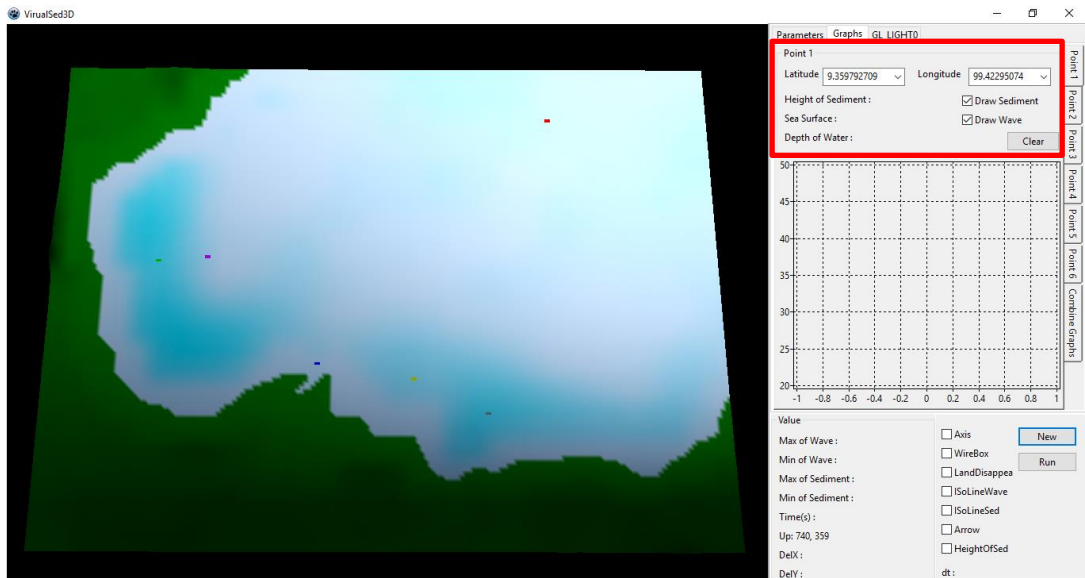
Figure 50 Latitude and longitude for the positions

3. Vary the various sliders to control the light as outlined in the figure below:
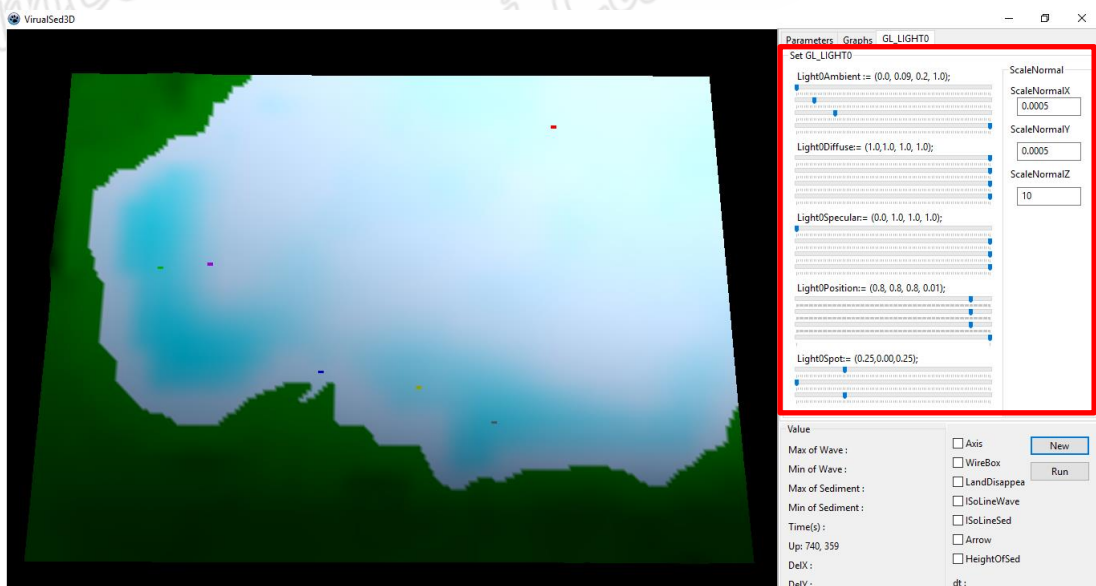
Figure 51 Sliders to control the light

4. Click the Run button to run the program as shown in the figure below:
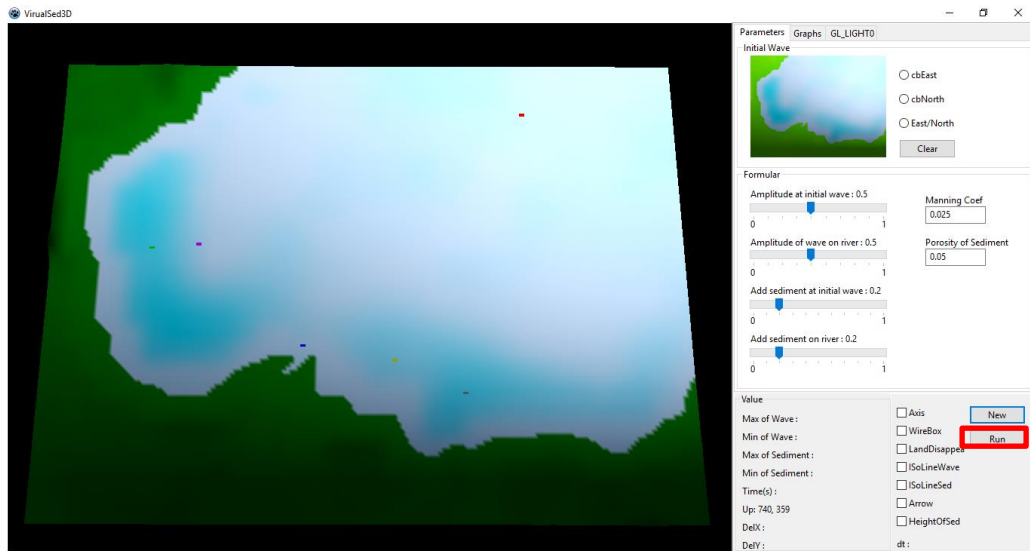
Figure 52 Run button to start the program

Algorithm of the program

The section 3.5.6 in Chapter 3 shows an overview of the algorithm for calculating the results from the model in this research. In the appendix I, the details from the flowchart in section 3.5.6 are described as follows.

<u>**Read Maps**</u>

This section describes loading the topography data.
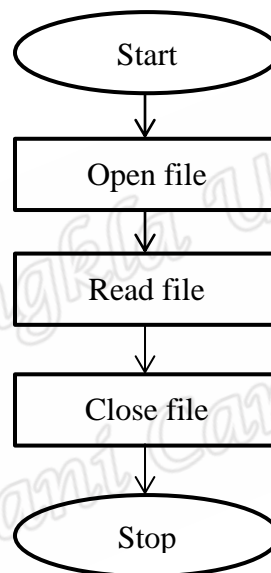
Figure 53 loading topography data

```
procedure ReadMapl();
        AssignFile(F,'C:\\ directory file');
        ReSet(F);
        Readln(F,dataMapW);          Readln(F,dataMapH);
        for j := 0 to dataMapH-1 do
        for i := 0 to dataMapW-1 do
        begin
                Read(F,Topo[i,j]);
        end;    CloseFile(F);
end;
```

Interpolate Data and Set Initial Values

This section describes the steps to interpolate and to set the initial data and this can be inputted by the user. The initial data that will be used in the simulation are the height of sediment (z), depth of water (h) and the rate of water flow per one unit in the x and y directions (uh, vh), respectively. The steps involved in the calculations are as follows
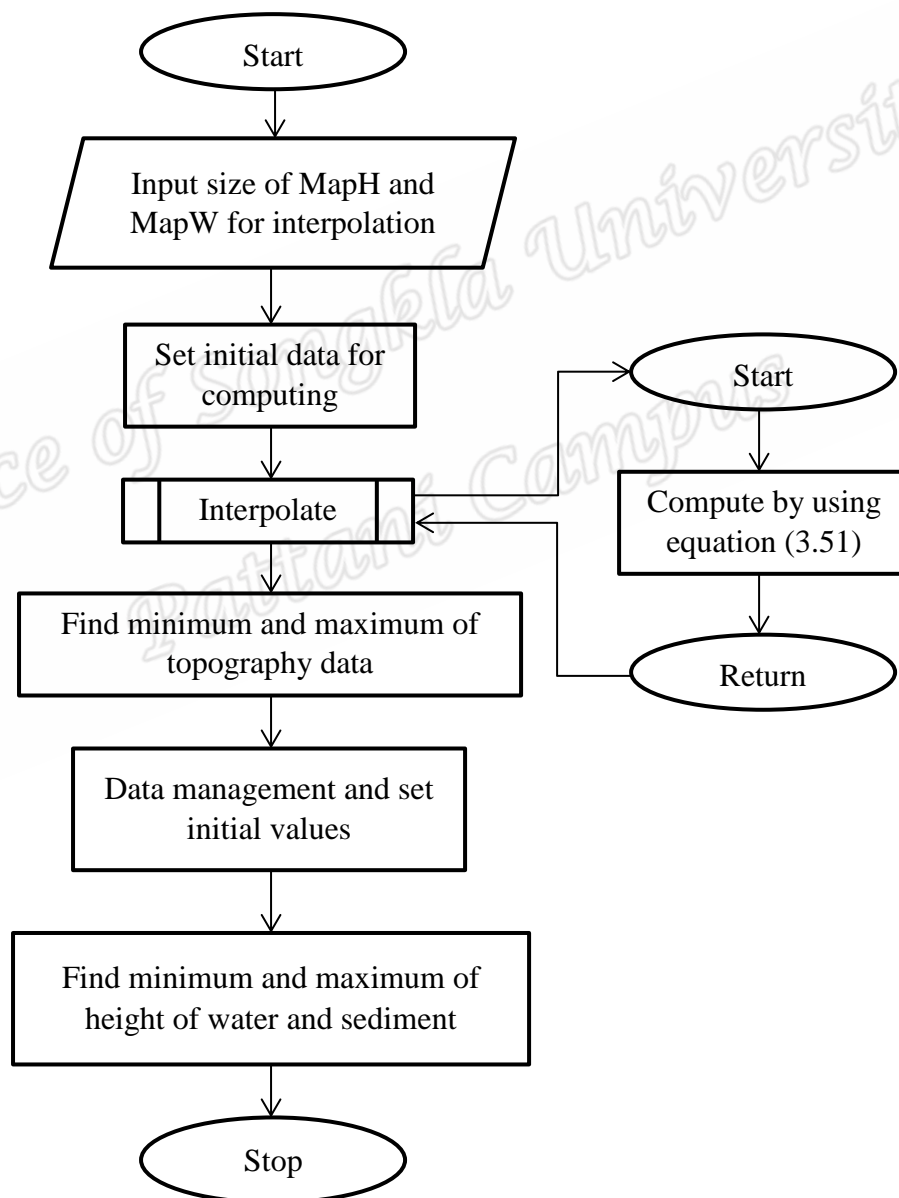
Figure 54 Set initial value and interpolate data

```
procedure SetInitialValue();
begin
        MapW  := size of data to interpolate;
        MapH  := size of data to interpolate;
        t:=0;              dt:=0;              umax := 0;         timestep := 0;
        dx := MapW;        dy := MapH;      FCoef := 0.025;    SCoef := 0.43;
        an := 0;           bn := 1;         cn := 2;


        for j:=0 to MapH-1 do
        for i:=0 to MapW-1 do
        begin
                Data[i,j] :=  Interpolate (i,j);


                if DataMin > Data[i,j] then
                begin
                        DataMin := Data[i,j];
                end
                else if DataMax < Data[i,j] then
                begin
                        DataMax := Data[i,j];
                end;
        end;


        for j := 0 to MapH-1 do
        for i := 0 to MapW-1 do
        begin
                U[an,i,j].uh  :=  0;
                U[an,i,j].vh  :=  0;
                U[an,i,j].h  :=  0;
                U[an,i,j].z  :=  abs(DataMin)+Data[i,j];
                U[an,i,j].h  :=  max(0,abs(DataMin)-U[an,i,j].z);
```

```
                U[bn,i,j]:=U[an,i,j];
                U[cn,i,j]:=U[an,i,j];


                if DataMinH > U[an,i,j].h then
                begin
                        DataMinH := U[an,i,j].h;
                end
                else if DataMaxH < U[an,i,j].h then
                begin
                        DataMaxH :=  U[an,i,j].h;
                end;
                if DataMinZ > U[an,i,j].z then
                begin
                        DataMinZ := U[an,i,j].z;
                end
                else if DataMaxZ < U[an,i,j].z then
                begin
                        DataMaxZ := U[an,i,j].z;
                end;
        end;
end;


function Interpolate(imap,jmap);
begin
        x := (imap)*(dataMapW-1)/(MapW-1);
        y := (jmap)*(dataMapH-1)/(MapH-1);
        i := floor(x);    j := floor(y);
        ee := topo[i,j]*(i+1-x)*(j+1-y)+topo[min(i+1,dataMapW-1),j]*(x-i)*(j+1-y)
            +topo[i,min(j+1,dataMapH-1)]*(i+1-x)*(y-j)+topo[min(i+1,dataMapW-1),
            min(j+1,dataMapH-1)]*(x-i)*(y-j);
        Settopography:=ee;
end;
```

Set Boundary

This section defines the 4 edges of the boundary. In this research, an open and closed boundary is considered. The steps for configuring are
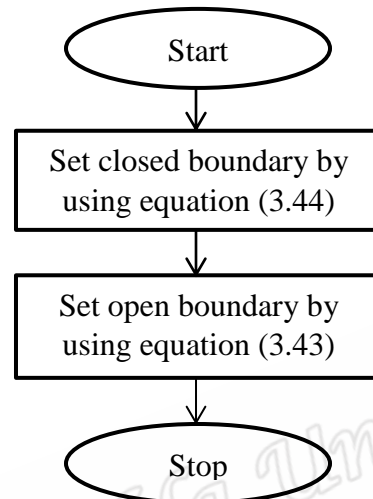
Figure 55 Set boundary condition

```
procedure Setboundary();
begin
        for j:=1 to MapH-2 do      //close boundary
        for i:=1 to MapW-2 do
        begin
                if (U[an,i,j].h = 0) then
                begin
                        U[an,i,j].h := 0;
                        U[an,i,j].uh:= 0;
                        U[an,i,j].vh:= 0;
                        ur[i,j]:=0;   ul[i,j]:=0;   uu[i,j]:=0;   ud[i,j]:=0;
                        vr[i,j]:=0;   vl[i,j]:=0;   vu[i,j]:=0;   vd[i,j]:=0;
                        hr[i,j]:=0;   hl[i,j]:=0;   hu[i,j]:=0;   hd[i,j]:=0;
                end;
        end;
```

```
for j:=0 to MapH-1 do  //open boundary
begin
      i := 0
      U[an,i,j] := U[an,i+1,j];
      U[bn,i,j] := U[an,i,j];
      U[cn,i,j] := U[an,i,j];
      u11 := sqrt(2) * (U[an,i,j].uh * U[an,i,j].h) / sqrt(power(U[an,i,j].h,4) +
            max(power(U[an,i,j].h,4),small));
      v11 := sqrt(2) * (U[an,i,j].vh * U[an,i,j].h) / sqrt(power(U[an,i,j].h,4) +
            max(power(U[an,i,j].h,4),small));
      ur[i,j] := u11;    ul[i,j] := u11;    uu[i,j] := u11;        ud[i,j] := u11;
      vr[i,j] := v11;    vl[i,j] := v11;    vu[i,j] := v11;        vd[i,j] := v11;
      v11 := U[an,i,j].h;
      hr[i,j] := v11;    hl[i,j] := v11;    hu[i,j] := v11;        hd[i,j] := v11;
      v11:=U[an,i,j].z;
      zr[i,j] := v11;    zl[i,j] := v11;    zu[i,j] := v11;        zd[i,j] := v11;

      i := MapW-1;
      U[an,i,j] := U[an,i-1,j];
      U[bn,i,j] := U[an,i,j];
      U[cn,i,j] := U[an,i,j];
      u11 := qrt(2) * (U[an,i,j].uh * U[an,i,j].h) / sqrt(power(U[an,i,j].h,4) +
            max(power(U[an,i,j].h,4),small));
      v11 := sqrt(2) * (U[an,i,j].vh * U[an,i,j].h) / sqrt(power(U[an,i,j].h,4) +
            max(power(U[an,i,j].h,4),small));
      ur[i,j] := u11;    ul[i,j] := u11;    uu[i,j] := u11;    ud[i,j] := u11;
      vr[i,j] := v11;    vl[i,j] := v11;    vu[i,j] := v11;    vd[i,j] := v11;
      v11:=U[an,i,j].h;
      hr[i,j]:=v11;      hl[i,j] := v11;    hu[i,j] := v11;    hd[i,j]:=v11;
      v11:=U[an,i,j].z;
      zr[i,j]:=v11;      zl[i,j]:=v11;      zu[i,j]:=v11;      zd[i,j]:=v11;
end;
```

```
for i:=0 to MapW-1 do
begin
        j:=0;
        U[an,i,j] := U[an,i,j+1];
        U[bn,i,j] := U[an,i,j];
        U[cn,i,j] := U[an,i,j];
        u11 := sqrt(2) * (U[an,i,j].uh * U[an,i,j].h) / sqrt(power(U[an,i,j].h,4) +
                max(power(U[an,i,j].h,4),small));
        v11 := sqrt(2) * (U[an,i,j].vh * U[an,i,j].h) / sqrt(power(U[an,i,j].h,4) +
                max(power(U[an,i,j].h,4),small));
        ur[i,j] := u11;    ul[i,j] := u11;    uu[i,j] := u11;    ud[i,j] := u11;
        vr[i,j] := v11;    vl[i,j] := v11;    vu[i,j] := v11;    vd[i,j] := v11;
        v11 := U[an,i,j].h
        hr[i,j] := v11;    hl[i,j] := v11;    hu[i,j] := v11;    hd[i,j] := v11;
        v11 := U[an,i,j].z;
        zr[i,j] := v11;    zl[i,j] := v11;    zu[i,j] := v11;    zd[i,j] := v11;

        j:=MapH-1;
        U[an,i,j] := U[an,i,j-1];
        U[bn,i,j] := U[an,i,j];
        U[cn,i,j] := U[an,i,j];
        u11 := sqrt(2) * (U[an,i,j].uh * U[an,i,j].h) / sqrt(power(U[an,i,j].h,4) +
                max(power(U[an,i,j].h,4),small));
        v11 := sqrt(2) * (U[an,i,j].vh * U[an,i,j].h) / sqrt(power(U[an,i,j].h,4) +
                max(power(U[an,i,j].h,4),small));
        ur[i,j]:=u11;    ul[i,j]:=u11;    uu[i,j]:=u11;    ud[i,j]:=u11;
        vr[i,j]:=v11;    vl[i,j]:=v11;    vu[i,j]:=v11;    vd[i,j]:=v11;
        v11:=U[an,i,j].h;
        hr[i,j]:=v11;    hl[i,j]:=v11;    hu[i,j]:=v11;    hd[i,j]:=v11;
        v11:=U[an,i,j].z;
        zr[i,j]:=v11;    zl[i,j]:=v11;    zu[i,j]:=v11;    zd[i,j]:=v11;
end;    end;
```

Set Initial Wave

This section defines the initial condition for the simulation.
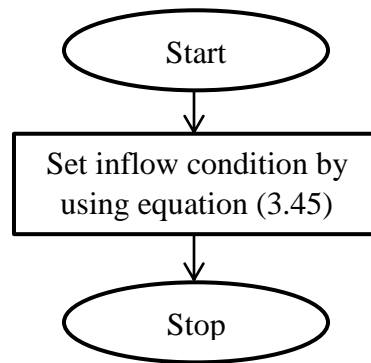
Figure 56 Set initial wave

```
procedure InitialWave();
begin
        for j := 0 to resizedbitmap.Height-1 do
        for i := 0 to resizedbitmap.Width-1 do
        begin
                if (Image1.Canvas.Pixels[i,j]=clBlack) then
                begin
                        if U[an,i,j].h > 0 then
                         begin
                                U[an,i,j].h:= max(0.1,(abs(DataMin)+Amp*sin
                                (timestep*pi/45))-U[an,i,j].z);
                           U[an,i,j].uh:=0;
                                U[an,i,j].vh:=0;
                                U[bn,i,j]:=U[an,i,j];
                                U[cn,i,j]:=U[an,i,j];
                        end;
                end;
        end;
```

```
if ((cbNorth.Checked = true) or (BothEastNorth.Checked = true)) then
begin
        for i:=0 to MapW-1 do
        begin   if U[an,i,1].h > 0 then
                begin
                        U[an,i,1].h:= max(0.1,(abs(DataMin) + Amp *
                                        sin(timestep * pi / 45)) - U[an,i,1].z);
                        U[an,i,1].z:=TmpNB[i,0]+Sed;
                        U[an,i,1].uh:=0;
                        U[an,i,1].vh:=0;
                        U[bn,i,1]:=U[an,i,1];
                        U[cn,i,1]:=U[an,i,1];
                end;
        end;
end;
if ((cbEast.Checked = true) or (BothEastNorth.Checked = true)) then
begin
        for j:=0 to MapH-1 do
        begin   if U[an,MapW-3,j].h > 0 then
                begin
                        U[an,MapW-3,j].h := max(0.1,(abs(DataMin) + Amp *
                                        sin(timestep * pi / 45)) -
                                        U[an,MapW-3,j].z);
                        U[an,MapW-3,j].z := TmpEB[0,j]+Sed;
                        U[an,MapW-3,j].uh:=0;
                        U[an,MapW-3,j].vh:=0;
                        U[bn,MapW-3,j]:=U[an,MapW-3,j];
                        U[cn,MapW-3,j]:=U[an,MapW-3,j];
                end;
        end;
end;
end;
```

Reconstruction

In this section, data at the edges of the 4 sides of each cell is created to calculate the flux and the results of the model. The details are as follows
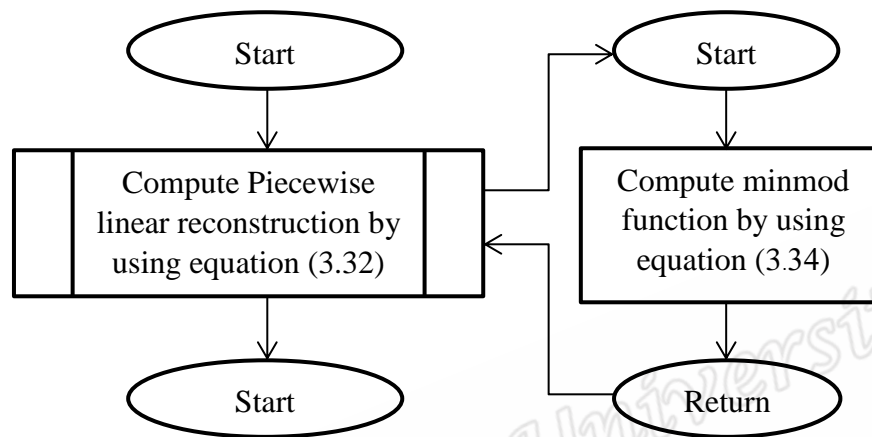

Figure 57 Reconstruction

procedure TForm1.reconstruction(nU);

begin

    for j:=1 **to** MapH-2 **do**

    for i:=1 **to** MapW-2 **do**

    begin

        u01 := dvz(U[nU,i-1,j].uh,U[nU,i-1,j].h);

        u11 := dvz(U[nU,i,j].uh,U[nU,i,j].h);

        u21 := dvz(U[nU,i+1,j].uh,U[nU,i+1,j].h);

        u10 := dvz(U[nU,i,j-1].uh,U[nU,i,j-1].h);

        u12 := dvz(U[nU,i,j+1].uh,U[nU,i,j+1].h);

        v01 := dvz(U[nU,i-1,j].vh,U[nU,i-1,j].h);

        v11 := dvz(U[nU,i,j].vh,U[nU,i,j].h);

        v21 := dvz(U[nU,i+1,j].vh,U[nU,i+1,j].h);

        v10 := dvz(U[nU,i,j-1].vh,U[nU,i,j-1].h);

        v12 := dvz(U[nU,i,j+1].vh,U[nU,i,j+1].h);

        dux := 0.5*minmod((u11-u01)/dx,(u21-u11)/dx)*dx;

```
ul[i,j] := u11-dux;
ur[i,j] := u11+dux;


duy := 0.5*minmod((u11-u10)/dy,(u12-u11)/dy)*dy;
uu[i,j] := u11-duy;
ud[i,j] := u11+duy;


dvx := 0.5*minmod((v11-v01)/dx,(v21-v11)/dx)*dx;
vl[i,j] := v11-dvx;
vr[i,j] := v11+dvx;


dvy := 0.5*minmod((v11-v10)/dy,(v12-v11)/dy)*dy;
vu[i,j] := v11-dvy;
vd[i,j] := v11+dvy;

u01 := U[nU,i-1,j].h;
u11 := U[nU,i,j].h;
u21 := U[nU,i+1,j].h;
u10 := U[nU,i,j-1].h;
u12 := U[nU,i,j+1].h;
dhx := 0.5*minmod((u11-u01)/dx,(u21-u11)/dx)*dx;
hl[i,j] := u11-dhx;
hr[i,j] := u11+dhx;
dhy := 0.5*minmod((u11-u10)/dy,(u12-u11)/dy)*dy;
hu[i,j] := u11-dhy;
hd[i,j] := u11+dhy;


u01 := U[nU,i-1,j].z+U[nU,i-1,j].h;
u11 := U[nU,i,j].z+U[nU,i,j].h;
u21 := U[nU,i+1,j].z+U[nU,i+1,j].h;
u10 := U[nU,i,j-1].z+U[nU,i,j-1].h;
u12 := U[nU,i,j+1].z+U[nU,i,j+1].h;
```

```
                    dzx := 0.5*minmod((u11-u01)/dx,(u21-u11)/dx)*dx;
                    zl[i,j] := u11-dzx-hl[i,j];
                    zr[i,j] := u11+dzx-hr[i,j];
                    dzy := 0.5*minmod((u11-u10)/dy,(u12-u11)/dy)*dy;
                    zu[i,j] := u11-dzy-hu[i,j];
                    zd[i,j] := u11+dzy-hd[i,j];

          end;

     end;


Function dvz(a,b);

begin

          dvz:=sqrt(2)*(a*b)/sqrt(power(b,4)+max(power(b,4),small));

end;


Function Minmod(a,b);

begin

          MM:=0.5*(sign(a)+sign(b))*min(abs(a),abs(b));

          Minmod:=MM;

end;
```

Calculate Flux

At this point, the data from the previous sections are used to calculate the flux function. Also, calculate the speed of wave and find out the maximum and minimum of the wave speed to compute $\triangle t$. The details are as follows
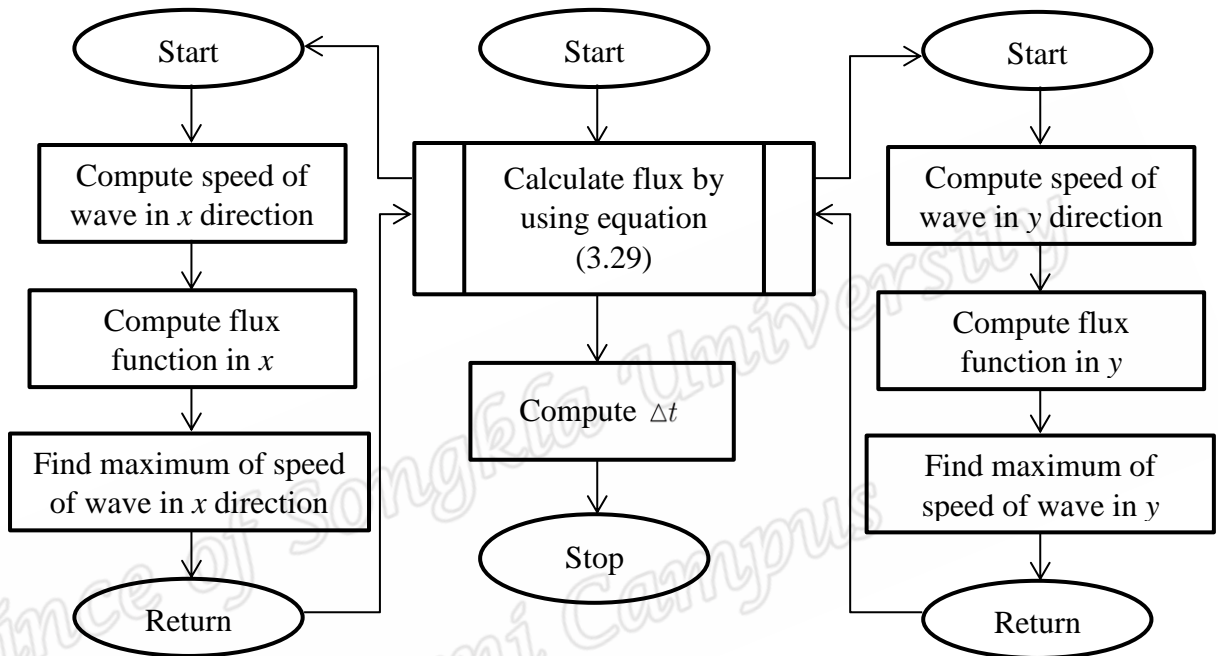

Figure 58 Calculate the flux function

Procedure CalFlux(nU);

begin

    umax:=0;

    for j:=1 **to** MapH-2 **do**

    for i:=1 **to** MapW-2 **do**

    begin

        fr[i,j] := NumericalFluxX(ur[i,j],vr[i,j],hr[i,j],zr[i,j],ul[i+1,j],vl[i+1,j],
hl[i,j+1],zl[i+1,j]);

        fl[i,j] := NumericalFluxX(ur[i-1,j],vr[i-1,j],hr[i-1,j],zr[i-1,j],ul[i,j],
vl[i,j],hl[i,j],zl[i,j]);

        fd[i,j] := NumericalFluxY(ud[i,j],vd[i,j],hd[i,j],zd[i,j],uu[i,j+1],
vu[i,j+1],hu[i,j+1],zu[i,j+1]);

```
                    fu[i,j] := NumericalFluxY(ud[i,j-1],vd[i,j-1],hd[i,j-1],zd[i,j-1],uu[i,j],
vu[i,j],hu[i,j],zu[i,j]);
                    fcx[i,j]:=(g/2)*(hl[i,j]*hl[i,j]- hl[i,j]*hl[i,j])+(g/2)*(hr[i,j]*hr[i,j]-
 hr[i,j]*hr[i,j])+(g/2)*(hl[i,j]+hr[i,j])*(zl[i,j]-zr[i,j]);
                    fcy[i,j]:=(g/2)*(hu[i,j]*hu[i,j]-hu[i,j]*hu[i,j])+(g/2)*(hd[i,j]*
 hd[i,j]-hd[i,j]*hd[i,j])+(g/2)*(hu[i,j]+hd[i,j])*(zu[i,j]-zd[i,j])
        end;

        if umax<>0 then
        begin
                dt := min(0.5*dx/umax,0.5*dy/umax);
        end else
        begin
                dt := min(dx/(2*g),dy/(2*g));
        end;
 end;

Function NumericalFluxX(ul,vl,hl,zl,ur,vr,hr,zr);
begin
        a1 := max(ul+sqrt(g*hl),ur+sqrt(g*hr));
        a1 := max(a1,0);
        a0 := min(ul-sqrt(g*hl),ur-sqrt(g*hr));
        a0 := min(a0,0);
        Flux.h := 0;
        Flux.uh := 0;
        Flux.vh := 0;

        if a1-a0 <> 0 then
        begin
                Flux.h := ((a1*(ul*hl)-a0*(ur*hr))+(a1*a0*(hr-hl)))/(a1-a0);
                Flux.uh := ((a1*(ul*ul*hl+g*hl*hl*0.5)-a0*(ur*ur*hr+g*hr*hr*0.5))
                        +(a1*a0*(ur*hr-ul*hl)))/(a1-a0);
```

```
            Flux.vh := ((a1*(vl*ul*hl)-a0*(vr*ur*hr))+(a1*a0*(vr*hr-vl*hl)))/(a1-a0);
            Flux.z := ((a1*(SCoef*ul*zl)-a0*(SCoef*ur*zr))+(a1*a0*(zr-zl)))/(a1-a0);
      end;
      umax:=max(umax,a1);
      umax:=max(umax,-a0);
      NumericalFluxX:=Flux;
end;


Function NumericalFluxY(uu,vu,hu,zu,ud,vd,hd,zd);
begin
      a1 := max(vu+sqrt(g*hu),vd+sqrt(g*hd));
      a1 := max(a1,0);
      a0 := min(vu-sqrt(g*hu),vd-sqrt(g*hd));
      a0 := min(a0,0);
      Flux.h := 0;
      Flux.uh := 0;
      Flux.vh := 0;

      if a1-a0 <> 0 then
      begin
            Flux.h :=((a1*(vu*hu)-a0*(vd*hd))+(a1*a0*(hd-hu)))/(a1-a0);
            Flux.uh:=((a1*(uu*vu*hu)-a0*(ud*vd*hd))+(a1*a0*(ud*hd-
                        uu*hu)))/(a1-a0);
            Flux.vh:=((a1*(vu*vu*hu+g*hu*hu*0.5)-a0*(vd*vd*hd+g*hd*hd*
                        0.5))+(a1*a0*(vd*hd-vu*hu)))/(a1-a0);
            Flux.z:=((a1*(SCoef*vu*zu)-a0*(SCoef*vd*zd))+(a1*a0*(zd-zu)))
                        /(a1-a0);
      end;
      umax:=max(umax,a1);
      umax:=max(umax,-a0);
      NumericalFluxY:=Flux;
end;
```

Calculate $\overrightarrow{W}^{(k)}$

This algorithm is a procedure for computing the results of the model by ignoring the source term $\triangle t \vec{S}_{i,j}$
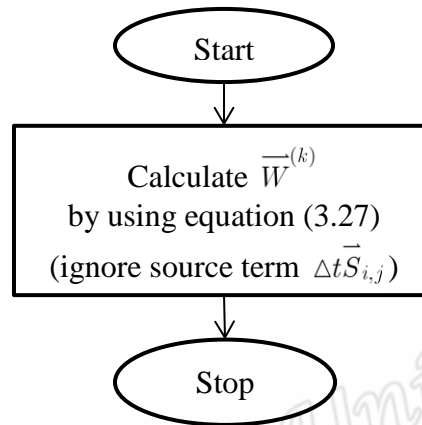

Figure 59 Computation the results of model by ignoring source term

```
procedure CalFlow(nU1,nU2);
begin
        for j:=1 to MapH-2 do
        for i:=1 to MapW-2 do
        begin
                if (U[nU2,i,j].h > 0) then
                begin
                        U[nU2,i,j].h := U[nU1,i,j].h-(dt/dx)*(fr[i,j].h-fl[i,j].h)-
                                        (dt/dy)*(fd[i,j].h-fu[i,j].h);
                        U[nU2,i,j].uh:= U[nU1,i,j].uh-(dt/dx)*(fr[i,j].uh-fl[i,j].uh)-
                                        (dt/dy)*(fd[i,j].uh-fu[i,j].uh)+(dt/dx)*fcx[i,j];
                        U[nU2,i,j].vh:= U[nU1,i,j].vh-(dt/dx)*(fr[i,j].vh-fl[i,j].vh)-
                                        (dt/dy)*(fd[i,j].vh-fu[i,j].vh)+(dt/dy)*fcy[i,j];
                        U[nU2,i,j].z := U[nU1,i,j].z-(dt/dx)*(fr[i,j].z-fl[i,j].z)-
                                        (dt/dy)*(fd[i,j].z-fu[i,j].z);
                end;
        end;
end;
```

Calculate Result $\overrightarrow{W}^{n+1}$

The calculation of the sediment transport including the source term $\triangle t \vec{S}_{i,j}$ can be found as follows

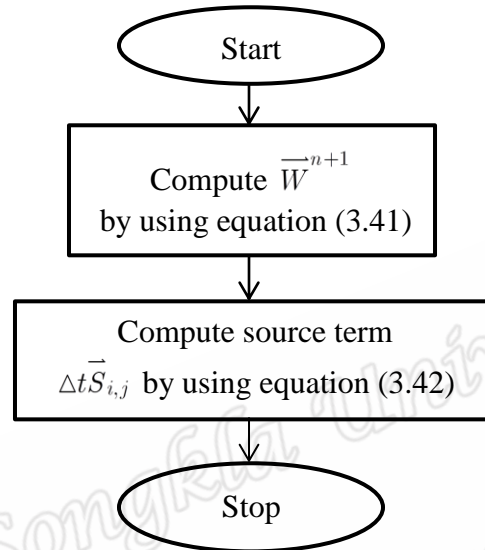**Figure 60** Computation the results of model including source term

```
procedure CalResult();

begin

        for j:=1 to MapH-2 do
        for i:=1 to MapW-2 do
        begin
                U[bn,i,j].h := (U[an,i,j].h+U[cn,i,j].h)*0.5;
                U[bn,i,j].uh := (U[an,i,j].uh+U[cn,i,j].uh)*0.5;
                U[bn,i,j].vh := (U[an,i,j].vh+U[cn,i,j].vh)*0.5;
                U[bn,i,j].z := (U[an,i,j].z+U[cn,i,j].z)*0.5;


                if U[bn,i,j].h > 0 then
                begin
                        ui := dvz(U[an,i,j].uh,U[an,i,j].h);
                        vi := dvz(U[an,i,j].vh,U[an,i,j].h);
```

$$U[bn,i,j].uh := U[bn,i,j].uh/(1+dt*g*(FCoef*FCoef*sqrt(ui*ui +vi*vi))/(power(U[bn,i,j].h,4/3)));$$

$$U[bn,i,j].vh := U[bn,i,j].vh/(1+dt*g*(FCoef*FCoef*sqrt(ui*ui +vi*vi))/(power(U[bn,i,j].h,4/3)));$$

end;

end;

end;

Draw Image

This section shows the step on how to compute the color RGB and draw the image from the results computed in the previous section.
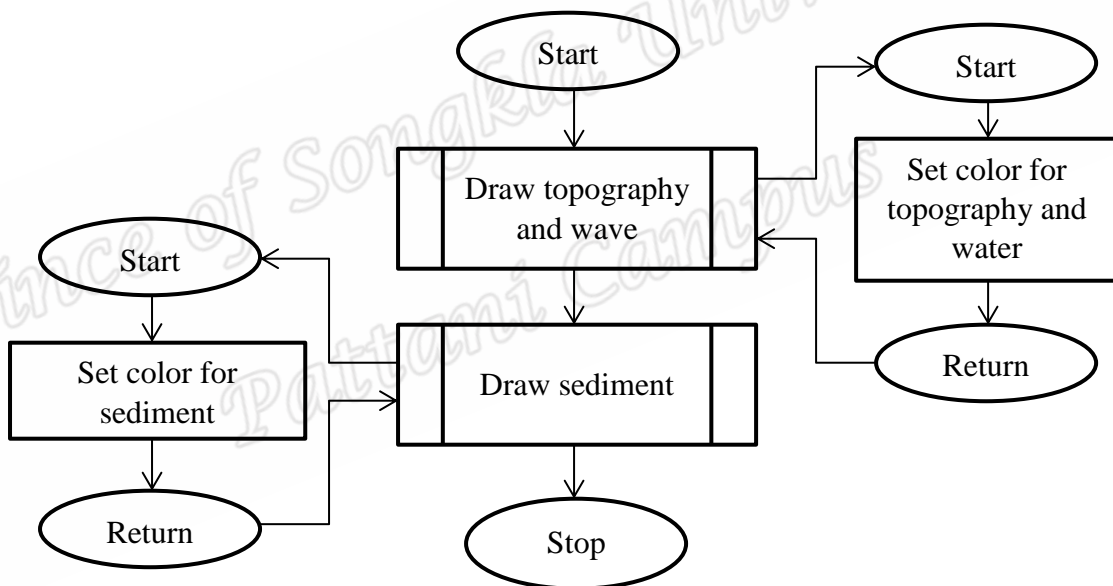

Figure 61 Compute color RGB and draw the image

procedure TForm1.DrawImage;

begin

DataRange := DataMax - DataMin;

DataRangeH := DataMaxH - DataMinH;

DataRangeZ := DataMaxZ - DataMinZ;

```
//------------- Draw Land -----------------
for j := 1 to MapH-3 Do
for i := 1 to MapW-3 Do
begin
        glBegin(GL_QUADS);
        CL := SetRGB(U[an,i,j].h,U[an,i,j].z);
        glColor4f(CL.r/255,CL.g/255,CL.b/255,1);
        glVertex3f(-1+i*(2/MapW), 0.1*((U[an,i,j].h+U[an,i,j].z)/
Datarange)+0.1, -1+j*(2/MapH));

        CL := SetRGB(U[an,i+1,j].h,U[an,i+1,j].z);
        glColor4f(CL.R/255,CL.G/255,CL.B/255,1);
        glVertex3f(-1+(i+1)*(2/MapW), 0.1*((U[an,i+1,j].h+U[an,i+1,j].z)/
Datarange)+0.1, -1+j*(2/MapH));

        CL := SetRGB(U[an,i+1,j+1].h,U[an,i+1,j+1].z);
        glColor4f(CL.R/255,CL.G/255,CL.B/255,1);
        glVertex3f(-1+(i+1)*(2/MapW),0.1*((U[an,i+1,j+1].h+U[an,i+1,j+1].z
)/Datarange)+0.1,-1+(j+1)*(2/MapH));

        CL := SetRGB(U[an,i,j+1].h,U[an,i,j+1].z);
        glColor4f(CL.R/255,CL.G/255,CL.B/255,1);
        glVertex3f(-1+i*(2/MapW),0.1*((U[an,i,j+1].h+U[an,i,j+1].z)/
Datarange)+0.1, -1+(j+1)*(2/MapH));
        glEnd();
    end;

    //----------- Draw Sediment -----------------
    for j := 1 to MapH-3 Do
    for i := 1 to MapW-3 Do
    begin
        glBegin(GL_QUADS);
```

```
            CZ := SetRGBZ(U[an,i,j].z);
            glColor4f(CZ.R/255,CZ.G/255,CZ.B/255,1);
            glVertex3f(-1+i*(2/MapW), 0.1*((U[an,i,j].z)/Datarange), -
1+j*(2/MapH));


            CZ := SetRGBZ(U[an,i+1,j].z);
            glColor4f(CZ.R/255,CZ.G/255,CZ.B/255,1);
            glVertex3f(-1+(i+1)*(2/MapW), 0.1*((U[an,i+1,j].z)/Datarange), -
1+j*(2/MapH));


            CZ := SetRGBZ(U[an,i+1,j+1].z);
            glColor4f(CZ.R/255,CZ.G/255,CZ.B/255,1);
            glVertex3f(-1+(i+1)*(2/MapW), 0.1*((U[an,i+1,j+1].z)/Datarange), -
1+(j+1)*(2/MapH));


            CZ := SetRGBZ(U[an,i,j+1].z);
            glColor4f(CZ.R/255,CZ.G/255,CZ.B/255,1);
            glVertex3f(-1+i*(2/MapW), 0.1*((U[an,i,j+1].z)/Datarange), -
1+(j+1)*(2/MapH));
                glEnd();
        end;
        OpenGLControl1.SwapBuffers;
end;


Function SetRGB(h,z);
begin
        if h>0 then   //blue
        begin
                ColorIndex := Round(253* (h-DataMinH) / DataRangeH);
                CL.r :=ColorWave[ColorIndex].R;
                CL.g :=ColorWave[ColorIndex].G;
                CL.b :=ColorWave[ColorIndex].B;
```

```
        end else
        begin   // green
                ColorIndex := Round(763* (z-DataMinZ) / DataRangeZ);
                CL.r :=ColorMap[ColorIndex].R;
                CL.g :=ColorMap[ColorIndex].G;
                 CL.b :=ColorMap[ColorIndex].B;
        end;
        SetRGB:=CL;
end;


Function SetRGBZ(zz);
begin
        if zz<= abs(DataMin) then
        begin
                ColorIndex := Round(253* zz/(abs(DataMin)));
                CZ.r :=ColorSediment[ColorIndex].R;
                CZ.g :=ColorSediment[ColorIndex].G;
                CZ.b :=ColorSediment[ColorIndex].B;
        end else
        begin
                CZ.r :=96;
                CZ.g :=96;
                CZ.b :=96;
        end;
        SetRGBZ:=CZ;
end;
```

Simulation

This section is a presentation of how the program works in the simulation and visualization of the sediment transport, which contains the procedures computed in previous sections.
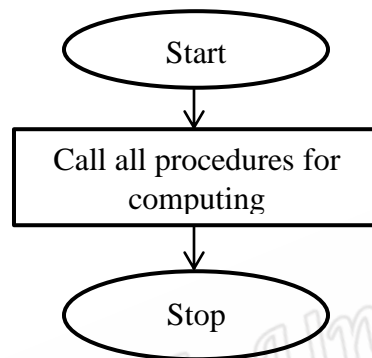

Figure 62 Call all procedure for computing

```
procedure Calflood();
begin
        ReadMap();
        Interpulate();
        SetinitialData();
        If (Run = True) then
        begin
                Setboundary();
                InitialWave();
                Reconstruction(an);
                CalFlux(an);
                CalFlow(an,bn);
                dt1:=dt;

                Setboundary();
                InitialWave();
                Reconstruction(bn);
```

```
            CalFlux(bn);
            CalFlow(bn,cn);
            dt2:=dt;

            dt:=(dt1+dt2)/2;
            CalResult();
            tmp:=an;
            an:=bn;
            bn:=tmp;
            DrawImage();
        end;
    end;
```

APPENDIX II

Map Data

Appendix II presents the map data used in the study. It was downloaded from the Global 30 Arc-Second Elevation Data Set. The data in this study considered longitude at 99.20416667 to 99.49583333 from the west to the east and latitude at 9.387500 to 9.170833 from the north to south. Therefore, from one latitude-longitude point, the measurement from the SRTM 30 is approximated to 1 kilometer which gives 36 kilometers from west to east and 27 kilometers from north to south. The raw data is shown below.
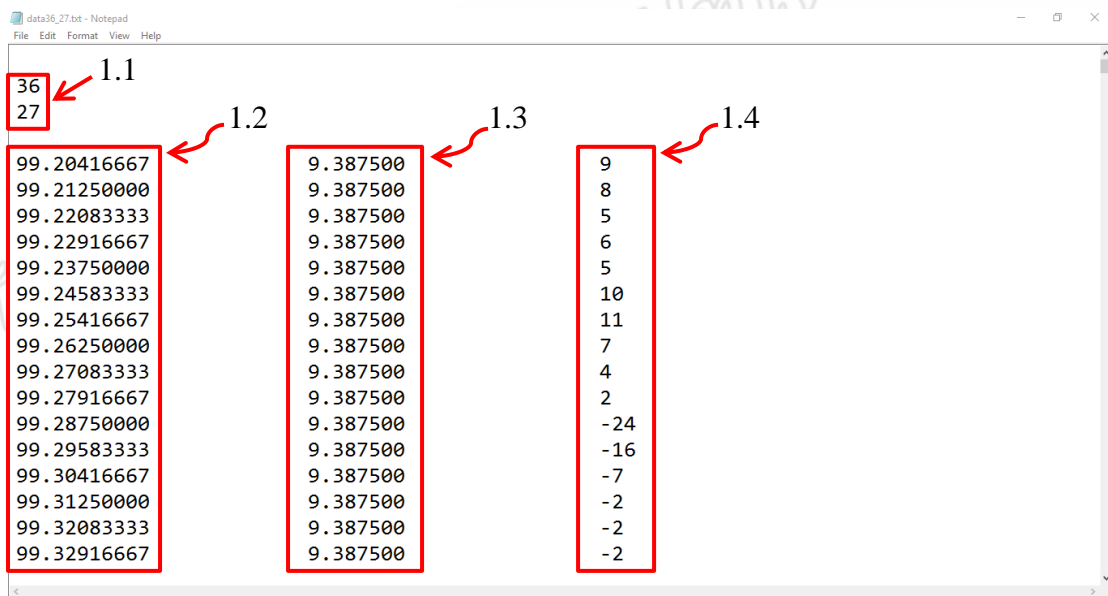

Figure 63 Data from GTOPO30 (Global 30 Arc-Second Elevation Data Set)

Map data with longitude having 36 points and latitude having 27 points.

1.1 Longitude data in the vertical section

1.2 Latitude data in the vertical section

1.3 Topography data

The data is then interpolated to 200 meters (explanation in section 4.2 in chapter 4 of this study) and this is shown in Figure 64.

Figure 64 Data after interpolation

After interpolation to a 200 meters, 180 points for longitude, that is from west to east and 135 points for latitude that is from north to south can be obtained. Figure 64 therefore shows the data after interpolation.

1.1 180 points and 135 points for longitude and latitude respectively.

1.2 Latitude and longitude from raw data.

1.3 Data after interpolation.

APPENDIX III

ภาควิชาคณิตศาสตร์และวิทยาการคอมพิวเตอร์

คณะวิทยาศาสตร์ จุฬาลงกรณ์มหาวิทยาลัย

ขอมอบเกียรติบัตรเพื่อแสดงว่า

นิธินันท์ พงษ์ศิริ

ได้นำเสนอผลงานและเข้าร่วม

การประชุมวิชาการทางคณิตศาสตร์ประจำปี 2559 ครั้งที่ 21 (AMM 2016)

การประชุมวิชาการคณิตศาสตร์บริสุทธิ์และประยุกต์ประจำปี 2559 (APAM 2016)

ณ คณะวิทยาศาสตร์ จุฬาลงกรณ์มหาวิทยาลัย

ระหว่างวันที่ 23 – 25 พฤษภาคม 2559

(ศาสตราจารย์ ดร.กฤษณะ เนียมมณี)
ประธานคณะกรรมการจัดการประชุม

(ศาสตราจารย์ ดร.ชิดชนก เหลือสินทรัพย์)
หัวหน้าภาควิชาคณิตศาสตร์และวิทยาการคอมพิวเตอร์

Mathematical Simulation and Visualization of Sediment Distribution at Bandon Bay in Surat Thani

Nitinun Pongsiri [1,1] and Somporn Chuai-Aree [2,2]

[1,2]Department of Mathematics and Computer Science,
Faculty of Science and Technology, Prince of Songkla University, Pattani Campus
[2]Centre of Excellence in Mathematics, CHE, Si Ayutthaya Rd., Bangkok 10400, Thailand
[1]pnitinun@gmail.com, [2]somporn.c@psu.ac.th

Abstract

Sediment transport plays a big role for changing the beach and bay properties. A mathematical model to study the sediment distribution at Bandon Bay, Surat Thani, Thailand is presented. The shallow water equations that is used in this study are based on some basic principles of the laws of conservation of mass and momentum. The Navier-Stoke equation was used to simplify the shallow water equations. The numerical method to solve the mathematical model was obtained by using the finite volume method. This was done on the basis of the integral form of the conservation laws based on the approximation to the integral of certain quantities over each volume. Simulation is carried out and visualized by VirtualSed3D programmed by Lazarus Free-Pascal software. It shows the sediment distribution depends on the continuous propagation of wave and also the depth of a particular area under consideration. The presented sediment transport model can be used to apply for other regions.

Mathematics Subject Classification: 68U20

Keywords: shallow water equations, sediment distribution and Grass model, simulation and visualization Bandon-Bay, VirtualSed3D

---

[1] Corresponding author

[2] The author is supported by the Centre of Excellence in Mathematics, Commission on Higher Education, Thailand.

1 Introduction

Mathematical models have been widely used in the study of environmental phenomena for sediment transport. Sediment transport is the movement of organic particles by current and water [7]. Water flow can be strong enough to suspend particles in the water column as they move downstream or particles push them along the bottom of a water way [10]. Sediment transport process may include mineral matter, chemicals, substances, pollutants and organic material [11].

Sediment distribution can cause some problems to groups of people who live near the coast and the marine organisms living along the coast in bays, shallow water and estuaries [9]. While sediment is needed to build aquatic habitats and reintroduce nutrients for grasses that grow along the coast, too much or little sediment can easily cause ecosystem and safety issues. Whether the concerns are caused by erosion or excessive turbidity the sediment transport rate is an essential environmental factor to be considered [12].

The area of interest for this research is Bandon Bay in Surat Thani, ThaiLand shown in figure 1.

Figure 1 Bandon Bay in Surat Thani, Thailand [5].

Surat Thani is the largest province in the southern part of Thailand with long coastal line of about 120 kilometers. There are 11 different rivers that flow into the bay. The bay is relatively shallow with water depths ranging from 1 to 5 meters.

This paper would primarily discuss about sediment distribution at Bandon Bay by using the shallow water equations (SWEs) and together with the sediment transport by following conservation of mass from shallow water equations and Grass models to analyze wave movement using the Lazarus programing software.

2 Methodology

The SWEs were used in the study of sediment transport at Bandon Bay. The advection diffusion model would be used in calculating for the movement of the sediment in the shallow water. The SWEs are derived based on some basic principles of the laws of conservation of mass and momentum [2]. The Navier-Stroke equation was used to simplify the formulated shallow water equations.
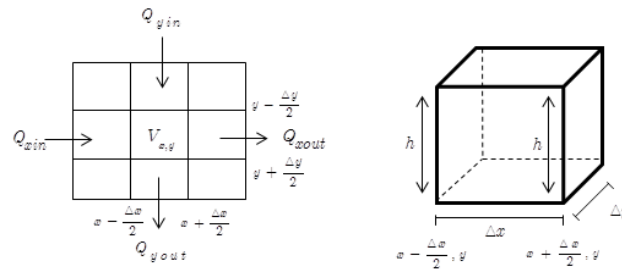
Conservation of Mass

Figure 2a Wave direction in grid form.   **Figure 2b** Depth of water.

Wave propagation is considered in the x and y directions as shown in figure 2a. The height of water (depth of water) is shown in figure 2b.

From figure 2a and 2b, the rate of change of volume of water at point in the x and y directions is

$$\frac{\partial V}{\partial t} = Q_{xin} - Q_{xout} + Q_{yin} - Q_{yout}. \tag{1}$$

The volume of the water (V) at points x and y is obtained by multiplying the water depth with the base area. This gives

$$\frac{\partial(\Delta x \Delta y h)}{\partial t} = (hu\Delta y)_{xin} - (hu\Delta y)_{xout} + (hv\Delta x)_{yin} - (hv\Delta x)_{yout}, \tag{2}$$

where u and v are the velocities of water flow in the x and y directions, respectively, h is the depth of water at point x and y, Δx and Δy are the length and width of volume control, respectively.

Dividing both side of equation (2) by constants Δx and Δy, we have

$$\frac{\partial h}{\partial t} = \frac{(uh)_{x-\Delta x/2,y} - (uh)_{x+\Delta x/2,y}}{\Delta x} + \frac{(vh)_{x,y-\Delta y/2} - (vh)_{x,y+\Delta y/2}}{\Delta y}. \tag{3}$$

Using the Taylor series expansion and omitting higher order terms in dx and dy, we have

$$\left.\begin{aligned}
(uh)_{x-\Delta x/2,y} &= (uh)_{x,y} - \frac{\partial(uh)}{\partial x}\frac{\Delta x}{2} + O(\Delta x^2), \\
(uh)_{x+\Delta x/2,y} &= (uh)_{x,y} + \frac{\partial(uh)}{\partial x}\frac{\Delta x}{2} + O(\Delta x^2), \\
(vh)_{x,y-\Delta y/2} &= (vh)_{x,y} - \frac{\partial(vh)}{\partial y}\frac{\Delta y}{2} + O(\Delta y^2), \\
(vh)_{x,y+\Delta y/2} &= (vh)_{x,y} + \frac{\partial(vh)}{\partial y}\frac{\Delta y}{2} + O(\Delta y^2).
\end{aligned}\right\} \tag{4}$$

Substituting (4) in to (3), we obtain

$$\frac{\partial h}{\partial t} = -\frac{\partial(uh)}{\partial x} - \frac{\partial(vh)}{\partial y}.$$

Therefore, the conservation of mass equation can be written quantitatively as

$$\frac{\partial h}{\partial t} + \frac{\partial(uh)}{\partial x} + \frac{\partial(vh)}{\partial y} = 0. \tag{5}$$

Conservation of Momentum

The conservation of mass is calculated in a similar manner as the conservation of momentum equation. The depth of water in equation (5) h is changed to be the momentum in the control volume (M) and which is equal to the net influx of momentum plus the net force acting on the control volume.

Therefore, we obtain

$$\frac{\partial M}{\partial t} + \frac{\partial (uM)}{\partial x} + \frac{\partial (vM)}{\partial y} = F \,, \tag{6}$$

where F is the force acting on the control volume.

The momentum in the control volume is $\rho Q_x \triangle x$ where ρ is the pressure of water and Q_x is the rate of flow of water in the x direction, therefore the rate of momentum in the control volume will be

$$\frac{\partial (\rho Q_x \triangle x)}{\partial t} + \frac{\partial (u\rho Q_x \triangle x)}{\partial x} + \frac{\partial (v\rho Q_x \triangle x)}{\partial y} = F \,. \tag{7}$$

Three forces acting on the control volume are the pressure force (F_p), gravitational force (F_g) and bed friction force (F_{fx}). These forces are calculated and the final equations are shown below,

pressure Force (F_p)

$$F_p = -\triangle x \triangle y h \frac{\partial (\rho g h)}{\partial x} \,, \tag{8}$$

gravitational Force (F_g)

$$F_g = -\rho g \triangle x \triangle y h \frac{\partial z}{\partial x} \,, \tag{9}$$

bed Friction Force (F_{fx})

$$F_{fx} = -\rho g \triangle x \triangle y h \frac{n^2 \sqrt{u^2 + v^2}\, u}{h^{4/3}} \,. \tag{10}$$

Therefore, the conservation of momentum equation in x direction can be written quantitatively as

$$\frac{\partial uh}{\partial t} + \frac{\partial u^2 h}{\partial x} + \frac{g}{2}\frac{\partial h^2}{\partial x} + \frac{\partial vuh}{\partial y} = -gh\frac{\partial z}{\partial x} - g\frac{n^2 \sqrt{u^2 + v^2}\, uh}{h^{4/3}} \,.$$

Similarly, the momentum in y direction is

$$\frac{\partial vh}{\partial t} + \frac{\partial vuh}{\partial x} + \frac{\partial v^2 h}{\partial y} + \frac{g}{2}\frac{\partial h^2}{\partial y} = -gh\frac{\partial z}{\partial y} - g\frac{n^2 \sqrt{u^2 + v^2}\, vh}{h^{4/3}} \,.$$

The equations above were used to simulate and visualize the movement of wave in the studied area.

Sediment Transport Equation

In this section, we present the sediment transport model by using conservation of mass equation from the shallow water equations and the Grass model as used by [4] in (11) and (12), respectively in one dimension to confirm the validity of the sediment transport model proposed in this study.

They are given as

$$\frac{\partial z}{\partial t} + \rho_x \frac{\partial uz}{\partial x} = 0\,,\tag{11}$$

$$\frac{\partial z}{\partial t} + \xi \frac{\partial q_{bx}}{\partial x} = 0\,,\tag{12}$$

where $\xi = \dfrac{1}{1 - \rho_x}$ and ρ_x is the porosity of the sediment layer, u represents the velocity in the x direction and z is the height of slope bed.

By following the Grass model as used by [4], the following formula for the solid transport discharge is given by

$$q_{bx} = A_g u \left| u \right|^{mg-1} ; 1 \le m_g \le 4\,,$$

where A_g is the constant determined from experimental data. This constant takes values between 0 and 1 and according to Grass model, the bed-load sediment transport begins as soon as the fluid starts to move.

This study focuses on a two dimensional sediment transport model by using conservation of mass equation from the shallow water equations in equation (13).

$$\frac{\partial z}{\partial t} + \rho_x \frac{\partial uz}{\partial x} + \rho_y \frac{\partial vz}{\partial y} = 0\,.\tag{13}$$

Finally, the shallow water equations and the sediment transport equations are put together as follows

$$\left.\begin{array}{c} \dfrac{\partial h}{\partial t} + \dfrac{\partial(uh)}{\partial x} + \dfrac{\partial(vh)}{\partial y} = 0, \\[2mm] \dfrac{\partial uh}{\partial t} + \dfrac{\partial u^2 h}{\partial x} + \dfrac{g}{2}\dfrac{\partial h^2}{\partial x} + \dfrac{\partial vuh}{\partial y} = -gh\dfrac{\partial z}{\partial x} - g\dfrac{n^2\sqrt{u^2+v^2}\,uh}{h^{4/3}}, \\[2mm] \dfrac{\partial vh}{\partial t} + \dfrac{\partial vuh}{\partial x} + \dfrac{\partial v^2 h}{\partial y} + \dfrac{g}{2}\dfrac{\partial h^2}{\partial y} = -gh\dfrac{\partial z}{\partial y} - g\dfrac{n^2\sqrt{u^2+v^2}\,vh}{h^{4/3}}, \\[2mm] \dfrac{\partial z}{\partial t} + \rho_x \dfrac{\partial uz}{\partial x} + \rho_y \dfrac{\partial vz}{\partial y} = 0. \end{array}\right\}\tag{14}$$

Boundary Conditions

In this study, an open and closed boundary were considered in the calculation of the entire area. In this way, the water can go out from the boundary without any restrictions. The value at the boundary is equal to the adjacent edges of the area. That is $z_{0,j} = z_{1,j}$, $z_{i,0} = z_{i,1}$,

$$z_{m_x-1,j} = z_{m_x-2,j}, \quad z_{i,m_y-1} = z_{i,m_y-2}, \quad \vec{w}_{0,j} = \vec{w}_{1,j}, \quad \vec{w}_{i,0} = \vec{w}_{i,1}, \quad \vec{w}_{m_x-1,j} = \vec{w}_{m_x-2,j} \quad \text{and}$$

$$\vec{w}_{i,m_y-1} = \vec{w}_{i,m_y-2}.$$

For the closed boundary, the depth of water (h) is set to 0 indicating land. This is a condition imposed on the system to stop the computation when h is equal zero.

Initial condition

The initial condition for the simulation process is obtained by using the following formula.

$$ic = s + amp * \sin(\Delta t * \pi / 45),$$

where s is the sea level and amp is the amplitude.

Numerical Method and Simulation

The numerical solution to the proposed mathematical model is obtained by using the finite volume method. This is done on the basis of the integral form of conservation laws based on the approximation to the integral of certain quantities over each volume. In the derivation of the 2-D conservation law, the numerical domain is subdivided into rectangular grid cells.

Equation (13) can be written in the vector form as

$$\frac{\partial \vec{w}}{\partial t} + \frac{\partial f(\vec{w})}{\partial x} + \frac{\partial g(\vec{w})}{\partial y} = -\vec{z} - \vec{s}. \tag{15}$$

The vector form is integrated and finally the solution can be written in the form

$$\vec{W}_{i,j}^{n+1} = \vec{W}_{i,j}^{n} - \frac{\Delta t}{\Delta x}\left[\vec{F}_{i+\frac{1}{2},j}^{n} - \vec{F}_{i-\frac{1}{2},j}^{n}\right] - \frac{\Delta t}{\Delta y}\left[\vec{G}_{i,j+\frac{1}{2}}^{n} - \vec{G}_{i,j-\frac{1}{2}}^{n}\right] - \Delta t \vec{Z}_{i,j}^{n} - \Delta t \vec{S}_{i,j}^{n}, \tag{16}$$

where $\vec{W}_{i,j}^{n}$ represents a cell average over the (i,j) grid cell at time t_n, i.e.,

$$\vec{W}_{i,j}^{n} \approx \iint_{c_{i,j}} \vec{W}(x,y,t)dxdy,$$

$\vec{F}_{i-\frac{1}{2},j}^{n}$ is an approximation of the average flux along $x = x_{i-\frac{1}{2},j}$, i.e.,

$$\vec{F}_{i-\frac{1}{2},j}^{n} \approx \frac{1}{\Delta t \Delta y} \int_{n}^{n+1} \int_{j-\frac{1}{2}}^{j+\frac{1}{2}} f(\vec{w}(x_{i-\frac{1}{2}},y,t))dydt,$$

$\vec{G}_{i,j-\frac{1}{2}}^{n}$ is an approximation of the average flux along $y = y_{i,j-\frac{1}{2}}$, i.e.,

$$\vec{G}_{i-\frac{1}{2},j}^{n} \approx \frac{1}{\Delta t \Delta x} \int_{n}^{n+1} \int_{i-\frac{1}{2}}^{i+\frac{1}{2}} g(\vec{w}(x,y_{i-\frac{1}{2}},t))dxdt,$$

$\vec{Z}_{i,j}^{n}$ is the gravity force vector, i.e.,

$$\vec{Z}_{i,j}^{n} \approx \frac{1}{\Delta t \Delta x \Delta y} \int_{n}^{n+1} \iint_{c_{i,j}} \vec{z}dxdydt,$$

and, $\vec{S}_{i,j}^{n}$ is the source vector, i.e.,

$$\vec{S}_{i,j}^{n} \approx \frac{1}{\Delta t \Delta x \Delta y} \int_{n}^{n+1} \iint_{c_{i,j}} \vec{s}dxdydt.$$

Topography Interpolation

The land data used in this study is based on a 1 kilometer average topography which was derived using the USGS SRTM30 gridded digital elevation model (DEM) data product. The DEM was created with data from the NASA shuttle radar topography mission [1]. It is possible for the grid cell resolution to be higher than the data obtained, therefore a topography interpolation is required. The bilinear interpolation technique was used to obtain the height of the topography interpolation [3]. The cell approximation at (i, j) is obtained by

$$Z_{i,j} = Z_{x,y}(x+1-m)(y+1-n) + Z_{x+1,y}(m-x)(y+1-n)$$
$$+Z_{x,y+1}(x+1-m)(n-y) + Z_{x+1,y+1}(m-x)(n-y),$$

where (x, y) is the spatial index of the topography data grid cell with $x = \lfloor m \rfloor$ and $y = \lfloor n \rfloor$.

Two indices as

$$m = i \times n_d^x n_c^x \text{ and } n = j \times n_d^y n_c^y$$

are the mapped indices of (i, j) onto the data grid cells, where n_d^x and n_d^y are the number of columns and rows of the topography data grids, n_c^x and n_c^y are the number of columns and rows of the computational grids, respectively.

3 Results and Discussion

In this section, simulation and visualization in the study were investigated by using the Lazarus programming namely VirtualSed3D software. The sediment transport model by following the conservation of mass equation from the shallow water equations used in this study is validated by comparing it with the Grass model.
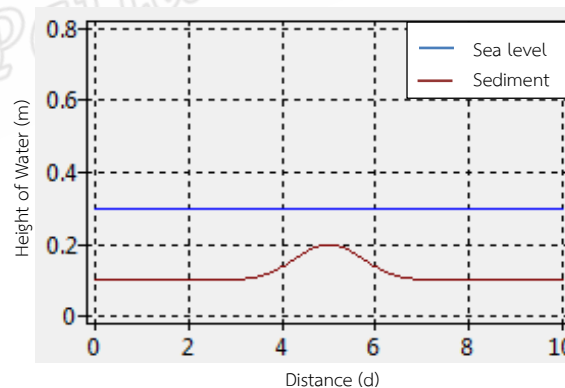

Figure 3 Initial condition for sediment transport in one-dimensional at time *t = 0*.

Figure 3 shows a one-dimensional shallow water equations model. At time *t = 0*, the level of water is at 0.3 meters and the level of the sediment is at 0.1 meters and rises at a point 0.2 meters.
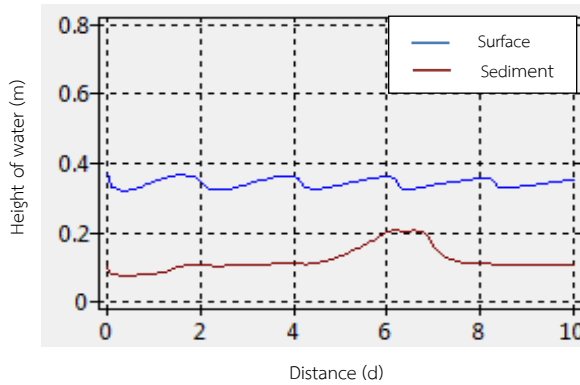
Figure 4a Graph of sediment transport from the conservation of mass equation at time $t = 10$ s.
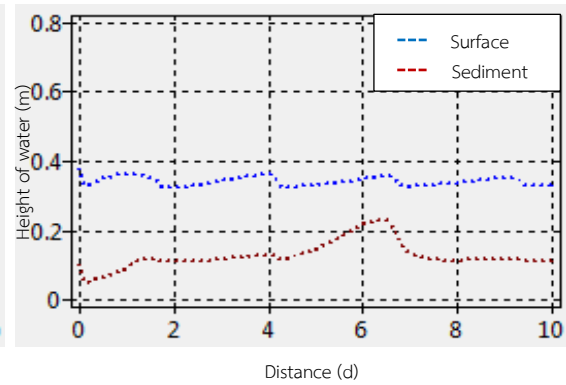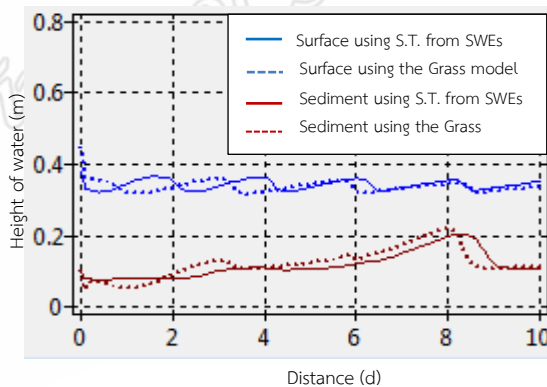
Figure 4b Graph of sediment transport by using the Grass model at time $t = 10$ s.

Figure 4a and 4b show the simulations that were carried out at the same time $t = 10$ s. for both the sediment transport model by following the conservation of mass equation from the shallow water equations (see figure 4a) and the Grass model (see figure 4b).

An A_g (Constant used in the Grass Model) of 0.3 is used and a porosity of sediment for fine sand of 0.43 in [8] is used for the Grass model and the sediment transport model by following the conservation of mass equation from the shallow water equations.

Figure 5a Graph of sediment transport from the conservation of mass equation and the Grass model at time $t = 20$ s.
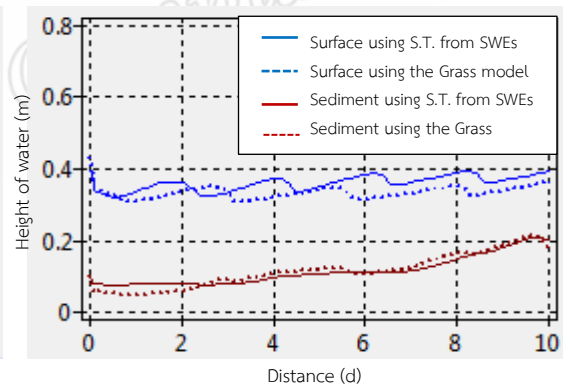
Figure 5b Graph of sediment transport from the conservation of mass equation and the Grass model at time $t = 30$ s.

The results are compared further in figure 5a and 5b, to know the validity of the sediment transport model. From figures 5a and 5b, the sediment distribution is evident in both models. A higher A_g in the Grass model results in a faster movement of the sediment and this can be varied in the model. The sediment transport model uses the porosity of the sediment from experimental data which makes it ideal in simulation.

A two-dimensional shallow water equations model together with the sediment transport model by using conservation of mass equations is used to read the topography data in VirtualSed3D software as shown in figure 6.
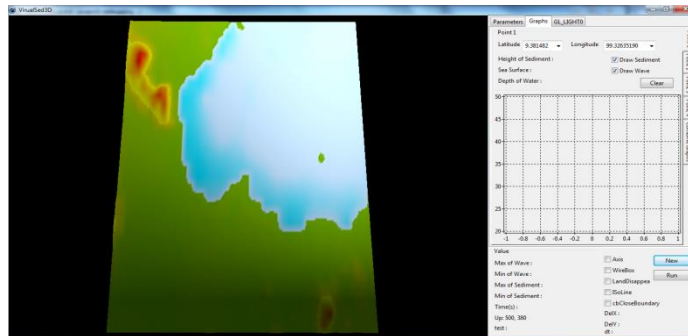

Figure 6 Map data as read by the program.

The map data in this study consider longitude at 99.12916667 to 99.49420379 from the west to the east and latitude at 9.404167 to 9.114120 from the north to south. Therefore, from one latitude-longitude point, the measurement from the SRTM 30 is approximated to 1 kilometer which gives 45 kilometers from west to east and 36 kilometers from north to south. The data is then interpolated using equation (16) to 200 meters.

The VirtualSed3D software is run by using the sediment transport model by following conservation of momentum equation together with the shallow water equations. In the program, the initial wave can be started from the east, north or both. The Manning constant which determines how fast or slow the sediment move is set to 0.025 as studied by [6]. The porosity of the sediment is chosen based on values ranging from 0.25 to 0.53 for sand (fine).
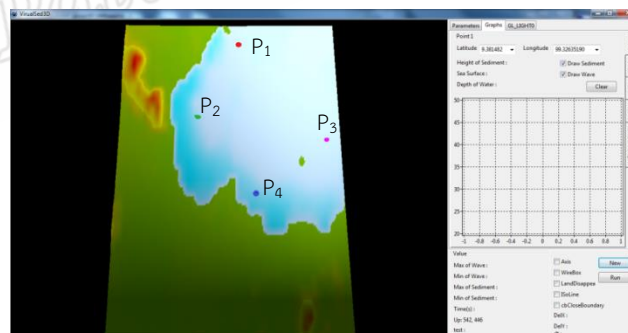

Figure 7 Observation points from simulation.

Arbitrary points (see figure 7) were chosen to know how the wave affect the transport of sediment. The wave is initialized from the east, and then propagates to rest of the area.

The sediment transport model by following conservation of mass from shallow water equations for the various points on the map at time *t = 150000* s are shown below.
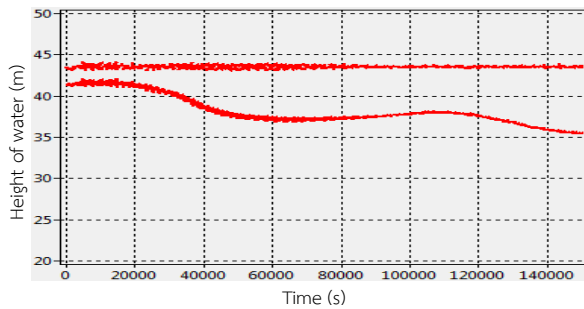
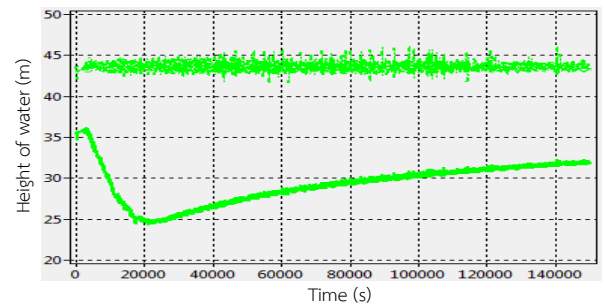**Figure 8a** Distribution of sand (fine) at point 1.

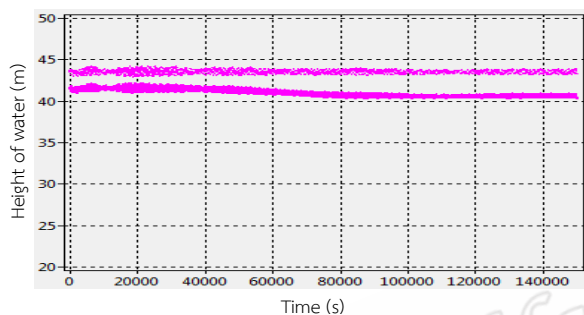**Figure 8b** Distribution of sand (fine) at point 2.

Figure 8c Distribution of sand (fine) at point 3.
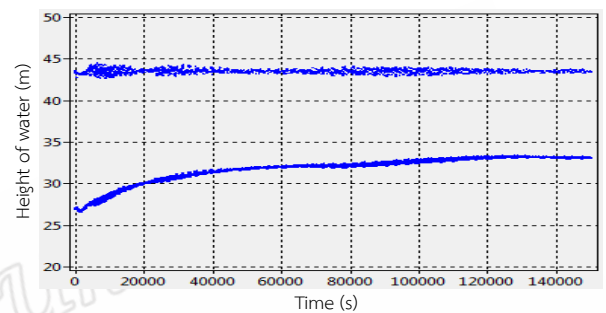

Figure 8d Distribution of sand (fine) at point 4.

Figure 8a, 8b, 8c and 8d show the distribution of sediment using the sediment transport model by following conservation of mass together with the shallow water equations for sand (fine) at time $t = 150000\,s$.

Each of the figures above presents two lines. The first line (upper line) shows the height of wave and the second line (lower line) the height of sediment. Each color displays arbitrary points that were chosen before initializing the wave in the system. The chosen points show the height of wave and the sediment transported as the wave propagation. The level of water is fixed at 44 meters and it could be seen in the first line of each figure. The sediment transport in a particular location is, however, dependent on how far it is to the shoreline and how deep it is. The movement of the wave is from the east but the program plot the graphs from the left to the right. Figure 8a and 8c show the graph of selected points at a location which is not in deep water. This can be seen from the fact that the sediment (below line) is close to the water level (upper line). Sediment in this location moves faster and they are close to the water as seen in the shorter wave lengths.

Figure 8b and 8d show the graph of chosen points at a deeper location in the bay. This is evident from the distance between the sea level and the sediment. As the wave is continuous propagation, the sediment moves depending on how strong the wave is as seen in figure 8b. The presented graph shows the distribution of sediment and how wave propagation affect to sediment distribution.

The sediment transport in shallow region is moved faster than the deep area with different amplitude and wave length.

4 Conclusion

The distribution of sediment at Bandon Bay, Surat Thani has been studied by using the sediment transport model from the shallow water equations and the Grass model. The Grass model is used in order to see the accuracy of the sediment transport model. From figures 4a, 4b,5 a and 5b, it could be seen that there is not much of a difference between the graph produced by the sediment transport model by using the conservation of mass equation from the shallow water equations and Grass model.

What has been achieved through simulation is the fact that sediment distribution depends on the continuous propagation of wave and also how shallow or deep a particular area under consideration is in the ocean. Also, the porosity of the sediment determines how fast they are transported as it can increase or decrease the velocity which it is moved by the wave. By using the latitude and the longitude in the program developed, any point of interest in the ocean can be chosen to see how the wave affects the distribution of sediment. Also the sediment transport model presented is ideal in the study of the sediment distribution by using the conservation of mass equation from the shallow water equations.

References

[1] J.J. Becker, D.T. Sandwell, W.H.F. Smith, J. Braud, B. Binder, J. Depner, D. Fabre, J. Factor, S. Ingalls, S-H. Kim, R. Ladner, K. Marks, S. Nelson, A. Pharaoh, R. Trimmer, J. Von Rosenberg, G. Wallace and P. Weatherall, Global Bathymetry and Elevation Data at 30 Arc Seconds Resolution: SRTM30_PLUS Marine Geodesy, 32:4, (2009), 355-371.

[2] A. Busaman, Mathematical Model for Simulation and Visualization of Flood. Master Degree Thesis, Chulalongkon University (2010).

[3] A. Busaman, K. Mekchay, S. Siripant and S. Chuai-Aree, Dynamically Adaptive Tree Grid Modeling for Simulation and Visualization of Rainwater Overland Flow, (2011), 980–989.

[4] S. Cordier, M.H. Le and T. Morales de Luna, Bedload Transport in Shallow Water Models: Why Splitting (may) Fail, How Hyperbolicity (can) Help. (2011), 980–989.

[5] Google 2001, Bandon Bay in Surat Thani, Thailand. [Online] Available: http://www.google.co.th/intl/th/earth/download/ge/agree.html. (Oct 8, 2015).

[6] Y.A. Kontar, V. Santiago-Fandino and T. Takahashi, Tsunami Events and Lessons Learned : Environment and Societal Significance (Springer Dordrecht Heidelberg, New York, London, 2014), pp. 218.

[7] M. Langland and T. Cronin, A Summary Report of Sediment Processes in Chesapeake Bay and Watershed (Water-Resources Investigations Report 03-4123, U S Geological Survey, 2003).

[8] B. McWhorter and K. Sunada, Ground - Water Hydrology and Hydraulics. [Online] Available :
    http://web.ead.anl.gov/resrad/datacoll/porosity.htm, [Feb 25, 2016].

[9] S. Robert, Oceanography in the 21th Century-An Online Textbook. [Online] Available:
    http://oceanworld.tamu.edu/resources/oceanography-book/coastalerosion.htm, (Feb 7, 2015).

[10] J. Southard, Introduction to Fluid Motions, Sediment Transport and Current-Generated
    Sedimentary Structures (Course Textbook. In MIT Open Courseware: Massachusetts Institute
    of Technology. 2006).

[11] U.S. Environmental Protection Agency, Sediments In Water: Pollution Prevention & Control,
    (2014).

[12] G. Zaimes and R. Emanuel, Stream Processes Part I: Basics. Arizona Watershed Stewardship
    Guide, Master Watershed Steward, (2006).

Vitae

Name   : Nitinun Pongsiri

Student ID   : 5620320707

Educational Attainment :

Degree	Name of Institution	Year
B. Sc. (Information Technology)	Prince of Songkla University	2012

Scholarship Awards during Enrolment

1. Research Assistantship (RA) Scholarship Supported by Centre of Excellence in Mathematics (CEM), Commission on Higher Education, Thailand.
2. Teaching Assistant Scholarship Supported by Graduate school, Prince of Songkla University.

Conference and Proceeding:

Proceeding

Pongsiri, N. and Chuai-Aree, S. 2016. Mathematical Simulation and Visualization of Sediment Distribution at Bandon Bay in Surat Thani. The 21st Annual Meeting in Mathematics & Annual Pure and Applied Mathematics Conference, Chulalongkorn University, Bangkok, Thailand, 23-25 May.